EFFECTS OF PIXEL NOISE AND STIMULUS STRUCTURE ON VISUAL DETECTION PERFORMANCE

HELJÄ TUULIKKI KUKKONEN

Doctor of Philosophy

THE UNIVERSITY OF ASTON IN BIRMINGHAM

March 1994

The University of Aston in Birmingham

EFFECTS OF PIXEL NOISE AND STIMULUS STRUCTURE ON VISUAL DETECTION PERFORMANCE

Heljä Tuulikki Kukkonen
Doctor of Philosophy
1994

Summary

This thesis consisted of two major parts, one determining the masking characteristics of pixel noise and the other investigating the properties of the detection filter employed by the visual system.

The theoretical cut-off frequency of white pixel noise can be defined from the size of the noise pixel. The empirical cut-off frequency, i.e. the largest size of noise pixels that mimics the effect of white noise in detection, was determined by measuring contrast energy thresholds for grating stimuli in the presence of spatial noise consisting of noise pixels of various sizes and shapes. The critical i.e. minimum number of noise pixels per grating cycle needed to mimic the effect of white noise in detection was found to decrease with the bandwidth of the stimulus. The shape of the noise pixels did not have any effect on the whiteness of pixel noise as long as there was at least the minimum number of noise pixel in all spatial dimensions. Furthermore, the masking power of white pixel noise is best described when the spectral density is calculated by taking into account all the dimensions of noise pixels, i.e. width, height, and duration, even when there is random luminance variation only in one of these dimensions.

The properties of the detection mechanism employed by the visual system were studied by measuring contrast energy thresholds for complex spatial patterns as a function of area in the presence of white pixel noise. Human detection efficiency was obtained by comparing human performance with an ideal detector. The stimuli consisted of band-pass filtered symbols, uniform and patched gratings, and point stimuli with randomised phase spectra. In agreement with the existing literature, the detection performance was found to decline with the increasing amount of detail and contour in the stimulus. A measure of image complexity was developed and succesfully applied to the data. The accuracy of the detection mechanism seems to depend on the spatial structure of the stimulus and the spatial spread of contrast energy.

Keywords

Spectral density of pixel noise
Critical size and shape of noise pixels
Spatial integration
Spatial image complexity
Human image processing

ACKNOWLEDGEMENTS

It is a pleasure to express my sincere gratitude to everybody who helped and supported me during this project in the University of Aston in Birmingham.

First and foremost, my sincere thanks are due to my supervisor Reader Jyrki Rovamo who provided continuing support, advice and encouragement during the project, and who made it possible for me to study in Birmingham.

I am deeply indebted to Dr Risto Näsänen for his patience, numerous invaluable discussions and suggestions, and his contribution as an observer. Furthermore, the research would hardly have been possible without his expert technical knowledge and continuous mathematical support.

My warm thanks also belong to my colleagues, Juvi Mustonen, Kaisa Tiippana, and Outi Ukkonen who showed great reliability and patience as observers.

I wish to thank the Head of the Department, Mr Derek Barnes, and the whole personnel of the Department of Vision Sciences at the University of Aston for enabling me to carry out my research.

The work was financially supported by Finnish Ministry of Education, Association of Finnish Ophthalmic Opticians, Information Centre of Optics Business in Finland, Finnish National Agency for Health and Welfare, Näköalaoptikot in Finland, and Finnish Culture Foundation.

Finally, my loving thanks go to my fiancé Serge and my family in Tohmajärvi for their love and support during the preparation of this thesis.

Heljä Kukkonen

March 1994

LIST OF CONTENTS

LIST OF TABLES

LIST OF FIGURES

1. INTRODUCTION

A common way to describe the response of the visual system to spatial patterns is to present observer's contrast sensitivity as a function of spatial frequency of a grating (e.g. Schade, 1956). The normal photopic contrast sensitivity for stationary gratings as a function of increasing spatial frequency has an inverted u-shape having a peak sensitivity around 1-4 c/deg, and decreasing both at high and low spatial frequencies. At high spatial frequencies contrast sensitivity is mainly attenuated by the optic's of the eye (e.g. Campbell & Green, 1965; Campbell & Gubish, 1966; Banks, Geisler & Bennet, 1987; Santamaria, Artal & Bescos, 1987; Deeley, Drasdo & Charman, 1991; Rovamo, Mustonen & Näsänen, 1994a). At low spatial frequencies the decrease of contrast sensitivity has been addressed to the neural transfer function of the visual pathway (Schade, 1956; Nachmias, 1968; Rovamo, Luntinen & Näsänen, 1993; Luntinen, Rovamo & Näsänen, 1994; Rovamo, Mustonen & Näsänen, 1994b) reflecting the effects of lateral inhibition (Ratliff & Hartline, 1959). In addition to optical and neural transfer functions, the shape of the contrast sensitivity function especially at low spatial frequencies is affected by the number of grating bars (Hoekstra, van der Goot, van den Brink & Bilsen, 1974; McCann, Savoy, Hall & Scarpetti, 1974; Savoy & McCann, 1975). When the number of grating bars within the stimulus field is kept constant at all spatial frequencies, the contrast sensitivity function at low spatial frequencies becomes flatter. This indicates spatial integration of contrast information at the level of signal detection. Finally, the visual system, like any sensory system, contains neural noise that limits its performance at threshold (e.g. Barlow, 1956, 1957, 1977).

The visual system could thus be regarded as an image processor, the performance of which is limited due to filtering properties of the signal transmission mechanism, introduction of neural noise, and inaccuracies at the stage of image interpretation (Rovamo & al., 1993; Rovamo, Mustonen & Näsänen 1994c; Rovamo, Ukkonen, Thompson & Näsänen, 1994d). Filtering at the level of signal transmission comprises the effects of the optical and neural transfer functions and can be called the modulation

transfer function of the visual system (Davila & Geisler, 1991; Rovamo & al., 1993). The modulation transfer function thus results in a decrease of foveal contrast sensitivity function at high and low spatial frequencies. After filtering at the early stage of visual processing, the detection of a visual stimulus is limited due to introduction of internal neural noise (e.g. Barlow, 1956, 1957, 1977; Pelli, 1981, 1990). Effectively, internal neural noise causes uncertainty at the level of image interpretation as to whether the received signal includes the visual stimulus or noise only. The decision of the presence of a visual signal is made at the level of image interpretation. The mechanism used at this level is able to integrate contrast information over space and hence improve the visual performance of the system. This feature of the detection mechanism is demonstrated by increasing sensitivity as a function of grating size, for example. The saturation of contrast sensitivity as a function of grating size, on the other hand, implies that the area over which the detection mechanism is able to integrate spatial information is limited.

By using complex spatial patterns, i.e. a kind of visual information that the visual system continuously has to deal with, we can obtain valuable information about the higher levels of visual processing. Unfortunately, the effect of the modulation transfer function of the visual system is difficult to estimate for complex spatial patterns. There is a way to "by-pass" the effects of both modulation transfer function and internal neural noise, however. By using external spatial noise of high spectral densities we can consider the external image noise to be the primary source of noise for the visual system and thus apply the concept of constant signal-to-noise ratio at threshold (e.g. Nagaraja, 1964; Pelli, 1981; Luntinen & al., 1994). When the stimulus to be detected is embedded in external noise of high spectral density, the filtering in the visual system affects both signal and noise similarly at each spatial frequency. The signal-to-noise ratio at each spatial frequency thus remains unaffected by the filtering. Therefore, when sufficient masking of the external image noise is obtained, the concept of constant signal-to-noise ratio allows us to investigate the properties of the visual system at the stage of image interpretation without the effects of internal neural noise and filtering at the early stages of image processing.

The work of this thesis attempts to clarify the critical features of the mechanism that is used by the visual system to detect various spatial patterns. In order to do so, detection thresholds were measured for spatial patterns of increasing complexity and results compared with an ideal detector whose performance is not limited by the spatial distribution of contrast information available but only by the magnitude of external image noise used. Therefore, and also in order to avoid the filtering in the early stages of vision, experiments were carried out in external spatial noise. Consequently, the first part of the thesis was dedicated to investigation of the properties and masking effects of external image noise produced on a computer display (i.e. pixel noise).

Contrast measures and interpreting results

The introduction of increasingly complex spatial patterns and visual noise as research tools has made it necessary to use new measures of contrast. As elementary as it might sound, in order to be able to interpret the results obtained, it is essential to comprehend how the various measures take into account the properties of spatial patterns and whether these properties are relevant for human visual performance. Therefore, *Section 2.4* of this thesis has been devoted to the three most common contrast measures used in contemporary studies of vision: They are Michelson contrast, r.m.s contrast, and contrast energy.

Section 2.4 shows that the shape of a contrast sensitivity function, which has traditionally believed to reveal important modulation transfer properties of the human visual system, can fundamentally change depending on the contrast measure used. A change in the shape of the contrast sensitivity function produced by a change in contrast measure is not, therefore, an indication of a change in the way signal is processed in the visual system, but rather reflects the properties of the spatial stimulus that the measure takes into account.

In addition, *Section 2.4* evaluates the validity of various contrast measures as

descriptors of human performance at threshold. It has been shown that the perceived contrast of a complex spatial pattern in comparison to a perceived contrast of a simple grating is best described in terms of the r.m.s contrast (e.g. Quick, Hamerly & Reichert, 1976; Moulden, Kingdom & Gatley, 1990, Tiippana, Näsänen & Rovamo, 1994). It is shown here that this conclusion can also be extended to threshold vision.

The effects of noise on the visual threshold

The masking effect of spatial noise, which refers to random luminance variation over space, is expressed in terms of the spectral density across the spatial frequency spectrum (e.g. Green & Swets, 1966; Pelli, 1981). In order to use external image noise as a tool for studying visual processes we need to keep in mind that the effective signal-to-noise ratio for the visual system can be unambiguously defined as the square of the ratio between contrast energy threshold and the external spectral density of image noise only by using white external noise, and only when the external noise is the dominant source of noise for the visual system, i.e. its effect exceeds the effects of other noise sources potentially affecting detection.

By definition, the spectral density of white spatial noise has a constant value at all spatial frequencies and we can thus describe the masking power of white external noise with one number. White noise, in the strict sense, is impossible to produce in the real world, however. Fortunately, our visual system is a band-limited detection system, which collects the signal as well as the noise within a limited bandwidth, and we thus need to satisfy the criteria of white noise only within the frequency range of the detection filter.

In addition to external image noise, there are mainly two other types of noise limiting visual performance: one is internal to the visual system and the other originates from the quantal nature of the light. Detection threshold is determined by the sum of all the noises present. However, when one of these noise sources is clearly dominating, the threshold measured is directly proportional to the spectral density of the dominant noise.

Therefore, if we want to evaluate the performance of the visual system on the basis of external image noise, the spectral density of the external noise has to be high enough to exceed the effects of the other noise sources affecting detection. Particularly high spectral densities of external noise are needed at low and high spatial frequencies (e.g. Luntinen & al., 1994) as well as at low levels of retinal illuminance (e.g. Nagaraja, 1964; Pelli, 1990).

Chapter 3 of this thesis searches for ways to maximise the masking power of white external spatial noise generated on a computer screen. Such a noise consists of discrete luminance samples, pixels. The spectral density of pixel noise can be increased by increasing either the r.m.s contrast of noise or the size of the noise pixels. When it is no longer possible to increase noise contrast, the only way to obtain higher spectral densities of pixel noise is to enlarge pixels. At the same time, however, the cut-off frequency of noise decreases. Therefore, in order to obtain the maximal masking effect of external noise we have to find the largest size of noise pixels that do not compromise the whiteness of external noise. It was found that the largest size of noise pixels depends on the bandwidth of the stimulus.

Furthermore, *Chapter 3* will demonstrate that the masking power of static pixel noise in a visual detection task is best described when the spectral density of white pixel noise is calculated by taking into account both spatial dimensions of the pixel, even when there is random luminance variation in only one dimension. This is in disagreement with the common view that the spectral density of spatial noise and its masking power can be adequately described by taking into account only the dimensions where random luminance variation takes place (e.g. Legge, Kersten & Burgess, 1987).

How is then the physical signal-to-noise ratio affected by changes in the experimental conditions? When the physical signal-to-noise ratio is kept constant, the changes in contrast threshold reflect changes in processing of the visual stimuli, if we assume that signal-to-noise ratio is constant at threshold. However, in some cases the change in threshold might be due to a change in the source of noise resulting from the changes in the experimental conditions (e.g. Rovamo, Franssila, Näsänen, 1992). In *Chapter 4*, detection thresholds were measured as a function of luminance, exposure

duration, and grating area both with and without external spatial noise in order to sort out various reasons for changes in detection threshold, when the physical signal-to-noise ratio is constant but experimental conditions vary. It was found that at low luminance levels, short exposure durations and small grating areas, the spectral density of external image noise has to be high in order to exceed the effect of other noise sources.

Chapter 4 also suggests that the effect of external noise on the performance of the visual system is best described when the spectral density of white external noise is calculated taking into account all the three dimensions of noise pixels, i.e. width, height, and duration.

Spatial integration and detection mechanisms

A large number of studies investigating the detection of grating stimuli have shown that contrast sensitivity increases as a function of stimulus area (e.g. Savoy & McCann, 1975; Howell & Hess, 1978; Virsu & Rovamo, 1979; Rovamo & al., 1993). Furthermore, for all spatial frequencies, contrast sensitivity is found to saturate at the same number of grating periods, when the height of the vertical grating is constant. Similarly, when only the height of the grating is varied, contrast sensitivity first increases but then saturates at a constant value of height expressed in terms of the number of grating periods. Spatial integration in the visual system thus has two main features: it is spatially limited and scale invariant.

The results obtained with grating stimuli are often explained by assuming that the visual system contains multiple channels each selectively sensitive to a limited range of spatial frequencies and orientations (e.g. Campbell & Robson, 1968; Graham, 1989). A channel is a collection of 'sub-units' with receptive fields of a given type, distributed across the visual field. A signal is detected when one of the sub-units reaches its individual threshold. In the spatial domain the receptive field of each sub-unit resembles a Gaussian-weighted grating patch containing a constant number of grating periods and

having a certain spatial frequency and orientation. Contrast sensitivity for a grating increases in direct proportion to the number of grating bars as long as the grating area is smaller than the receptive field of an individual sub-unit most sensitive to that particular pattern. When the grating area exceeds the size of the receptive field, the increase of contrast sensitivity does not immediately saturate, however. Instead, as a result of the further increase in grating area, the grating is assumed to excite several, adjacent sub-units sensitive to that particular spatial frequency and orientation, but occupying a different part of the visual field. The output of the multiple sub-units is then combined using the statistical procedure of probability summation (e.g. Quick, 1974; Graham, 1989). In practice probability summation means that as the number of stimulated sub-units and channels increases, the probability that one of them will exceed its threshold increases.

Although, there is an extensive amount of physiological evidence for the existence of such selectively sensitive cells in the primate visual cortex (e.g. Hubel & Wiesel, 1962, 1968; De Valois, Albrecht & Thorell, 1982), it seems that we cannot explain visual perception with a model based on probability summation across cortical cells. The problem with the multiple channel model is its rigidity: without any further assumption prior information of the signal expected should not have any effect on the detection performance (e.g. Davis & Graham, 1981; Davis, Kramer & Graham, 1983). This has clearly been shown not to be the case with human observers whose performance decreases with uncertainty of the signal (e.g. Lappin & Uttal, 1976; Davis & Graham, 1981; Davis & al., 1983; Burgess & Ghandeharian, 1984a, b; Burgess, 1985; Ukkonen, Rovamo & Näsänen, 1993). Therefore, multiple channels, rather than being responsible of the visual performance of a human observer, are nowadays considered as a means of preliminary coding of the visual information (e.g. Burgess, 1990). This coded information is then suitably weighted and combined at higher levels of visual processing. The mechanism that is responsible for the perception of the stimulus clearly has to be adaptive and able to use a priori information. The detection filter could therefore be, for example, a local matched filter with a limited area of spatial integration, as has been suggested by

Burgess (1990), and in association with a more complete model of the human contrast detection mechanism by Rovamo et al. (1993;1994c, d).

A critical study of how this adaptive detection mechanism operates and what limits its performance is to investigate the spatial integration of complex spatial patterns. The complexity of the spectral and spatial dimensions of the stimulus can be separately manipulated, and by doing so it is possible to find out whether the critical determinant of spatial integration is the spectral or spatial characteristics of the stimulus, or both. The multiple channel model would suggest that the main determinant is the spatial frequency spectrum of an image whereas in a system in which channels only code the information which is then interpreted by a matched filter with a limited integration capacity, both spectral and spatial characteristics would affect performance.

Chapter 5 introduces four studies carried out with visual patterns of varying spatial and spectral complexities. By using spatial noise of a sufficiently high spectral density, the effects of early filtering in the visual system, as well as the effects of internal noise in the visual system could be ignored. The detection thresholds measured were then compared with detection thresholds of an ideal, statistically determined detector (matched filter), which is able to use all spatial information. The performance of an ideal detector operating on a signal that is exactly known is thus limited only by external image noise.

The detection efficiencies obtained for complex spatial patterns seemed to be determined by the amount of contour and detail in the image i.e. their spatial features, rather than their spatial frequency spectrum. However, the amount of contour and detail in the image was not the only determinant of spatial integration: even when the number of details was kept constant, but the spread of the contrast information was increased, detection efficiency decreased. The human visual system thus seems to be able to use a limited amount of spatial information at a time (e.g. Verghese & Pelli, 1992) and the ability to collect the visual information decreases as the distance from the centre of attention increases (e.g. Burgess, 1990; Nakayama, 1990; van Essen, Olshausen, Anderson & Gallant, 1991).

2. GENERAL METHODOLOGY

2.1. APPARATUS

The experiments were performed using two different apparatus both consisting of a high resolution computer monitor (CRT) and a VGA graphics board driven by a computer. Both apparatus were set up by Dr R Näsänen.

The main difference between the two apparatus was in the colour channel summation used to increase the number of available grey levels to allow contrast sensitivity measurements with sufficient accuracy. Without any modification, an achromatic signal of 64 grey levels could be produced. However, this number of grey levels is insufficient for detection threshold measurements with sinusoidal and even with square wave gratings: With 64 grey levels, the luminance of a pixel can vary from 0 to 63 on a relative range. The maximum contrast range available for a grating would thus extend from 1 [(63-0)/(63+0)] to 0.016 [(32-31)/(32+31)] at a constant mean luminance level (proportional to 32). Except for the highest spatial frequencies, the minimum contrast is clearly too great for presenting a square-wave grating at thresholds. The minimum contrast available could be reduced by increasing the mean luminance but this, on the other hand, would result in a reduced range of available contrasts. On the basis of the above example, we can therefore conclude that 64 is not a sufficient number of grey levels to measure thresholds even for square wave gratings, not mentioning sinewave stimuli which require a finer scale of luminance steps to present the gradual changes in luminance across space.

A colour image is produced on the monitor screen by separately driving the three colour guns in the monitor. Since the achromatic contrast sensitivity measurements, such as those described in this thesis, do not need colour, the number of grey levels can be increased by suitably combining the signals of three colour guns. Two summation methods, one designed by Dr R Näsänen and the other one built according to Pelli and Zhang (1991), were used in the two different apparatus.

Both apparatus are introduced below. According to a series of control experiments, the two summation methods yielded similar contrast threshold values. The Apparatus 1 was used in the experiments described in chapters 3, 4, and 5.4-5.6 whereas Apparatus 2 was used in all the other experiments of this thesis.

2.1.1 Apparatus 1

Apparatus 1 consisted of a 16" RGB multiscan monitor (Eizo Flexscan 9080i with a fast phosphor B22), and a VGA graphics board (Orchid's Pro Designer VGA plus) driven by an ALR Business Veisa 486/33 computer. The monitor could show 1280 x 800 pixels but the graphics board was used in a mode of 640 x 480 pixels leading to the pixel size of 0.42 x 0.42 mm^2 on the screen. The pixel size chosen allowed measurements at a sufficient resolution and high enough frame rate which was 60 Hz. The display was used in white mode. The average photopic luminance of the display was measured with a Minolta Luminance Meter LS-110 and set at 50 cd/m^2.

A VGA board can simultaneously show 256 colours (8 bits) chosen from a palette of 262144 colours (6+6+6 = 18 bits). The maximum number of intensity levels of each colour channel is only 64 (6 bits).

To obtain a monochrome signal of 1024 intensity levels (10 bits) from a monochrome palette of 65536 (16 bits), the red, green and blue outputs of the VGA board were combined by using a video summation device built according to Pelli and Zhang (1991): For red and green colour gun only the four most significant bits were used to represent the signal in order to avoid inaccuracies in voltages corresponding to less significant bits which may cause some distortion in the contrast response. For blue colour gun the whole range of six bits was used. By using a combination of precision resistors the green output was first attenuated by a factor of about 1/13 and the blue output by a factor of about 1/182 in comparison to the red channel. The optimal combination of the resistors was thereafter found by generating a square-wave flicker near the mean

luminance by using only the red output and an amplitude equal to one quantization interval. The voltage from the green output was then added to the minimum luminance in order to cancel the flicker. If the resistor was too low, the flicker could not be cancelled even with the maximum input of green channel, and vice versa. The correct setting was obtained as a mean of several estimations (30-50). The same kind of tuning procedure was carried out for the blue output using green output as a standard. This calibration procedure is difficult and needs a very high flicker sensitivity.

After the tuning, all outputs were added together to form a single monochrome output. This procedure resulted in an 8-bit signal from a palette of 14 (4+4+6) bits. The red output thus mediated the most significant bits. Two additional bits were obtained by adding a periodic dither signal of a very small contrast and high spatial frequency before intensity quantization.

This type of ordered dither technique is commonly used in order to produce an impression of various shades of grey in printed images. The masking effect produced by a periodic dither signal (Näsänen, 1989) resembles the masking produced by gratings (e.g. Legge & Foley, 1980; Georgeson & Georgeson, 1987; Ross & Speed, 1991): it decreases with increasing distance between signal's spatial frequency and the spatial frequency of the mask (periodic dither signal in this case), and the magnitude of masking produced is a power function of the effective contrast of the masking signal (Legge & Foley, 1980; Näsänen, 1989). Näsänen (1989) studied the masking effect of a high-contrast periodic dither signal and found that the masking effect halves at about one octave from the dither frequency. This result is in agreement with the high-contrast masking bandwidth found for gratings by Legge and Foley (1980), for example. As Legge and Foley (1980) showed the masking bandwidth of low-contrast grating masks was considerably narrower. Therefore, by keeping the size and contrast of the dither signal small enough, the number of grey levels can be increased by using a periodic dithering signal without undesirable masking effects.

The size of the dither period used was 2x2 pixels leading to the lowest spatial frequency of 11.9 c/cm on the screen which is 1.58 octaves higher than the highest

spatial frequencies (4 c/cm) of the stimuli used. On the other hand, the amplitude of the dither signal was one quantization interval. For example, at the stimulus contrast of 1.25×10^{-3}, contrast of the dither was only 1.05×10^{-4}. This guarantees that the dither could not have any masking effects even when thresholds were measured without external noise. Furthermore, in the presence of external spatial noise, as in most of the experiments of this thesis, the proportion of dither signal is negligible.

The dither signal was $d(0,0)=0$, $d(0,1)=0.75$, $d(1,0)=0.5$, $d(1,1)=0.25$. The dither signal thus increased the number of grey levels by four. The dithering algorithm was

$$g_q(x,y) = \text{int}[g(x,y)+d(x,y)], \qquad (2.1)$$

where int [.] denotes rounding to the nearest integer, $g_q(x,y)$ is the quantized signal with dither, $g(x,y)$ is the continuous luminance signal, and $d(x,y)$ is the dither signal.

The monochrome signal was connected to the red input of the monitor. The colour of the screen was changed to white by means of a switch in the monitor. The range of 16 bits allowed measurement of contrast sensitivity with sinusoidal gratings consisting of about 49 grey levels at a Michelson contrast of 0.00125 (see page 24 for more details).

Calibration of the luminance response

The luminance response of the display in the white mode was measured as a function of the 6-bit index value (0-63) with the Minolta Luminance Meter LS-110. When plotted in linear coordinates, the luminance values followed an exponential function of the input values, as shown in Figure 2.1. The luminance increased from about 0.01 cd/m^2 to about 100 cd/m^2 when the index value increased from 0 to 63.

In order to find a function describing the relationship between the luminance and the index values, the data were plotted in a double logarithmic coordinates. When plotted

in this way the logarithm of the luminance response was linearly proportional to the logarithm of the intermediate index values and a least squares line could be fitted to this part of the data. The luminance response function obtained for Apparatus 1 was of the form $L(I) = 0.005298\ I^{2.409}$, where L is the luminance in cd/m^2 and I is the index value. The solid line in Figure 2.1 shows the luminance response function of the Apparatus 1 in linear coordinates.

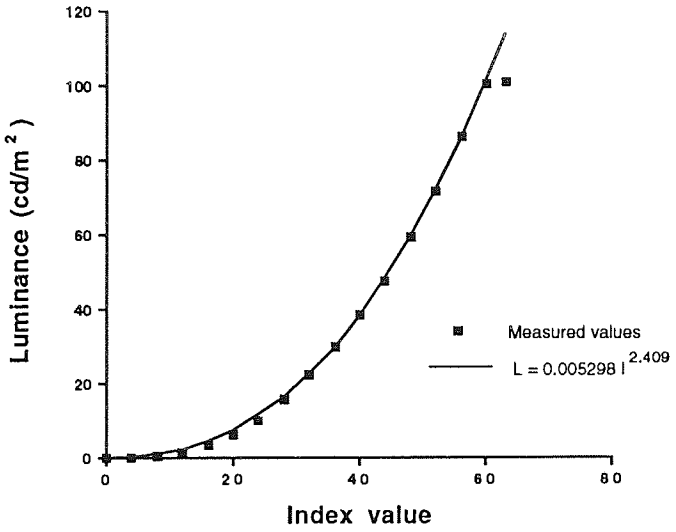

Figure 2.1
The measured luminance response of the monitor of Apparatus 1.

The inverse of the function obtained was then used to linearise the luminance response of the screen. The function $I = [L(I)/0.005298]^{1/2.409}$ thus gave the index value for each requested luminance. This gamma-correction was performed when computing the stimulus images.

Naturally gamma-correction is the most accurate within the luminance range which was used to find the least squares line. In order to produce the stimuli as accurately as possible, we mainly want to use the most accurate luminance range. Therefore, as the luminance of the stimuli used in this thesis was varied symmetrically around mean luminance, the mean luminance was set at 50 cd/m^2, which was approximately in the middle of the luminance range used to find the least squares line.

The function $L(I) = 0.005298\ I^{2.409}$ describes the luminance response of the screen when sampled with 64 index values ranging from the minimum to maximum luminance. However, the 14 bit system consist of the total of 16,384 (2^{14}) luminance steps within the same luminance range i.e. each of the 64 steps comprised 256 additional luminance steps. When the gamma-function is converted to correspond to the total number of luminance steps, it gets a form $L(I_e) = 0.005298\ (I_e/256)^{2.409}$ $= 8.369 \times 10^{-9}\ I_e^{2.409}$, where I_e is the extended index value. In order to estimate the number of grey levels for the stimulus contrast of for example 0.00125 at the mean luminance of 50 cd/m^2, we need to calculate the index values for corresponding minimum (49.9375 cd/m^2) and maximum (50.0625 cd/m^2) luminances by means of the inverse of the luminance response function. According to the extended gamma-function they were 11,429 and 11,441, respectively. There was thus 13 grey levels produced by video summation device (Pelli & Zhang, 1991) only. The random dither used added three more steps between each step produced by the video summation across the colour channels, and therefore the total number of about 49 grey levels were obtained at Michelson contrast of 0.00125. The nominal number of grey levels at various contrasts is showed below.

Michelson contrast	Number of grey levels
0.000625	25
0.00125	49
0.0025	97
0.005	189
0.01	381
0.02	761
>0.027	1024

Table 2.1
The nominal number of grey levels at various contrasts for Apparatus 1.

Because the amplitude of the dither signal equals to the amplitude of one step produced by video summation, we can estimate the contrast of the dither signal at various

contrasts of the signal. For example, at Michelson contrast of 1.25×10^{-3} the maximum and minimum luminances correspond to a step from index value of 11,435 to 11,436. From the extended luminance response function, we obtain an estimate of 1.05×10^{-4} for the contrast of the dither signal at the stimulus contrast of 1.25×10^{-3}. However, at Michelson contrast of 1, the dither signal corresponds to a step size of an 8 bit signal. The extended luminance response function for an 8 bit signal is $L(I_e) = 1.88 \times 10^{-4} I_e^{2.409}$. The mean luminance of 50 cd/m^2 corresponds to an index value 179. The Michelson contrast for a step from index value 179 to 180 is thus 6.71×10^{-3}.

2.1.2 Apparatus 2

Apparatus 2 consisted of a 16" RGB high-resolution colour monitor (Eizo Flexscan 9070S), a VGA graphics board (Orchid's Pro Designer VGA plus) driven by a WYSE PC-386 computer. In practice, Apparatus 2 differed from Apparatus 1 only by the luminance response of the display, the colour channel summation method used, and the number of grey levels.

To obtain a monochrome signal of 1024 intensity levels (10 bits) from a monochrome palette of 16,384 (14 bits), the red and green outputs of the VGA board were combined using a method designed by Dr R Näsänen. The method had the same theoretical principle as the one used for Apparatus 1, but now only the red and green outputs were added together to produce a single monochrome output. In comparison to the red output the green output was first attenuated by a factor of about 1/64 using an adjustable resistor. The red and green outputs were then added together and a fine tuning of the resistor was thereafter performed using the visual criterion that a sine-wave with high contrast and low spatial frequency did not have any visible steps and looked as smooth as possible. Again, the red output mediated the most significant bits. This operation allowed us to use a signal of 8 bits from a monochrome palette of 12 (6 + 6) bits. Two additional bits were obtained by using a periodic dither signal as in Apparatus 1.

The non-linear luminance response of the monitor was found to be of the form $L(I) = 0.177\ (I-12)^{1.69}$. Apparatus 2 produced about 9 grey levels at Michelson contrast of 0.00125. The contrast of the dither signal at the corresponding stimulus contrast was 4.68×10^{-4}. The nominal number of grey levels at various Michelson contrasts is shown below. All the other details of the Apparatus 2 were identical to Apparatus 1.

Michelson contrast	Number of grey levels
0.000625	5
0.00125	9
0.0025	21
0.005	45
0.01	85
0.02	173
0.04	341
0.08	685
>0.12	1024

Table 2.2
The nominal number of grey levels at various contrasts for Apparatus 2.

2.1.3 Contrast response of the monitor

The contrasts of the gratings used for experiments were measured with Minolta Luminance Meter LS-110. In order to measure the contrast response across spatial frequencies, six sets of sinusoidal gratings with spatial frequencies of 0.25 - 4 c/cm were created. Three orientations were tested (0°, 45°, and 90°) using two contrast levels of 0.1 and 0.5.

Each set of gratings was studied separately by measuring the maximum and minimum luminance of the grating displayed on the screen by the Minolta Luminance Meter LS-110 with a close up lens No 110 having a spot diameter of 0.4 mm on the screen. The maxima and minima could be displayed at the same location on the screen by changing the phase of the displayed grating by 180 degrees. Measurements were

performed as a function of spatial frequency. For each grating at least three measurements of maximum and minimum luminances were recorded and an average was used to calculate the contrast of the grating displayed on the screen.

The curves obtained are shown in Figure 2.2a. At first the measured contrast stayed constant and equal to the contrast requested. Then the transfer function of the display system caused a decrease in displayed contrast. The displayed contrast was found to be independent of spatial frequency and orientation approximately up to 2 c/cm. At spatial frequency of 4 c/cm, which was the highest spatial frequency used in the experiment of this thesis, the contrast response was attenuated by 0.12 $\log_{10}$ units.

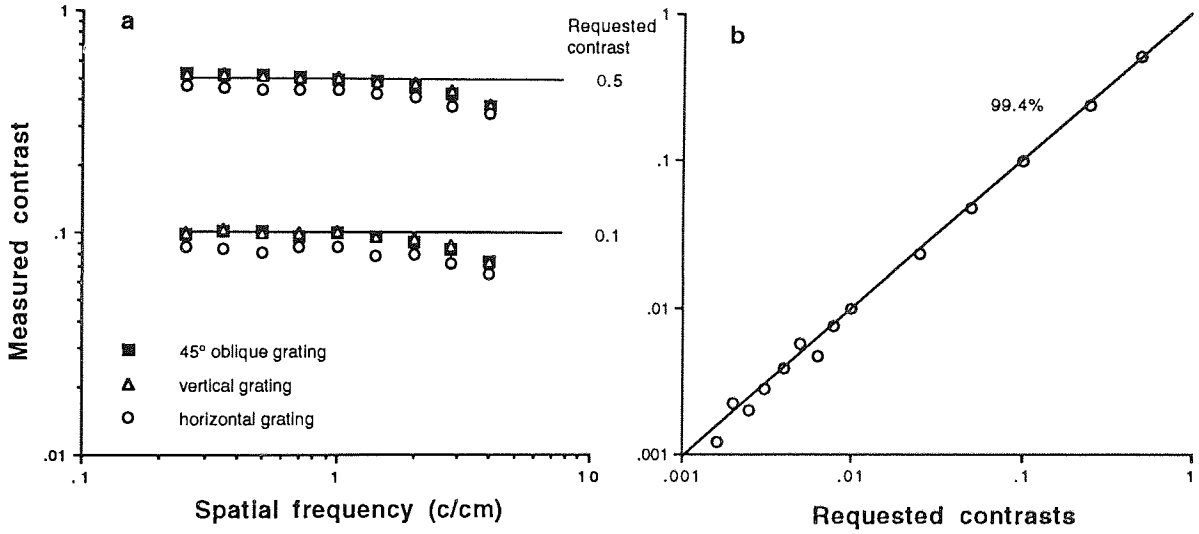

Figure 2.2
The contrast response of the display system of Apparatus 1.

Figure 2.2b shows the contrast response of the monitor across a contrast range of 0.0016-0.5. It was measured for a very low spatial frequency displayed on the screen. The spot diameter of the Minolta Luminance Meter LS-110 was about 2 cm on the screen. The maximum and minimum luminances were recorded by changing the phase of the grating from 0 to 180 degrees, as explained above. The measured contrast is plotted as a function of requested contrast. The solid line in Figure 2.2b shows the optimal situation when the measured contrast is equal to the requested contrast down to very low

contrasts. As Figure 2.2b shows, the measured and requested contrasts were equal down to the smallest contrast measured which was 0.0016 corresponding to sensitivity of 625. The explained variance of the solid line, calculated according to Appendix 1, was 99.4%. At small contrasts the measurements are somewhat noisy which leads to random deviations from the solid line.

2.2 STIMULUS GENERATION

Stimuli were generated and manipulated digitally by means of the software developed by Dr R Näsänen. The software was written using Microsoft Professional BASIC 7.0. The software utilised the graphics subroutine library of Professional HALO 2.0 developed by Media Cybernetics.

The stimuli were drawn on the screen with coordinates (x,y) varying between (0,0) and (639, 479). The maximum stimulus size allowed by the apparatus was 16 x 16 cm^2.

The required stimuli were first computed and stored on the hard disk. Before starting an experiment the stimulus files needed were copied to the part of 16 MB main memory that was used as a fast RAM-disk in order to speed up and equalize the search times of the stimulus needed. The stimuli were transferred to the VGA frame buffer upon request. The stimulus was rapidly switched on and off by changing the colour look-up table during the vertical retrace period of the display.

2.3 THRESHOLD DETERMINATION

Detection threshold, in its strict sense, means a value (e.g. contrast) at which a stimulus can just be detected: at the values below threshold, stimulus is never detected and at the values above threshold, stimulus is always detected. In terms of a psychometric function, the probability of detection would be a single step function of the variable. However, in any biological system there is no single threshold value, but the probability of correct response changes gradually as a function of the variable. In case of contrast detection, probability of detection increases from a minimum level, which is determined by the probability of correct guessing, to 1.0 correct as the contrast of the stimulus increases. This produces a shallow s-shaped function. Therefore, threshold is normally defined as a value which produces a certain percentage of correct responses.

In this thesis detection thresholds were determined using a forced-choice algorithm with a staircase routine. Thresholds were determined in non-randomised order for one stimulus at a time. Either a two-alternative or a two-interval forced-choice algorithm was used. In a two-alternative algorithm the stimulus (e.g. signal + noise) and the comparison stimulus (e.g. noise alone) were presented simultaneously whereas in a two-interval algorithm the stimulus and the comparison stimulus were presented in successive exposures. The observer had to indicate in which stimulus window/exposure the stimulus was by pressing one of two keys on a computer keyboard. The response time was unlimited and a new trial began 250 msec after the subject's response. These algorithms produce a minimum of 50% correct responses.

The subject was given an auditory feedback about the correctness of the response in order to help him/her to achieve the best possible performance. All the subjects used were experienced and well motivated colleques (postgraduate students and postdoctoral fellows) but usually naive about the aim of the study.

This thesis concentrated on the foveal vision only. Therefore, all the experiments were performed in a dark room to avoid the stimulation of peripheral vision. The only light

source was the computer screen. Its horizontal and vertical dimensions were 26.9 and 20.2 cm.

2.3.1 The staircase routine

A staircase routine was used to estimate the threshold contrasts. The up-and-down transformed response (UDTR) rule, described by Wetherill and Levitt (1965), allows us to vary the probability level of correct responses by changing either the number of consecutive correct responses that produce a decrease in the contrast level of the stimulus, or the number of incorrect responses that produce an increase in the contrast level of the stimulus, or both. The contrast level is changed using a fixed step size on a logarithmic scale.

The up-and-down transformed response (UDTR) rule is a modification of a straightforward up-and-down rule where only one correct response is required to produce a decrease of the contrast level and only one incorrect response in required to produce an increase of the contrast level. This basic form of the up-and-down rule yields the probability level of correct responses equal to the level that would be obtained by purely quessing. Thus, when the two-alternative or the two-interval algorithm is used, the 1-1 up-and-down rule results in a probability level 50% of correct responses. When the number of incorrect responses that produce an increase of contrast level is kept constant at one and the number of correct responses required for a change in contrast level is varied, the probability of a correct response at any probability level x follows a function $x^n = 0.50$, where n is the number of correct responses required. Therefore, the number of consecutive correct responses required determines the probability level by:

$$x = \sqrt[n]{0.50} \tag{2.2}$$

For the threshold measurements introduced in this thesis the up-and-down transformed response (UDTR) rule was used in a mode that four consecutive correct answers produced a decrease in stimulus contrast by one step and each incorrect response produced an increase in stimulus contrast by one step. Thus the probability of 0.84 ($0.50^{1/4}$) correct responses was obtained. The step size was constant at 0.1 $\log_{10}$ units.

In order to eliminate the effect of the starting contrast on the threshold value, the estimation of threshold contrast took place in two consecutive phases for each threshold measurement. The first phase established a subthreshold starting point for the final threshold estimation independently of the initial contrast selected.

The first contrast shown for each threshold measurement was clearly above threshold in order to reduce observers uncertainty of the stimulus to be detected. During the first phase of threshold determination, each correct choice reduced contrast by 0.1 $\log_{10}$ units. Although, the first wrong choice increased stimulus contrast, it was not recorded as a turning point, on which the calculations of threshold contrast were based. The first phase of threshold determination continued until the second wrong choice initiated the final phase. The contrast at which the second wrong choice took place was normally below the threshold level by an amount depending on the hit rate of subject's guesses at near threshold contrasts.

The second and final phase of contrast estimation procedure started after this first phase. During the final phase the 1-4 up-and-down transformed rule was applied. Every wrong choice thus increased contrast by 0.1 $\log_{10}$ units and four consecutive correct responses led to a contrast decrement by the same amount; a smaller number of correct choices had no effect.

The final phase of contrast estimation continued till 9 reversals of the direction of contrast change occurred; hence, the estimation always terminated after a string of correct responses. The threshold contrast was estimated as the arithmetic mean of the last 8 reversal contrasts. Figure 2.3 shows a sketch of a plausible string of trials for one

threshold measurement. Each data point presented in this thesis represents the average of at least three threshold estimates.

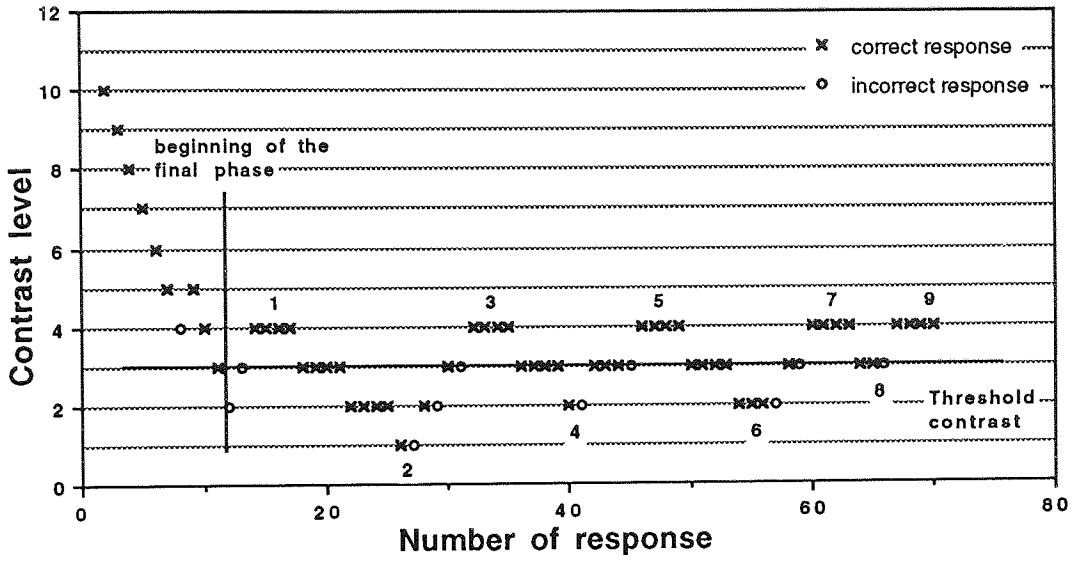

Figure 2.3
A plausible string of trials for one threshold measurement.

2.4 CONTRAST MEASURES

2.4.1 Introduction

One way to describe human performance in the experiments of spatial vision, is to define the minimum contrast i.e. contrast threshold at which the stimulus can be detected or discriminated. As explained above, threshold contrast is generally defined as a contrast level at which a desired percentage of correct responses is obtained. Results are then expressed either in terms of contrast threshold or contrast sensitivity, which is the inverse of the threshold value.

The definition of contrast is often selected on the basis of the stimulus. For an isolated stimulus element, like a single spot or line, contrast is traditionally expressed in terms of Weber fraction (e.g. Graham, Brown & Mote, 1939; De Vries, 1943; Rose, 1948, Baumgardt, 1972):

$$c_{Weber} = \frac{\Delta L}{L_b}, \tag{2.3}$$

where ΔL refers to luminance increment or decrement and L_b to the background luminance. When the stimulus element is small in respect to the background, as is often the case with spots or line stimuli, the background luminance approximately equals to the mean luminance.

However, Weber fraction is not applicable for stimuli whose luminance varies both below and above the mean luminance, as is the case with grating stimuli. For a simple periodic stimulus, such as sinusoidal or square-wave grating, contrast is conveniently expressed in terms of Michelson contrast:

$$c_{Michelson} = \frac{L_{max} - L_{min}}{L_{max} + L_{min}}, \tag{2.4}$$

where L_{max} and L_{min} are the maximum and minimum and luminances, respectively. Following the classical paper of Campbell and Robson (1968), Michelson contrast has

been widely used in the studies of grating detection. Campbell and Robson (1968) studied the detection and discrimination of sine, square, rectangular and saw-tooth gratings. They showed that contrast threshold for various waveforms (square, rectangular or saw-tooth gratings) over a wide range of spatial frequencies was determined by the amplitude (Michelson contrast) of the fundamental Fourier component of the waveform and that they were distinguished from a sinewave only when the higher harmonics reached their independent thresholds. It was suggested that the visual system behaves as a multiple channel detector comprising a range of relatively narrow-band detection filters each optimally tuned to detect a band of spatial frequencies in the Fourier space.

As equation (2.4) shows, Michelson contrast expresses contrast in terms of the maxima and minima in the stimulus. Therefore, for a given pair of L_{max} and L_{min} values Michelson contrast gets a constant value despite of the introduction of any number of intermediate luminances. This characteristic of Michelson contrast is problematic when the perception of non-periodic complex stimuli, such as compound gratings or random stimuli with random luminance distribution, is investigated. The perceived contrast of these non-periodic stimuli does not agree with the perceived contrast of simple gratings when their physical contrasts are expressed in terms of Michelson contrast (Quick & al., 1976; Mayhew & Frisby, 1978; Moulden & al., 1990; Tiippana & al., 1994). Instead, the perceived contrasts seem to match when their physical contrasts are expressed in terms of the luminance distribution of the stimulus rather than its peak values. A contrast measure that takes into account the luminance distribution of the stimulus is the root-mean-square i.e. r.m.s contrast. To obtain the r.m.s contrast of the stimulus, the squares of the local contrasts are averaged across the stimulus area. The square root of the average then provides the r.m.s contrast

$$c_{r.m.s.} = \left[\frac{1}{nm}\sum_{i=0}^{n-1}\sum_{j=0}^{m-1} c^2(i,j)\right]^{0.5} \qquad (2.5)$$

The local contrast c(i,j) is obtained by:

$$c(i,j) = \frac{L(i,j) - L_0}{L_0}, \qquad (2.6)$$

where L(i,j) is the local luminance and L_0 is the mean luminance of the screen. The r.m.s contrast is thus equal to the standard deviation of luminance distribution calculated pixel by pixel across the screen and divided by the average luminance. For simple cosine gratings, the r.m.s contrast is approximately equal to Michelson contrast divided by $\sqrt{2}$. The relationship between the r.m.s and Michelson contrasts of a cosine grating is described in detail in Appendix 2.

The usefulness of the r.m.s contrast as a descriptor of perceived suprathreshold contrast has been proved by Quick et al. (1976), Mayhew and Frisby (1978), and Tiippana et al. (1994), for example. They showed that the perceived contrasts of simple gratings and complex spatial stimuli are equal when their r.m.s contrasts are equal. Quick et al. (1976) adjusted the overall contrast of either the two-component grating or random-noise gratings (one-dimensional low-pass filtered static noise) with various bandwidths to match the perceived contrast of a simple grating. The compound gratings consisted two vertical gratings at spatial frequencies of either 4, 12 or 20 c/deg added in peaks-add or peaks-subtract phase. The random-noise gratings, on the other hand, contained all spatial frequencies up to the cut-off frequency which varied from approximately 1 to 20 c/deg. Contrast of the complex test stimulus and simple grating matched when their physical contrasts, expressed in terms of the r.m.s contrast, were equal. Quick et al. (1976) pointed out that their results were consistent both with multiple channels combined by a square-law summation mechanism or with a single channel model in which perceived contrast is directly proportional to the r.m.s contrast. Mayhew and Frisby (1978) came to the same conclusion in their study with band-pass filtered random textures. The spatial frequency of the band-pass filtered textures was kept approximately constant, but they contained either one orientation or two orthogonal orientations. The task of the subject was to find the best contrast match between a set of random textures comprising a single orientation and another set comprising two orthogonal orientations. The most frequent best match of perceived contrasts was obtained when the r.m.s contrasts of both standard and test stimuli were equal. In accordance, Tiippana et al. (1994) showed that the perceived contrast of gratings comprising 1-4 orientation components of the same

spatial frequency and phase and having different luminance distributions were equal when their physical r.m.s contrasts were equal. In addition, Moulden et al. (1990) demonstrated that the adaptive power of various random-dot stimuli is determined by the standard deviation of their luminances, that is by a measure proportional to the r.m.s contrast, rather than their luminance maxima and minima, which is proportional to Michelson contrast.

All the studies cited above suggest that r.m.s contrast is a better measure of perceived contrast for various spatial stimuli than Michelson contrast. Because this thesis investigates detection of both simple gratings and more complex spatial stimuli, one aim of this study was to test whether the above conclusion can also be extended to threshold vision.

Another contrast measure, contrast energy, was included mainly because it is used when the human detection performance is expressed in terms of detection efficiency (see Chapter 5 of this thesis). It is therefore important to understand the relationship between contrast energy and other more conventional contrast measures at threshold. Contrast energy is calculated by numerically integrating the square of the local contrast of signal [equation (2.6)] across the stimulus area:

$$E = \sum_{i=0}^{n-1} \sum_{j=0}^{m-1} c^2(i,j) p^2, \tag{2.7}$$

where p^2 is the pixel area.

The relationship between the r.m.s contrast and contrast energy is then given by

$$c_{r.m.s.} = \sqrt{\frac{E}{A}}, \tag{2.8}$$

where A is the stimulus area.

In order to compare the descriptive power of these contrast measures, the detection thresholds for simple cosine gratings and band-pass filtered random stimuli were

measured and expressed in terms of Michelson contrast, r.m.s contrast and contrast energy.

2.4.2 Methods

The experiments were carried out using Apparatus 1, which is introduced in detail in Section 2.1.1.

Stimuli

The stimuli consisted of one-dimensional simple cosine gratings and two-dimensional band-pass filtered random stimuli. The sharp-edged circular stimulus window was surrounded by an equiluminous field limited to a circular aperture of 20 cm a diameter by placing a black cardboard mask in front of the screen.

The random stimuli were produced by band-pass filtering a sample of two-dimensional white static noise. Noise was produced by adding a random number from an even distribution with zero mean to each pixel of 0.42x0.42 mm^2 in size. The Fourier transform of the basic stimulus was then band-pass filtered using a circularly symmetric log-Gaussian transfer function:

$$MTF(f_r) = e^{-\ln^2(f_r/f_c)/b^2\ln(2)}, \tag{2.9}$$

where f_r is the radial spatial frequency, and f_c is the radial centre frequency of the filter. The radial spatial frequency is given as $f = (f_x^2 + f_y^2)^{0.5}$, where f_x and f_y are the spatial frequencies along horizontal and vertical spatial frequency axes, respectively. When

$$MTF(f_r) = 1/2, \tag{2.10}$$

then

$$\frac{f_r}{f_c} = 2^b, \qquad (2.11)$$

which shows that b is the half-bandwidth at half height in octaves. The bandwidth of the band-pass filter was either 0.5 or 1 octaves, and its radial centre frequencies (f_c) were chosen to correspond to the spatial frequencies of the one-dimensional cosine gratings.

Detection thresholds were measured for stimuli with either a constant stimulus area or a constant number of grating cycles per stimulus window. For the stimuli with a constant stimulus area, the diameter of the circular stimulus window was 16 cm on the screen. Spatial frequencies varied between 0.0625 and 4 c/cm with 1 octave steps. From the viewing distance of 228 cm, the stimulus area in solid degrees was 12.7 deg^2, and the spatial frequency of the grating varied between 0.249 and 15.9 c/deg. The band-pass filter for the random stimuli had corresponding radial centre frequencies and the bandwidth of 1 octave.

The gratings with a constant number of cycles contained 12 cycles per stimulus diameter at all spatial frequencies. The number of cycles was kept constant by reducing the diameter of the circular stimulus field in proportion to increasing spatial frequency. The circular stimulus windows had diameters of 12, 8.75, 6, 4.29, and 3 cm on the screen and corresponding spatial frequencies of 1, 1.4, 2, 2.8, and 4 c/cm, respectively. From the viewing distances of 57.3 and 319 cm, the spatial frequencies ranged from 1 to 22.3 c/deg at approximately half an octave steps. An additional spatial frequency of 0.5 c/deg was obtained by using the stimulus diameter of 12 cm, spatial frequency of 1 c/cm and viewing distance of 28.6 cm. Corresponding stimulus areas and radial centre frequencies were used for band-pass filtering the random stimuli. The filter bandwidth was 0.5 octave.

Figure 2.4 shows an example of a one-dimensional vertical grating and the corresponding two-dimensional random stimulus used in the experiments. Both stimuli comprise 12 cycles across the circular stimulus window. For the two-dimensional band-pass filtered random stimulus the measure of cycles per stimulus diameter is based on the radial centre frequency of the band-pass filter.

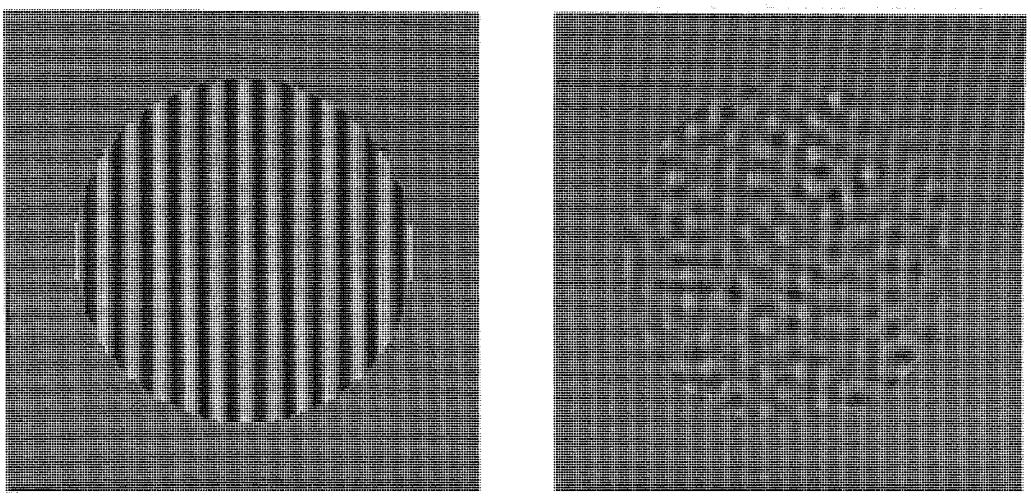

Figure 2.4
A simple one-dimensional cosine grating and a two-dimensional band-pass filtered random stimulus with a corresponding radial centre frequency of the filter.

The simple cosine grating and the complex random stimulus in Figure 2.4 have the same Michelson contrast. Figure 2.4 thus demonstrates the fact that the perceived contrasts of simple gratings and more complex stimuli comprising relatively more intermediate grey levels are not equal when their Michelson contrasts are equal.

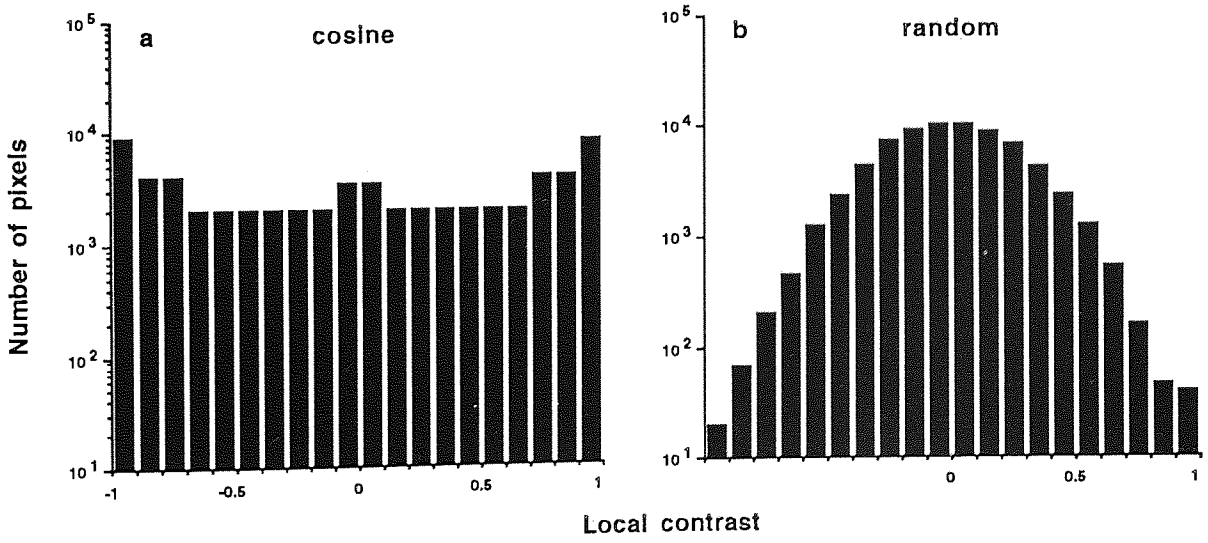

Figure 2.5
The contrast histogram for the simple cosine grating and the two-dimensional random stimuli of Figure 2.4.

Figure 2.5 shows the contrast signal histogram for the two stimuli presented in Figure 2.4. The local contrast, calculated according to equation (2.6), can get values from -1 to +1. The histogram shows the total number of pixels at each value of local contrasts within the stimulus area.

Procedures

Contrast sensitivity refers to the inverse of contrast at detection threshold. The thresholds were determined at the probability of 0.84 of correct responses using the forced-choice algorithm described in detail in Section 2.3.1. All data points are based on geometric means of at least three threshold estimates.

The two-interval forced-choice procedure was used. Each trial consisted of two exposures of 500 msec, only one of which contained the signal with non-zero contrast. Exposures were separated by 600 msec and accompanied by a sound signal to indicate the occurrence of exposures. The observer indicated which exposure contained the stimulus with non-zero contrast by pressing one of the two keys on a computer keyboard. An auditory feedback indicated the correctness of the response. A new trial began 250 msec after the observer's response. Between the two exposures and during the intertrial intervals the observer saw only the homogenous field having the mean luminance of the stimulus.

The experiments were performed in a dark room; the only light source was the display. A chin-rest was used to stabilise the head of the observer. No fixation point was used, but subjects were asked to fixate approximately at the centre of the stimulus. Viewing was binocular with natural pupils.

Subjects

Two subjects, aged 25 and 27 years, served as observers. KT was a corrected non-astigmatic myope (od. -6.00 DS / os. -4.00 DS) with binocular Snellen acuity of 1.5. HK was an uncorrected hyperope (+0.5 DS oa.) with binocular Snellen acuity of 1.5.

2.4.3 Results

In Figure 2.6 contrast sensitivity for simple cosine gratings and corresponding band-pass filtered random stimuli was expressed in terms of Michelson contrast. Contrast sensitivity was plotted as a function of the spatial frequency of the stimuli. The spatial frequency on a horizontal axis of Figure 2.6 corresponds to the nominal spatial frequency of the grating and the centre spatial frequency of the band-pass filtered random stimuli. Both gratings and random stimuli had either a constant stimulus area of 12.7 deg^2 or a constant number of 12 cycles per stimulus window as described above. Figure 2.6a shows the results for HK, and 2.6b for KT.

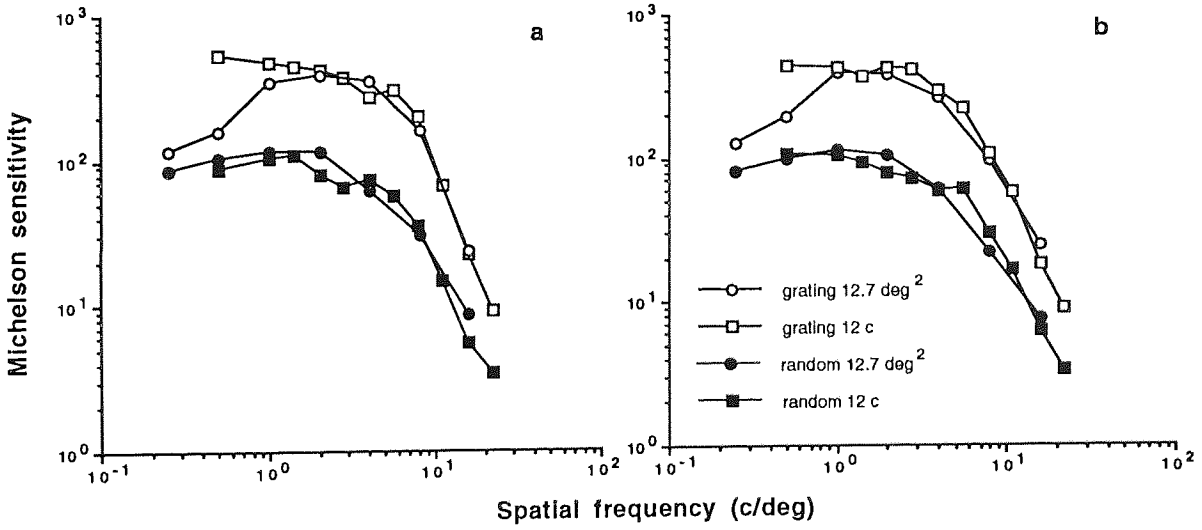

Figure 2.6
Contrast sensitivity for simple cosine gratings and complex band-pass filtered random stimuli expressed in terms of Michelson contrast.

As Figure 2.6 shows, Michelson contrast sensitivity was better for gratings than for random stimuli at all spatial frequencies and stimulus types. Michelson contrast sensitivity function for gratings with constant stimulus area had a familiar "inverted U" shape reaching its maximum at about 2 c/deg. At high spatial frequencies contrast sensitivity is mainly reduced by the point spread function of the ocular optics (e.g.

Campbell & Gubish, 1966; Deeley & al., 1991, Rovamo & al., 1994a). At low spatial frequencies the small number of grating cycles reduced contrast sensitivity (e.g. Hoekstra & al., 1974; Howell & Hess, 1978; Rovamo & al., 1993). For gratings with constant area of 12.7 deg^2 the number of visible cycles increased with spatial frequency. Consequently, contrast sensitivity increased up to the spatial frequency of approximately 1 c/deg, after which the contrast sensitivity function for the grating with constant stimulus area (12.7 deg^2) approximately followed the contrast sensitivity function for gratings with constant number of cycles (12 cycles) which had a low-pass shape without a decline at low spatial frequencies.

Michelson contrast sensitivity for random stimuli had a low-pass shape irrespective of whether stimulus area or the number of cycles was kept constant. The bandwidth of random stimuli was either 0.5 or 1 octaves. Hence, when the filter centre frequency was 0.25 or 0.5 c/deg, they were probably detected on the basis of their higher spatial frequencies. The low-pass shape of the contrast sensitivity function for random stimuli with a constant stimulus area agrees with experiments with square wave gratings (e.g. Campbell & Robson, 1968). Up to the spatial frequency of about 1 c/deg, contrast sensitivity for square-wave gratings is constant and clearly higher than contrast sensitivity for sinusoidal gratings of the corresponding spatial frequency. This suggests that at lower spatial frequencies the detection of the square-wave gratings is aided by their higher harmonics to which the visual system is more sensitive.

In Figure 2.7 contrast sensitivity for the cosine gratings and corresponding random stimuli was expressed in terms of r.m.s contrast and plotted again as a function of the spatial frequency of the stimulus. Other details were as in Figure 2.6.

For cosine gratings r.m.s contrast is in practice equal to Michelson contrast divided by $\sqrt{2}$. Thus, contrast sensitivity functions for gratings shown in Figure 2.6 were only shifted upwards by a factor of $\sqrt{2}$ without any change in shape. Neither was the shape of the contrast sensitivity function for random stimuli appreciably affected by the change in contrast metrics. However, the change from Michelson to r.m.s metrics resulted in an increase in contrast sensitivity by a factor of about four at all spatial frequencies for

the random stimuli. As a result, the difference in contrast sensitivities for one-dimensional simple gratings and two-dimensional random stimuli greatly reduced and the two functions almost superimposed.

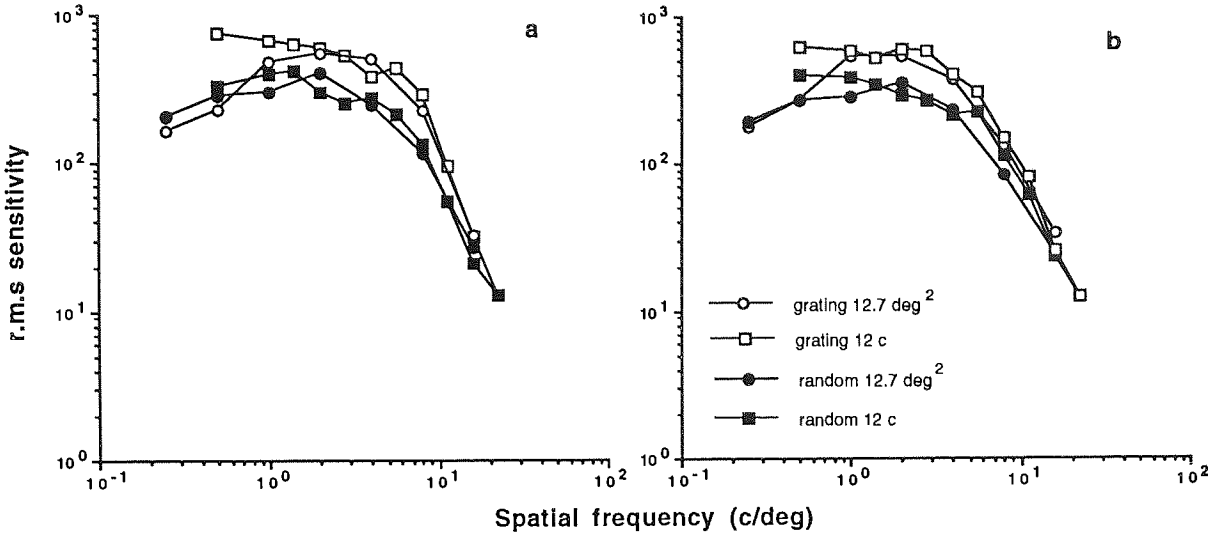

Figure 2.7
Contrast sensitivity for the simple cosine gratings and complex band-pass filtered random stimuli expressed in terms of r.m.s contrast.

The scrutinity of Figure 2.7 shows that there were some small systematic differences between thresholds, however. At low spatial frequencies ($\leq$ 1 c/deg) r.m.s contrast sensitivity was best for gratings having a constant number of cycles (12 cycles) per stimulus window. When spatial frequency increased, r.m.s contrast sensitivity became similar for both kinds of grating stimuli while it stayed slightly lower for random stimuli. This probably reflects differences in the spatial integration of simple gratings and complex stimuli, as will be discussed later on in Chapter 5. At the highest spatial frequencies ($\geq$ 10 c/deg), however, sensitivities became similar for all the stimuli used.

In Figure 2.8 contrast sensitivity for the cosine gratings and corresponding random stimuli was expressed in terms of contrast energy and plotted as a function of the spatial frequency of the stimulus. Other details were as in Figure 2.6.

Contrast energy for stimuli within a sharp-edged window can be calculated by multiplying the square of r.m.s contrast by stimulus area in deg^2. Therefore, contrast

energy sensitivity functions for gratings and random stimuli with constant stimulus area of 12.7 deg^2 shown in Figure 2.8 were identical in shape to their corresponding r.m.s contrast sensitivity functions in Figure 2.7. There was only a shift in the vertical direction resulting from squaring the r.m.s contrast sensitivity and division by the stimulus area.

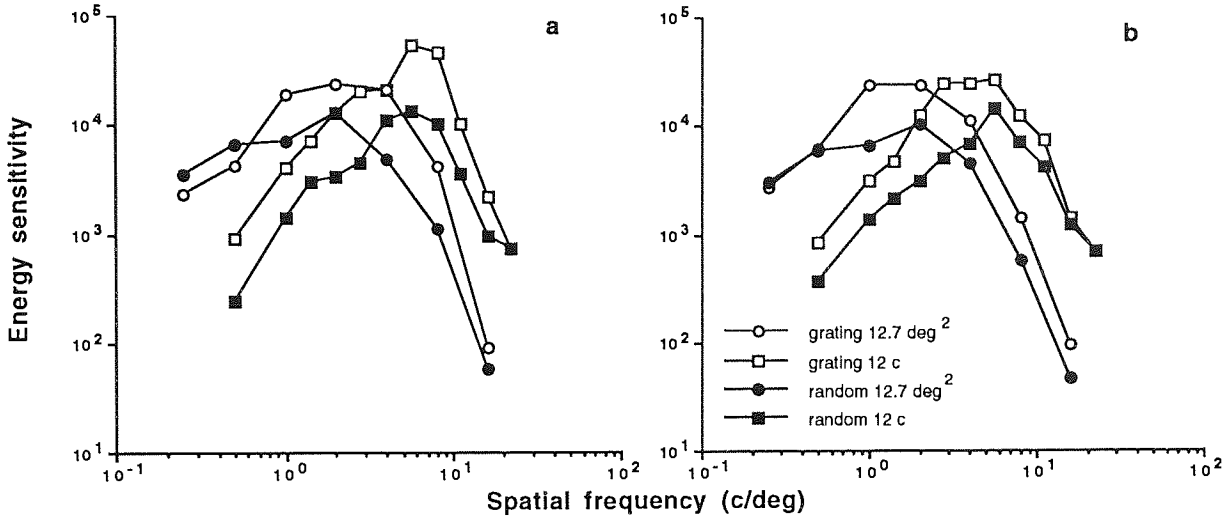

Figure 2.8
Contrast sensitivity for the simple cosine gratings and complex band-pass filtered random stimuli expressed in terms of contrast energy.

For both grating and random stimuli with constant number of cycles per stimulus window (12 cycles), the shape of the contrast energy sensitivity function was affected by the decrease of stimulus area with increasing spatial frequency. Therefore, in comparison with the shape of the r.m.s contrast sensitivity function in Figure 2.7, energy sensitivity was reduced by the large stimulus area at low spatial frequencies and increased by the small stimulus area at high spatial frequencies.

As Figure 2.8 shows, contrast energy sensitivities were better for stimuli with constant stimulus area (12.7 deg^2) at spatial frequencies <3 c/deg where the number of cycles per stimulus area was smaller than 12 cycles whereas the reverse happened at spatial frequencies >3 c/deg where there was more than 12 cycles per stimulus area. Contrast energy sensitivity functions measured with constant area and constant number

of cycles crossed each other at 3 c/deg, where the stimulus area in deg^2 of the visual field and the number of cycles per stimulus area were the same for both stimuli.

2.4.4 Discussion

The results obtained showed that, irrespective of the spatial frequency of the stimulus, Michelson contrast sensitivity is clearly higher for simple gratings than for narrow-band two-dimensional random stimuli. However, r.m.s contrast sensitivity was almost equal to gratings and random stimuli irrespective of the stimulus area. As contrast energy takes into account the area of the stimulus, the contrast energy sensitivity at each spatial frequency was better the smaller the stimulus area being, however, fairly independent of the stimulus structure (simple grating or complex random stimuli).

The result that r.m.s contrast sensitivity was equal for gratings and random stimuli is in agreement with the suprathreshold studies (Quick & al.,1976; Mayhew & Frisby, 1978; Moulden & al, 1990; Tiippana & al, 1994) which have shown that perceived contrasts of simple gratings and complex two-dimensional stimuli are equal when their r.m.s contrasts are equal. The same rule applies at threshold: the r.m.s contrast is a more generally applicable measure of contrast than Michelson contrast irrespective of whether the human visual performance is studied at or above threshold.

The finding that detection threshold for simple gratings and random stimuli was similar in terms of the r.m.s contrast provides an explanation for the finding that Michelson contrast sensitivity was better for gratings than random stimuli: The r.m.s contrast is proportional to the standard deviation of the stimulus luminance distribution whereas Michelson contrast is proportional to the total luminance range of the stimulus. As Figure 2.5 demonstrates the proportion of pixels with luminances close to the maximum or minimum luminance is greater in gratings than random stimuli. Therefore, to obtain the same standard deviation (i.e. r.m.s contrast) a smaller range (i.e. Michelson contrast) is needed in gratings than in random stimuli. In accordance, when cosine

gratings and random stimuli were both at threshold, their r.m.s contrasts were equal whereas the Michelson contrast was smaller for cosine gratings than for random stimuli. Consequently, Michelson contrast sensitivity was better for gratings than for random stimuli.

Contrast energy is a measure of contrast related to the r.m.s contrast. However, as contrast energy of the stimulus is affected by its area, the shape of the contrast energy sensitivity curve depends on the area of the stimulus. Therefore, contrast energy does not have one critical property of a contrast measure which is scale invariance, i.e. the independence of viewing distance, magnification or minification of the stimulus. This is important because contrast of a stimulus on the screen remains constant irrespective of the viewing distance. However, the value of contrast energy is affected by the viewing distance in the sense that when the viewing distance increases, the stimulus area decreases in terms of deg^2 of the visual field and thus causes a decrease in contrast energy. In order to be a contrast measure as good as other two contrast metrics, contrast energy should be made scale invariant by multiplying it by spatial frequency squared, for example.

Although contrast energy in its basic form is not a suitable measure of contrast it allows us to compare human visual performance with an ideal detector as will be explained in Chapter 5. Furthermore, as contrast energy is only affected by areas where local contrast differs from zero, its value does not depend on a pre-chosen stimulus area. This is an advantage over the r.m.s (and of course Michelson contrast), when the contrast of a stimulus with an uneven luminance distribution is described. In such cases, the value of the r.m.s contrast depends on the choice of the area across which it is calculated. When the local contrast of the stimulus decreases with increasing distance from the stimulus centre, as is the case, for example, in Gaussian weighted gratings, the r.m.s contrast decreases with increasing area. Therefore the form of the r.m.s contrast sensitivity function depends on the pre-chosen stimulus area.

In conclusion, the contrast metric chosen had a significant effect on the shape of the contrast sensitivity functions for different stimuli. There may be good reasons for

using any of the contrast measures discussed above: Michelson contrast is a useful descriptor for the modulation transfer function of a lens or a computer display, for example, whereas r.m.s contrast seems to be a more reliable measure for describing human detection performance. Contrast energy, which cannot be considered as a pure contrast metric due to its lack of scale invariance, is needed for definition of detection efficiency.

3. THE WHITENESS AND MASKING POTENCY OF PIXEL NOISE[1]

3.1 INTRODUCTION

This thesis concentrates on contrast detection in external spatial noise. Noise was produced on a computer display screen where any achromatic picture is drawn by defining a certain luminance for each square shaped picture element, pixel. It follows that spatial noise produced on a computer screen also consist of discrete picture elements, pixels, and can thus be called pixel noise. This chapter introduces the specific features of pixel noise based on general definitions of visual noise (e.g. Green & Swets, 1966; Pelli, 1981).

In spatial noise, the luminance value of a sample (e.g. pixel) varies randomly from one sample to another and the luminance values of neighbouring samples do not correlate. Whether noise is called one- or two-dimensional, depends on the spatial dimensions over which random luminance fluctuation takes place. Pixel noise is called static two-dimensional noise when each pixel has a random luminance value. If the luminance value of each sample or pixel fluctuates randomly in time, noise is spatio-temporal two-dimensional noise. In one-dimensional spatial noise, on the other hand, random luminance variation takes place only in one spatial dimension being constant in the other. Thus, in static one-dimensional pixel noise each row of pixels has a random luminance. Again, if the luminance of each row of pixels fluctuates randomly in time, pixel noise is called dynamic one-dimensional noise.

Figure 3.1 attempts to visualise the appearance of static pixel noise. On the left there is a field of static one-dimensional pixel noise and on the right a field of static two-dimensional pixel noise. Spatio-temporal two-dimensional noise, on the other hand, looks like "snow-fall" on a television screen, and Figure 3.1 thus shows only one frame of spatio-temporal two-dimensional pixel noise. Figure 3.1 should be viewed from some distance in order to avoid the distortion produced by halftoning in the printed images.

---

[1]Here pixel noise refers to spatial noise produced by generating a random luminance value for each pixel; not producing images which are coarsely sampled and quantized (See e.g. Harmon & Julesz, 1973).

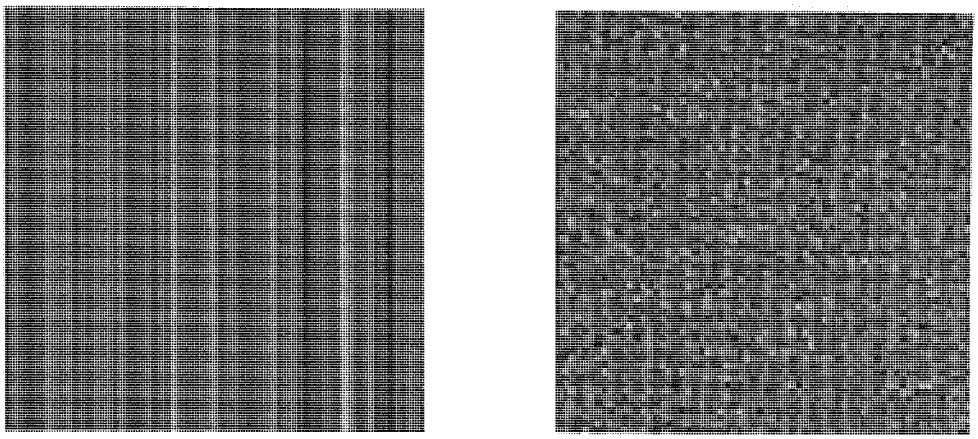

Figure 3.1
Examples of one- and two-dimensional static pixel noise.

3.1.1 The spectral density function of pixel noise

The masking effect of external image noise is described by the spectral density of noise at each spatial frequency, i.e. spectral density function. In theory, white visual noise means that its spectral density is constant at all spatial and temporal frequencies and it thus masks all spatial and temporal frequencies similarly. In spatial domain this is obtained when a noise field consist of infinitely small luminance samples whose value varies randomly from one sample to another. Therefore, in order to produce spatial white pixel noise the luminance value of each pixel should be uncorrelated and the size of the noise pixels should be infinitely small.

To understand the connection between sample size and noise bandwidth, it is helpful to consider the Fourier transform of an impulse stimulus: When the spatial size of an impulse stimulus is infinitely small, its Fourier transform has the same value at all spatial frequencies. A finite spatial extent, however small, results in a band-limited function in Fourier domain. It is impossible to produce an impulse stimulus of an infinitely small size, and it is equally impossible to realise an infinitely small pixel. Therefore, in practice pixel noise always has a limited bandwidth, which depends on the size of the

pixel, and pixel noise is white only at the spatial frequencies that are low in respect to the cut-off frequency.

The spectral density of pixel noise in one dimension is derived in Appendix 3. The spectral density function of static one-dimensional noise, where the luminance of each row of pixels gets a random value, is traditionally defined only in the direction of luminance modulation (e.g. Pelli, 1981; Legge & al., 1987). The spectral density function of one-dimensional pixel noise is thus given by:

$$N(f_x) = p_x c_n^2 [\frac{\sin(\pi f_x p_x)}{\pi f_x p_x}]^2, \tag{3.1}$$

where p_x is the noise pixel width in degrees of the visual field, c_n is the r.m.s contrast of noise, and f_x is the spatial frequency along the horizontal spatial frequency axis. How valid this definition is for describing the effects of one-dimensional pixel noise on the detection of one-dimensional gratings, will be investigated in Section 3.4 of this thesis.

The noise spectral density function for two-dimensional static pixel noise is a straightforward extension of the one-dimensional case and is given by

$$N(f_x, f_y) = p_x p_y c_n^2 [\frac{\sin(\pi f_x p_x)}{\pi f_x p_x}]^2 [\frac{\sin(\pi f_y p_y)}{\pi f_y p_y}]^2, \tag{3.2}$$

where p_x and p_y are the noise pixel width and height, and f_x and f_y are the spatial frequencies along the horizontal and vertical frequency axes, respectively.

According to equations (3.1) and (3.2), the spectral density function for pixel noise is first constant and then dies out oscillating. At the lowest spatial frequencies the latter part of equation (3.2) approximately equals to 1:

$$[\frac{\sin(\pi f_x p_x)}{\pi f_x p_x}]^2 [\frac{\sin(\pi f_y p_y)}{\pi f_y p_y}]^2 \approx 1 \tag{3.3}$$

At these low spatial frequencies, the noise spectral density thus gets a constant value, and pixel noise is by definition white. Therefore, the spectral density of white two-

dimensional pixel noise can be calculated with a sufficient accuracy as the product of the noise pixel area and the r.m.s. contrast of noise squared:

$$N_0 = c_n^2 p_x p_y \tag{3.4}$$

Accordingly, on the basis of equation (3.1), the spectral density of white one-dimensional pixel noise is calculated by multiplying the noise pixel width (in case of vertical one-dimensional noise) by the r.m.s contrast squared ($c_n^2 p_x$).

In order to define the cut-off frequency for white pixel noise i.e. the frequency where the spectral density function ceases of being flat, we can apply an approach introduced for spatial noise by Pelli (1981): Suppose a spatial noise, whose spectral density is constant up to a cut-off frequency (f_c) and zero beyond it. When the noise sample is scanned using circular sampling apertures of various areas, the aperture area multiplied by the r.m.s contrast of noise squared measured within the aperture (i.e. aperture-power product) is constant only for large apertures. The smallest diameter of the sampling aperture that still produces a constant aperture-power product is $1/(2f_c)$ i.e. half of the period of the cut-off frequency f_c. When this approach is applied to pixel noise so that its pixel size is considered to be the smallest aperture still producing a constant aperture-power product, the cut-off frequency f_c of underlying spatial noise is then given as follows:

$$\frac{1}{2f_c} = p \Rightarrow f_c = \frac{1}{2p}, \tag{3.5}$$

where p is a side length of the square shaped noise pixel. Along the horizontal ($f_y = 0$) and vertical ($f_x = 0$) frequency axes the spectral density of two-dimensional pixel noise, calculated by equation (3.2), has decreased to 40.5% of its maximum value. Along the oblique frequency axis ($f_x = f_y$) the spectral density of two-dimensional pixel noise with square shaped noise pixels has decreased to 16.4% of its maximum value.

3.1.2 The masking potency of white pixel noise

The noise spectral density function represents the mean power spectrum of a noise field. The actual power spectrum of a single noise field varies greatly because of the random luminance variation across pixels. In fact, the spectral density indicates the variance of the contrast of noise at each spatial frequency. The variance is reflected in the response of the detection mechanism at each spatial frequency as an uncertainty of the presence of the signal and it consequently leads to a reduction in detection performance. The greater the variance of the luminance of each noise pixel, the greater the spectral density of pixel noise at each spatial frequency, and consequently the poorer the performance of the detection mechanism. However, external image noise affects detection threshold only if its magnitude is great enough in comparison to other noise sources affecting the detection mechanism. When the spectral density of noise is great enough, the ratio between contrast energy at threshold and the spectral density of image noise is constant (e.g. Pelli, 1981; see Section 3.1.3).

Although several studies have shown that noise is collected only from a limited bandwidth (see Section 3.1.4), there is no single answer as to what this bandwidth is. Therefore, in order to simplify the definition of the masking effect of external noise, the assumption of whiteness of noise used for masking in a visual task is important because the spectral density of white noise is constant at all spatial frequencies. Consequently, the masking effect can be described by one number, the spectral density of noise, irrespective of the spatial frequency or the bandwidth of the detection mechanism, from which the noise is collected. We thus avoid making assumptions of the bandwidth of the detection filter used. On the other hand, external noise with a limited bandwidth can be used to determine the bandwidth of the detection mechanism for a particular task and stimulus (e.g. Stromeyer & Julesz, 1972; Pelli, 1981; see Section 3.1.4).

The spectral density of pixel noise gets a constant value only at low spatial frequencies, and pixel noise can be therefore called white only at these low spatial frequencies. The spectral density of white two-dimensional pixel noise is given by

equation (3.4) as the product of the r.m.s contrast of noise squared and the area of noise pixels ($c_n^2\ p_x\ p_y$). This means that both noise contrast and noise pixel size affect the spectral density and, consequently, masking potency of pixel noise at low spatial frequencies where noise can be considered as white.

Figure 3.2 demonstrates the effects of contrast and pixel size on the spectrum of two-dimensional pixel noise along the horizontal and vertical frequency axes. Along an oblique frequency axis spectral density decreases more rapidly. Spectral density functions for two-dimensional pixel noise in Figure 3.2 are calculated according to equation (3.2).

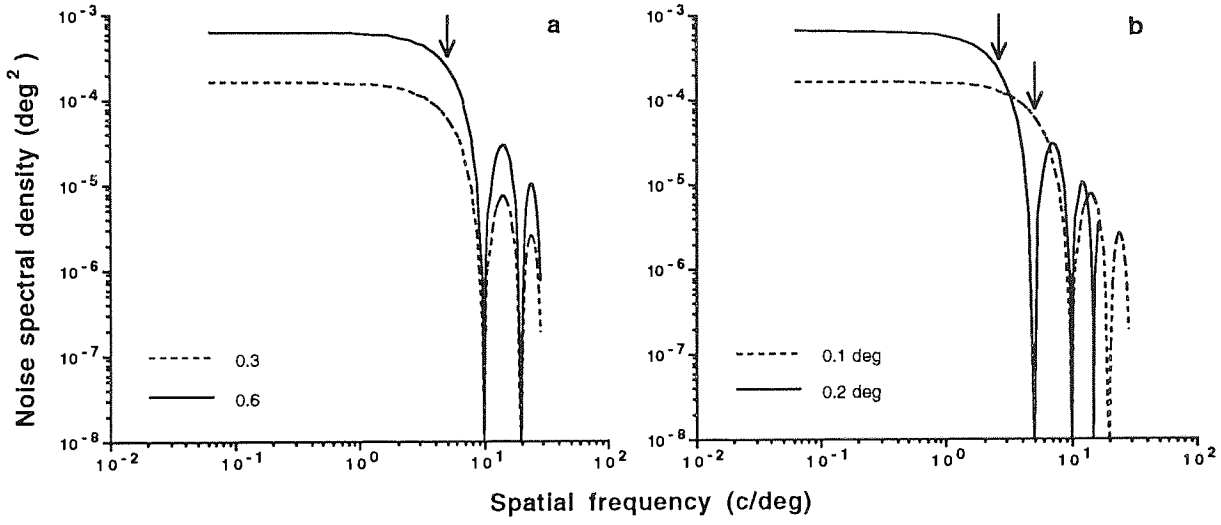

Figure 3.2
The effects of the r.m.s contrast of noise (a), and the size of the noise pixels (b) on the spectral density function of two-dimensional pixel noise.

Figure 3.2a shows the effect of noise contrast on the spectral density function. By doubling the r.m.s. contrast of noise from 0.3 to 0.6, its spectral density at low spatial frequencies is increased by four. Naturally, the increase in noise contrast does not affect the cut-off frequency of noise.

Figure 3.2b, on the other hand, demonstrates the effect of noise pixel size on the spectral density function. The side length of a square shaped noise pixel is doubled by increasing it from 0.1 to 0.2 degrees whereas noise contrast is kept constant at 0.3. As expected, the spectral density is increased by four at low spatial frequencies and the cut-off frequency of noise is halved due to the doubling of noise pixel side length. An increase

in the size of the noise pixels thus causes an increase in the spectral density at low spatial frequencies, where the spectrum is flat and the definition of white pixel noise applies.

3.1.3 Contrast detection in white external noise

The aim of the following literary review is to describe how white spatial noise limits contrast detection and provide some experimental evidence that at detection threshold the ratio between the signal contrast energy and the noise spectral density and, therefore signal-to-noise ratio is constant.

As noted above, the spectral density of external image noise has to exceed a certain value before it has any apparent effect on detection threshold. When the spectral density of external noise is increased from very low spectral densities, contrast energy threshold is first constant and only after certain value starts to increase in direct proportion to the spectral density of external noise (e.g. Nagaraja, 1964; Pelli, 1981, 1990; Luntinen & al., 1994). This result suggests that at low spectral densities of external noise, the masking caused by external image noise is too low in respect to the other noise sources affecting detection threshold. Therefore, detection threshold is not affected by external image noise, because its contribution is negligible.

Nagaraja (1964) studied the effect of increasing spectral density of external white noise on contrast detection threshold by using disk signals of various sizes. He measured detection threshold as a function of the spectral density of one-dimensional white noise at three luminance levels (0.03, 0.3, and 3.0 cd/m^2). When the spectral density of noise was increased, contrast detection threshold first stayed constant but then started to increase in proportion to increasing r.m.s contrast of noise, suggesting that signal-to-noise ratio is constant at threshold. On the other hand, the r.m.s contrast of external noise, at which the transition took place, depended on the luminance level: the lower the luminance the higher was the r.m.s contrast of external noise needed to make the contrast threshold proportional to the r.m.s contrast of external noise.

In agreement, Pelli (1981) measured detection thresholds for grating patches embedded in spatiotemporal two-dimensional white external noise with increasing spectral density of noise, and found that contrast threshold was first constant but then, beyond a critical value of noise spectral density, increased in proportion to the square-root of the spectral density of external noise. This critical spectral density of external noise was named as equivalent noise as it was considered to be equal to the internal neural noise in the visual system expressed in terms of the spectral density of external noise. In agreement with Nagaraja (1964), Pelli (1981) found that the equivalent noise, at which contrast energy threshold became proportional to the spectral density of external noise, was higher the lower the luminance levels.

Luntinen et al. (1994) measured detection thresholds for gratings at various spatial frequencies and grating areas as a function of the spectral density of white external noise. They used a constant luminance of 50 cd/m^2. They found that detection threshold was constant and independent of the spectral density of external noise up to a critical spectral density after which thresholds became proportional to the spectral density of external noise. According to their result, the critical spectral density of external spatial noise decreased with increasing spatial frequency up to 2 c/deg and started to increase after that. In accordance, Pelli (1990) who used two-dimensional spatio-temporal noise, showed that the equivalent noise level is higher at low spatial frequencies.

All the studies above suggest that, in addition to the external image noise, there are at least two other noise sources limiting detection threshold: one that is inherent to the visual system and the other which is introduced with decreasing luminance level, and therefore referred to as quantal or light-dependent noise. Because detection threshold at high levels of external noise becomes proportional to the square-root of the spectral density of external noise, we have good reasons to assume that threshold is always determined by constant signal-to-noise ratio irrespective of the noise source. Noise can be internal to the visual system, external light-dependent noise or external image noise added to the stimulus. The lower the luminance level the higher is the value of quantal noise (for details, see chapter 4) in respect to the internal neural noise. Therefore, at low luminance

levels contrast energy threshold is mainly determined by quantal noise unless the spectral density of external image noise is sufficiently high: the lower the luminance the higher is the spectral density of external noise needed to exceed the effect of quantal noise (e.g. Nagaraja, 1964; Pelli, 1981; Rovamo & al., 1994c). Consequently, at high luminance levels, the effect of internal neural noise dominates over the quantal noise. The magnitude of internal neural noise can be assumed to be constant over the spatial frequency range (i.e. internal noise is white). However, because the external image noise is filtered by optics of the eye and the neural transfer function that especially affect high and low spatial frequencies, the spectral density of external noise needed to exceed the effect of internal neural noise depends on the spatial frequency of the stimulus (e.g. Pelli, 1990; Luntinen & al., 1994).

When the experiments are performed in white external noise with spectral density high enough to exceed the effects of other noise sources, contrast energy thresholds become proportional to the spectral density of external image noise giving experimental evidence to the assumption that the signal-to-noise ratio is constant at detection threshold (Coltman & Anderson, 1960; van Meeteren & Boogaard, 1972; Stromeyer & Julesz, 1972; Chesters, 1973; van Meeteren & Valeton, 1988; Rovamo & al., 1992).

Chesters (1973) measured detection thresholds in the presence of white two-dimensional noise produced using magnified photographic granularity and showed that the detection thresholds for disk signal of various sizes increased in proportion to a square root of the power of external noise. Because the energy threshold is a squared contrast measure (see Chapter 2.4), the square-root relation between the spectral density of external noise and contrast threshold indicates constant signal-to-noise ratio.

For grating stimuli, the direct proportionality between the spectral density of external noise and contrast energy threshold has been demonstrated by van Meeteren and Boogaard (1972), Stromeyer and Julesz (1972), and van Meeteren and Valeton (1988), for example. Van Meeteren and Boogaard (1972) imitated photon noise by producing "speck-images" of sine-wave gratings, where speck density was modulated sinusoidally as a function of spatial dimension. The noise spectral density in such a case is inversely

proportional to speck density (Pelli, 1981). It follows, that when the number of specks per unit area increases, the noise spectral density decreases. Thus, when intensity of the specks is increased from moderate luminance levels, the number of visible specks increases and the noise spectral density consequently decreases. Van Meeteren and Boogaard (1972) showed, that at high speck intensities, where the detection of specks was not limited by photon noise, contrast sensitivity was proportional to the square root of speck-density. As contrast sensitivity squared is inversely related to the contrast energy at threshold and speck density is inversely related to the spectral density of noise, the result of Van Meeteren and Boogaard (1972) indicates that signal-to-noise ratio is constant at detection threshold.

Stromeyer and Julesz (1972) measured contrast thresholds for stationary sinusoidal gratings at spatial frequencies of 1.77, 5.0, and 10.0 c/deg embedded in spatio-temporal one-dimensional noise i.e. the luminance of each row of pixels fluctuated randomly in time. The spatial cut-off frequency of noise was 54 c/deg. The temporal frequency was 60 Hz (60 cycles/sec). Noise was thus considered as white for the stimuli used. They found that contrast sensitivity decreased in direct proportion to average noise contrast and signal-to-noise ratio thus stayed constant at threshold. In accordance, van Meeteren and Valeton (1988) showed that two-dimensional white pixel noise reduced contrast sensitivity measured without external noise similarly at spatial frequencies below 20 c/deg. At higher spatial frequencies contrast sensitivity was approximately similar for noise and no-noise condition. This result suggests that contrast threshold at spatial frequencies higher than 20 c/deg was in fact determined by the internal neural noise.

Another evidence for constant signal-to-noise ratio at threshold is provided by experiments measuring contrast threshold in external spatial noise as a function of viewing distance. Because the increase in viewing distance reduces similarly both the energy of the signal and the spectral density of the external noise, the physical signal-to-noise ratio stays constant as a function of viewing distance, which should keep detection threshold constant. Coltman and Anderson (1960) measured detection thresholds for sinusoidal gratings embedded in white noise presented on a television monitor. They

found out that detection threshold in external noise stayed almost constant when viewing distance increased from 0.5 to 7 meters. Similar result has recently been obtained by Rovamo et al. (1992), who studied the effect of viewing distance on contrast sensitivity both with and without noise. They showed that sensitivity to a grating stimulus stayed constant as a function of viewing distance, when contrast sensitivity was determined by external spatial noise i.e. sensitivity in spatial noise was lower than sensitivity measured without external image noise.

3.1.4 Detection threshold in non-white noise

The review above pointed out that signal-to-noise ratio is constant at detection threshold in white external noise whose spectral density is high enough to exceed the effect of other noise sources affecting detection. When the spectral density of external noise is kept high, and its cut-off frequency is varied, one can find out how different spatial frequency components of noise affect the detection threshold of a spatial stimulus, what is the critical bandwidth across which noise is collected by the visual system, and how the bandwidth depends on the spatial characteristics of the stimulus (e.g. Carter & Henning, 1971; Stromeyer & Julesz, 1972; Harmon & Julesz, 1973; Chesters, 1973; Pelli, 1981; Henning, Hertz & Hinton, 1981; van Meeteren & Valeton, 1988).

Carter and Henning (1971) measured detection thresholds for grating stimuli consisting of either one or 160 cycles per stimulus window, i.e. stimulus had either a broad or narrow spectral bandwidth. Detection thresholds were measured in the presence of strong narrow- or broad-band one-dimensional dynamic noise. They found that in the presence of broad-band noise detection thresholds did not differ much for broad and narrow band stimulus, respectively. When only narrow-band noise was used, detection threshold was lower for broad-band stimulus than for narrow-band stimulus. The narrow-band noise alone thus masked better the grating with a narrow spectral bandwidth. This demonstrates the fact that the spectral bandwidth of the stimulus affects the effective

bandwidth of the spatial noise.

Stromeyer and Julesz (1972) measured detection thresholds for gratings embedded in high- and low-pass filtered one-dimensional spatio-temporal noise, and in one-dimensional spatio-temporal noise which was centred at the spatial frequency of the stimulus, but whose band-width varied. Spatial frequencies ranged from 2.5 to 10 c/deg within a constant stimulus field of 2.5 deg width and 1 deg height. The masking produced by both low- and high-pass filtered noise decreases as the cut-off frequency of noise moved away from the spatial frequency of the stimulus. The masking effect decreased symmetrically around the spatial frequency of the stimulus to one-half of its maximum when the noise cut-off was moved ± 0.5 - ± 0.75 octaves away from the grating frequency. When the band-pass filtered noise was centred on the spatial frequency of the stimulus with a constant spatial frequency bandwidth, and the bandwidth of the noise was increased, masking increased as the band of noise widened, up to a critical bandwidth of about ± 1 octave, and did not increase further when the band was widened beyond this range. Stromeyer and Julesz (1972) did not study the effect of stimulus bandwidth on the critical bandwidth of noise.

Henning et al. (1981) used both static and dynamic one-dimensional noise which were spatially either low- or high-pass filtered. The cut-off frequency of noise was increased or decreased until it was equal to the spatial frequency of the grating. As the cut-off frequency of noise approached the stimulus spatial frequency, detection thresholds increased. In static noise, the increase in threshold was asymmetrical around the spatial frequency of the stimulus having a steeper slope at spatial frequencies below the stimulus frequency when plotted in a logarithmic coordinates. However, when the experiments were repeated in dynamic noise, the increase in threshold became symmetrical around the spatial frequency of the stimulus, in agreement to Stromeyer and Julesz (1972).

Similarly, Pelli (1981) investigated the effects of spatially low-, high-, and band-pass filtered one-dimensional dynamic noise on the detectability of grating stimuli (2.5-4 c/deg). In agreement with Stromeyer and Julesz (1972), Pelli (1981) found that squared threshold rose in proportion to the spatial frequency bandwidth of narrowband noise

centred to the spatial frequency of the stimulus, up to the critical bandwidth of ± 1 octaves. Approximately similar approximation of the critical bandwidths were found, when detection thresholds were measured as a function of the cut-off frequency of either low- or high-pass spatial noise. However, Pelli pointed out that the masking effect of the three different noise conditions were not consistent with the idea that a single channel was used for detection in all conditions. Instead, on the basis of the masking effect of noise, Pelli (1981) suggested that the observer might learn to use off-frequency looking in order to improve his detection performance when noise contained frequencies only below or above the spatial frequency of the stimulus.

Van Meeteren and Valeton (1988), on the other hand, studied detection of grating stimuli at 1-50 c/deg embedded in fine, medium and coarse grain noise. The number of cycles varied with spatial frequency from 1-50 cycles per grating area. Fine noise represented white noise in their experiment whereas medium and coarse noise were low-pass filtered with cut-off frequencies of about 20 and 5.0 c/deg. As expected, they found that coarse noise masked only low spatial frequencies and sensitivity at high spatial frequencies in the presence of coarse noise was almost equal to contrast sensitivity measured without noise. Furthermore, their result showed that changing from fine noise to medium noise, the removal of high-frequency noise components reduced contrast sensitivities at medium and high (5-20 c/deg) spatial frequencies, but did not change the contrast sensitivity at low spatial frequencies. In their experiment, the spectral density of spatial noise at low spatial frequencies, where the noise was white, increased as the cut-off frequency decreased. This caused the decrease in contrast sensitivity at medium and high but not at low spatial frequencies when the fine grain noise was changed to medium grain noise. Hence, it is probable that at low spatial frequencies, where the effect of internal noise is high (e.g. Luntinen & al., 1994), the magnitude of the fine and medium grain noise was not high enough to exceed the effect of internal noise and thresholds at low spatial frequencies were thus approximately similar in fine-, medium- and no-noise conditions.

Although Carter and Henning (1971) found that the critical bandwidth for noise

depends on the bandwidth of the stimulus i.e. number of grating bars, the other studies attempting to find the critical bandwidth did not control the stimulus bandwidth together with the spatial frequency. The results of Stromeyer and Julesz (1972), Henning et al. (1981) and Pelli (1981) suggest that the critical bandwidth is ± 1 octaves around the spatial frequency of the stimulus for a variety of stimulus frequencies and bandwidths. However, as Pelli (1981) pointed out, the estimation of bandwidth and/or the centre frequency of the detection filter actually depends also on the characteristics of noise, that is whether the noise is high- or low-pass filtered. Pelli (1981) suggested that a detection mechanism with a constant stimulus bandwidth combined with the ability of off-frequency looking could explain the differences in estimations of bandwidth found in his study.

The experiments of this chapter attempt to expand the existing knowledge of the effects of grating bandwidth on the critical bandwidth of the detection filter. In addition, as the cut-off frequency of pixel noise decreases in proportion to the size of the noise pixels, it is important to know how well the theoretical and empirical cut-off frequency of pixel noise agree. Therefore, in order to study how near to the nominal spatial frequency of the stimulus the cut-off frequency of noise can decrease and still mimic the effect of white noise, the following experiments test the effect of the noise pixel size and shape, and noise contrast on the detection threshold for vertical and circular gratings having various spatial frequencies and bandwidths. Two main questions were thus addressed: what is the largest noise pixel size that still mimics the effect of white noise in the visual system, and how this value depends on the characteristics of the stimulus, such as bandwidth, i.e. when can we assume that pixel noise used for masking the detection of a spatial pattern is white for the visual system?

3.2 THE CRITICAL SIZE OF NOISE PIXELS

As the above literary review showed, detection threshold is determined by the external image noise only when its effect exceeds the effect of other noise sources affecting detection threshold, such as internal neural noise (e.g. Watson, Barlow & Robson, 1983; Pelli, 1990; Luntinen & al., 1994) in bright light and quantal or light dependent noise in dim light (e.g. Nagaraja, 1964; Pelli, 1990; Rovamo & al, 1994c). Therefore, in certain conditions, e.g. when detection thresholds in noise are measured at high or low spatial frequencies (Luntinen & al., 1994) or in dim light (e.g. Rovamo & al., 1994c), fairly high spectral densities of external noise are needed in order to exceed the effect of other noise sources.

The spectral density of pixel noise can be increased by increasing the r.m.s contrast of external noise and/or the size of noise pixels (See Section 3.1.2). Increasing the r.m.s contrast of noise is a safe method, because it increases the spectral density of noise without affecting the spatial frequency range where noise is white. However, in any experimental apparatus the maximum contrast available is 1. When the effect of external noise on contrast detection is investigated, the maximum contrast has to be suitably shared between the stimulus (to be detectable when embedded in external noise) and the spatial noise (to exceed the other noise sources affecting detection). Therefore, it might be necessary to increase the spectral density of pixel noise further by increasing the size of noise pixels.

When the spectral density of pixel noise is increased by increasing the size of noise pixels, the cut-off frequency of noise decreases and thus the spatial frequency range where noise can be considered white is reduced. However, according to studies introduced in Section 3.1.4, the magnitude of the effect of spatial noise on grating detection is determined by its spectral density within the spatial frequency range of the stimulus or rather, within the spatial frequency range of the detection filter used for perceiving the stimulus (e.g. Carter & Henning, 1971; Stromeyer & Julesz, 1972; Pelli, 1981; Henning & al., 1981; van Meeteren & Valeton, 1988). Therefore, the spectral

density of pixel noise can be increased without compromising the whiteness of pixel noise by increasing the size of noise pixels as long as the cut-off frequency of noise is high in respect to the spatial frequency of the stimulus.

The question therefore arises as to what is the largest noise pixel size that still mimics the effect of white noise in grating detection and how this value depends on stimulus bandwidth. Gratings of various areas and spatial frequencies were embedded in pixel noise and the size of noise pixels was increased. The cut-off frequency of pixel noise thus decreased with increasing size of noise pixels first reaching and then even going below the spatial frequency of the grating. Two-dimensional pixel noise was considered to mimic the effect of white noise when contrast energy threshold was directly proportional to the noise spectral density of white pixel noise, calculated by multiplying the r.m.s contrast of noise by pixel area [see equation (3.4)].

3.2.1 Methods

The experiments were carried out using the Apparatus 1 introduced in Chapter 2. Chapter 2 also gives details about stimulus generation and threshold determination.

Stimuli

The stimuli consisted of vertical cosine gratings within a sharp-edged square window, the size of which varied between 1.3 x 1.3 cm^2 to 16 x 16 cm^2. The stimulus window was surrounded by an equiluminous field, which was limited to a 20 x 20 cm^2 square by placing a black cardboard mask in front of the screen. Spatial frequencies varied between 0.75 and 4.0 c/cm on the screen. The viewing distances of 43 to 458 cm resulted in spatial frequencies of 1.5, 3.0 and 6.0 c/deg.

Stimuli were embedded in two-dimensional pixel noise, which was produced by

adding to each noise pixel within the grating area a random number drawn independently from a Gaussian distribution. The Gaussian distribution of random numbers had a zero mean and it was truncated at ± 2.5 times the standard deviation.

Each noise pixel consisted of n x n image pixels. The side length of the square shaped noise pixel (p_n) varied from 1 to 64 image pixels. The luminances of the neighbouring noise pixels were uncorrelated. Thus, noise was white at low spatial frequencies having a cut-off frequency at a spatial frequency of $1/2p_n$ as described in Section 3.1.1.

The noise spectral density was defined as a product of the r.m.s contrast of noise squared (c_n) and the noise pixel area (p_n^2): $N_e = c_n^2 p_n^2$, where r.m.s contrast is the standard deviation of the local contrasts of noise. This formula describes the noise spectral density within the low spatial frequencies where the spectral density function of noise is flat (See Section 3.1.2) and noise can thus be called white. The spectral density of noise either increased due to increasing r.m.s contrast of noise or the increasing size of noise pixels, or it was kept constant by reducing the r.m.s contrast of noise squared in inverse proportion to increasing area of noise pixels.

Each trial comprised one exposure with signal-plus-noise and one with noise only. For the grating-plus-noise exposure, five different noise samples were computed for each contrast level of the grating. One of them was chosen randomly for each exposure. The total of 20 contrast levels, i.e. 100 signal plus noise samples, was used for each threshold estimation. For the noise only exposure, one noise sample from a set of 20 samples was chosen randomly for each trial.

Procedure

The contrast energy thresholds (See Section 2.4) were determined at the probability level of 0.84 of correct responses using a forced-choice algorithm described in detail in Section 2.3.1. All data points are based on geometric means of at least three

threshold estimates.

The two-interval forced-choice procedure was used. Each trial consisted of two exposures (signal plus noise or noise only exposure) of 500 msec, separated by 600 msec and accompanied by a sound signal to indicate the occurrence of exposure. The observer indicated which noise exposure contained the grating by pressing one of the two keys on a computer keyboard. An auditory feedback was given to the observer about the incorrectness of the response. A new trial began 250 msec after the observer's response. Between the two exposures and during the intertrial intervals the observer saw only the homogenous field having the mean luminance of the stimulus.

The experiments were performed in a dark room; the only light source was the display. A chin-rest was used to stabilise the head of the observer. No fixation point was used, but subjects were asked to look approximately at the centre of the stimulus. Viewing was binocular with natural pupils.

Subjects

Four subjects, aged 25, 27, 28, and 30 years, served as observers. KT was a corrected non-astigmatic myope (od. -6.00 DS / os. -4.00 DS) with binocular Snellen acuity of 1.5. OU was a corrected non-astigmatic anisotrope (od. +0.75 DS / os. -0.75 DS) with binocular Snellen acuity of 1.5. HK was an uncorrected hyperope (+0.5 DS oa.) with binocular Snellen acuity of 1.5. JM was a corrected astigmatic myope (od. -1.5 DS / os. -0.50/-0.50 x 180) with binocular Snellen acuity of 1.7.

3.2.2 Results

Figure 3.3 presents the results of an experiment, where the pixel size of two-dimensional noise was kept constant at 1 x 1 image pixel but the noise spectral density

was increased from 9.62 x 10^{-9} to 3.94 x 10^{-5} deg^2 by increasing the r.m.s contrast of noise. Contrast energy thresholds were plotted as a function of the r.m.s contrast of noise. The spatial frequency of cosine grating was 1.5 c/deg in Figure 3.3a and 6 c/deg in Figure 3.3b. The area of the grating was constant at 15.8 deg^2 resulting in either 6 (Figure 3.3a) or 24 (Figure 3.3b) cycles per stimulus width.

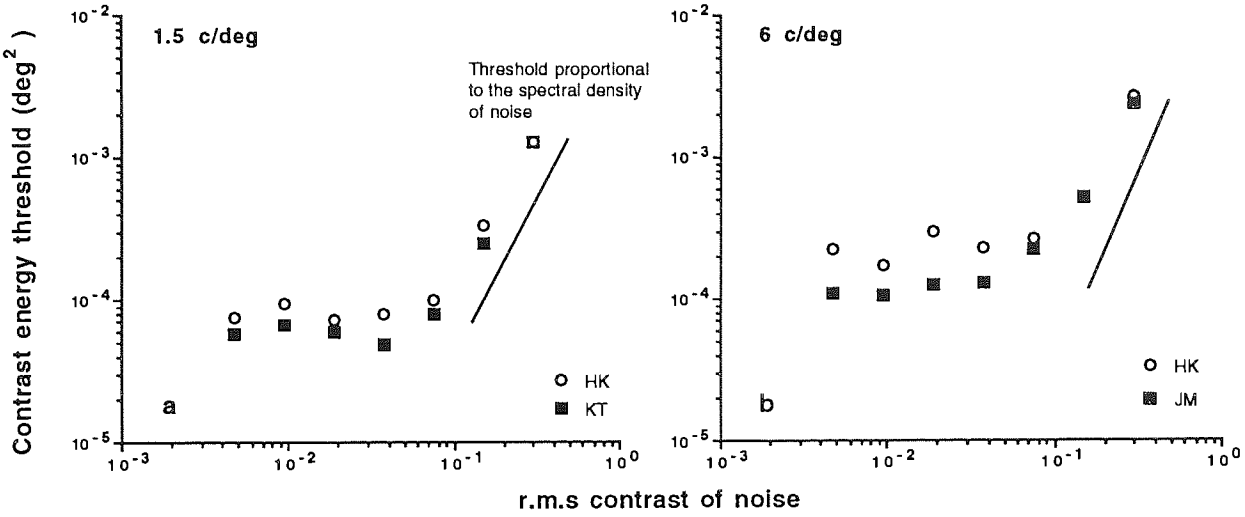

Figure 3.3
Contrast energy thresholds for cosine gratings embedded in white pixel noise as a function of the r.m.s contrast of noise. Subjects as indicated.

As expected, contrast energy threshold was first constant and equal to the threshold measured without external noise, but then it increased in proportion to increasing noise contrast. Detection thresholds remained constant and similar to threshold measured without spatial noise, when the r.m.s contrast of the pixel noise was low. This means that the effect of internal neural noise was greater than the effect of external spatial noise and thresholds were determined by internal neural noise. At high noise contrast levels contrast energy threshold increased with a slope of 2 in double-logarithmic coordinates. Contrast energy threshold thus increased in direct proportion to the spectral density of external noise calculated as a product of noise pixel area and squared r.m.s contrast of noise.

In Figure 3.4 binocular contrast energy thresholds were measured in two-dimensional pixel noise as a function of the increasing size of square shaped noise pixels.

Noise contrast was constant at 0.35, but the area of square shaped noise pixels increased from 1 x 1 to 64 x 64 image pixels. The spectral density of noise, calculated according to equation (3.4), thus increased with increasing noise pixel size from 3.38×10^{-6} to 0.221 deg^2 in Figure 3.4a and from 2.40×10^{-5} to 1.57 deg^2 in Figure 3.4b. Spatial frequencies of 1.5, 3 and 6 c/deg were obtained from viewing distances of 115, 229 and 458 cm in Figure 3.4a and 43, 86 and 172 cm in Figure 3.4b. Gratings contained either 4 or 16 cycles, as indicated in the graphs, corresponding to the bandwidths of 0.43 and 0.11 octaves at the half height across the Fourier spectrum of the stimuli.

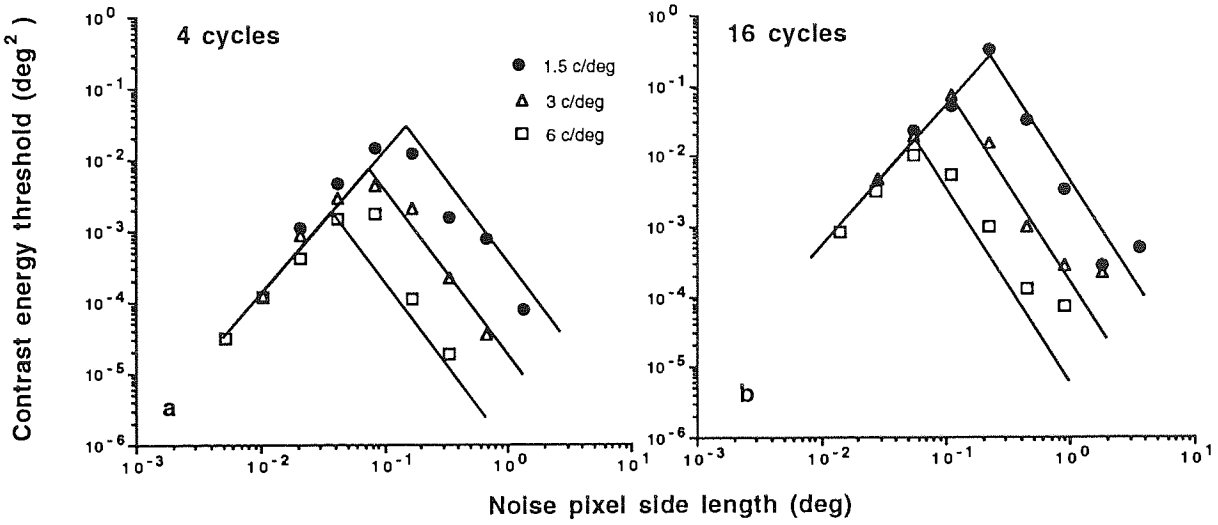

Figure 3.4
Contrast energy thresholds for cosine gratings embedded in pixel noise. The spectral density of noise was increased by increasing the size of the noise pixels. Subject was KT at 3 c/deg in Figure 3.4a and at 1.5 c/deg in Figure 3.4b, but HK in the other conditions.

As Figure 3.4 shows, contrast energy thresholds first increased and then decreased with increasing noise pixel side length at all spatial frequencies. During the increase contrast energy thresholds were similar for all spatial frequencies. However, the decrease started earlier the higher the spatial frequency of the grating.

In double logarithmic coordinates, the slope of increase in contrast energy threshold was +2. Contrast energy threshold thus increased in direct proportion to the noise spectral density calculated as the product of noise pixel area and the r.m.s contrast of noise squared. The decrease of contrast threshold was parallel at all spatial frequencies. The decrease of threshold indicates that the noise cut-off frequency had become too low

in respect to the spatial frequency of the stimulus, resulting in a decrease of the average spectral density of pixel noise in the vicinity of the spatial frequency of the grating used. Therefore, the spectral density of white pixel noise, calculated by equation (3.4), no more determined the threshold for grating detection.

The side length of the square-shaped noise pixel, where the transition from increase to decrease in contrast energy threshold occurred, is here called a critical noise pixel side length and it is marked by the intersection of the rising and declining least squares lines, which were fitted to the whole data set in each frame: contrast energy thresholds (E) were first expressed in terms of cm^2 on the screen and plotted as a function of the side length of noise pixels (P) also expressed in terms of cm on the screen. When plotted this way, the data for the three spatial frequencies superimposed at all noise pixel side lengths. A least squares line of the form $\log E = 2\log P + k$ was fitted to the increasing part of the data with the slope of $+2$ in double logarithmic coordinates. Another least squares line of the form $\log E = a \log P + b$ was fitted to the decreasing part of the data. The solid lines in Figure 3.4 were then obtained by again expressing contrast energy thresholds in deg^2 and pixel side length in deg of the visual field.

For gratings with 4 cycles the critical noise pixel side length, where the transition from increase to decrease in contrast energy threshold occurred, increased from 0.038 to 0.15 deg when spatial frequency decreased from 6 to 1.5 c/deg whereas for the gratings with 16 cycles the critical noise pixel side length increased from 0.057 to 0.23 deg. The critical noise pixel side length was thus inversely proportional to the spatial frequency of the grating. As a result, the critical number of noise pixel per grating cycle, calculated by dividing the length of the grating period by the critical noise pixel side length, was constant at 4.4 noise pixels per grating cycle for the grating comprising 4 cycles, and at 2.9 noise pixels per grating cycle for the grating comprising 16 cycles, irrespective of spatial frequency. Accordingly, the theoretical cut-off frequency of noise corresponding to the critical noise pixel size $f_c = 1 / 2p_c$ (See Section 3.1.1 for details) was 2.2 and 1.5 times higher than the spatial frequency of the grating consisting of 4 and 16 cycles, respectively.

The result of Figure 3.4a is demonstrated in Figure 3.5 which shows examples of a grating consisting of 4 cycles embedded in pixel noise. The size of the noise pixels is 1x1 and 8x8 image pixels in the top and bottom frame of the left column, and 64x64 image pixels on the right. The r.m.s contrasts of both grating and noise are constant in all frames.

Figure 3.5 shows that when the size of the noise pixels increases from 1x1 to 8x8 image pixels, the masking effect of pixel noise increases with increasing spectral density of noise. At the noise pixel size of 8x8 image pixels the number of noise pixels per grating cycle is 4 i.e. approximately equal to the critical number of noise pixels per grating cycle for a grating comprising 4 cycles. When the size of the noise pixels further increases to 64x64 image pixels, the number of noise pixels per grating cycle decreases to 0.5 i.e. below the critical number. Then the grating becomes visible inside each noise pixel, and the masking effect of noise decreases.

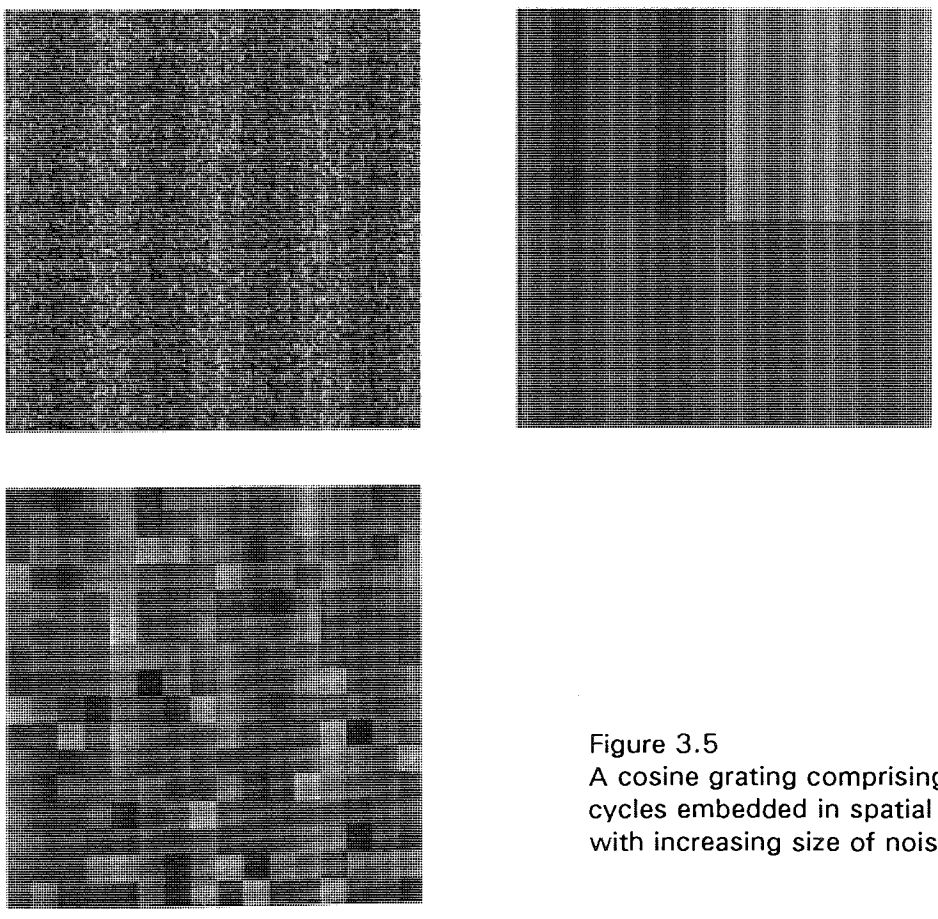

Figure 3.5
A cosine grating comprising 4 cycles embedded in spatial noise with increasing size of noise pixels.

In Figure 3.6 contrast energy thresholds in two-dimensional pixel noise were again measured as a function of noise pixel side length. However, the spectral density of noise was now kept constant at those spatial frequencies where the spectrum of noise is flat by reducing the r.m.s contrast of noise in proportion to increasing noise pixel side length. The noise spectral density was 21.5, 5.41, and 1.35 x 10^{-5} deg^2 in Figure 3.6a and 38.4, 9.61, and 2.40 x 10^{-5} deg^2 in Figure 3.6b at spatial frequencies of 1.5, 3, and 6 c/deg, respectively. In other respects the stimuli used were as in Figure 3.4.

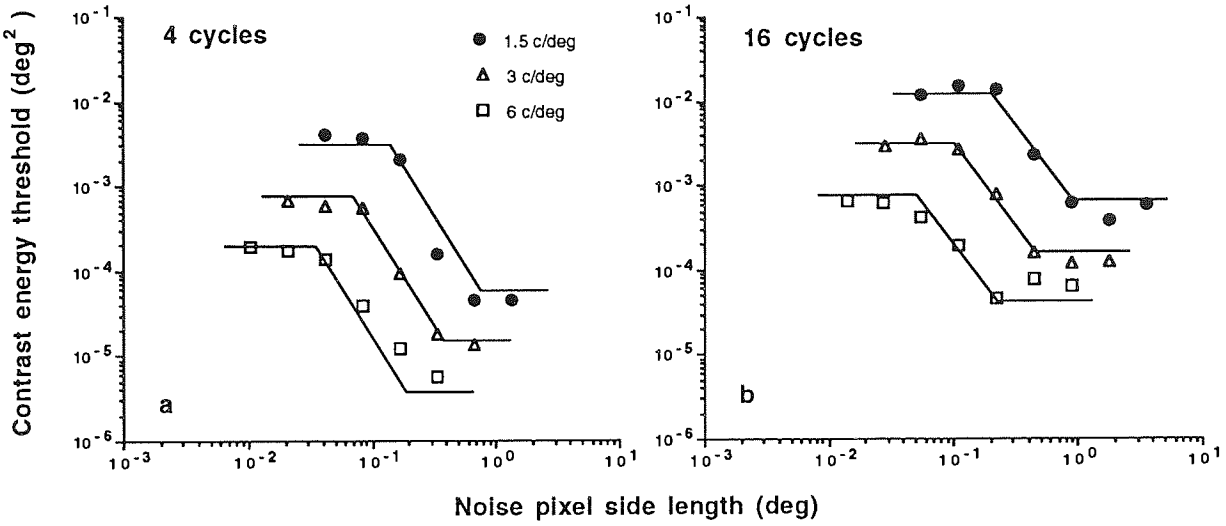

Figure 3.6
Contrast energy thresholds for cosine gratings embedded in pixel noise with increasing size of noise pixels. The spectral density of noise was kept constant by reducing the r.m.s contrast of noise in proportion to increase in pixel side length. Subject was KT at 3 c/deg in Figure 3.6a and at 1.5 c/deg in Figure 3.6b, but HK in the other conditions.

As Figure 3.6 shows, constant noise spectral density first kept contrast energy thresholds constant at all spatial frequencies studied. However, contrast thresholds were constant only up to the critical noise pixel side length. Thereafter contrast thresholds decreased with increasing noise pixel side length until they hit the floor determined by the contrast energy threshold without noise where the detection performance is limited by internal neural noise.

The critical noise pixel side length now refers to the transition from the constant contrast energy threshold to the decrease in threshold, and is marked by an intersection between the upper horizontal and decreasing solid lines. The solid lines were fitted to the

whole set of data in each frame in a similar way as in Figure 3.4: When contrast energy thresholds (E) in cm^2 on the screen were plotted as a function of the side length of noise pixels (P) in cm on the screen, the data for three spatial frequencies superimposed. Horizontal lines correspond to the respective averages of the upper and lower horizontal parts of the data in each frame. Least squares lines of the form $\log E = a \log P + b$ were fitted to the decreasing part of the data. The solid lines in Figure 3.6 were obtained by expressing contrast energy thresholds in deg^2 and pixel side lengths in deg of the visual field.

In agreement to the experiment above, the critical noise pixel side length increased when spatial frequency decreased from 6 to 1.5 c/deg. The critical noise pixel size increased from 0.035 to 0.14 deg for gratings comprising 4 cycles and from 0.052 to 0.21 deg for gratings comprising 16 cycles. The critical number of noise pixels per grating cycle was 4.8 for the grating consisting of 4 cycles and 3.2 for the grating consisting of 16 cycles. The theoretical cut-off frequency of noise corresponding to the critical pixel size $f_c = 1 / 2p_c$ (See Section 3.1.1 for details) was thus 2.4 and 1.6 times higher than the spatial frequency of the grating consisting of 4 and 16 cycles, respectively.

According to the results of Figures 3.4 and 3.6, the critical number of noise pixels per grating cycle was independent of spatial frequency and only depended on the bandwidth of the stimulus - the critical number of noise pixels was smaller the narrower the stimulus bandwidth. In order to test a larger range of grating bandwidths, the experiments of Figure 3.4 were repeated in Figure 3.7 by using gratings at 3 c/deg consisting of 1 and 64 cycles within the square-shaped stimulus area. The corresponding bandwidths were 1.56 and 0.03 octaves at half height across the Fourier spectrum of the stimuli.

The r.m.s contrast of noise was constant at 0.30 and the area of the noise pixels increased from 1x1 to 16x16 image pixels. The gratings consisting of 1 and 64 cycles were obtained using spatial frequencies of 0.77 and 4.0 c/cm at the viewing distances of 223 and 43 cm, respectively. The noise spectral density, calculated by multiplying the noise pixel area with the r.m.s contrast of noise squared , varied from 0.105 to

26.8 x 10^{-4} deg^2 and from 0.282 to 72.1 x 10^{-3} deg^2 for the gratings of 1 and 64 cycles.

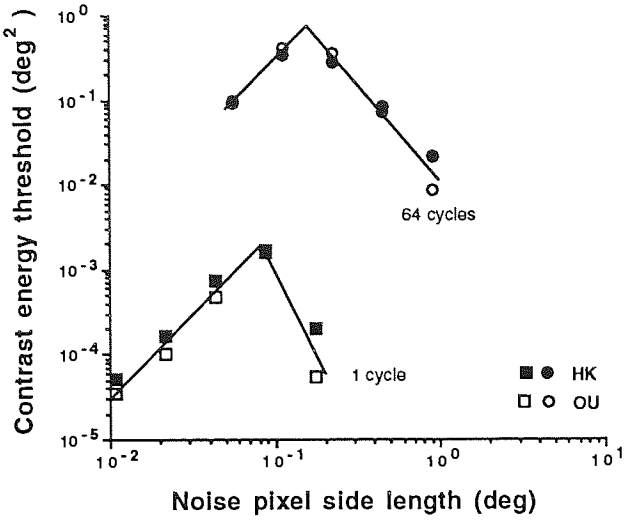

Figure 3.7
Contrast energy thresholds for cosine gratings comprising 1 and 64 cycles embedded in pixel noise. The noise spectral density increased with increasing size of the noise pixels. Subjects as indicated.

As Figure 3.7 shows, contrast energy threshold first increased and then decreased with increasing noise pixel side length for both stimuli. In agreement with the experiments of Figure 3.4, the slope of increase was +2. Contrast energy threshold thus increased in direct proportion to the noise spectral density calculated as a product of the r.m.s contrast of noise squared and the area of the noise pixels.

The least squares lines of the form logE = 2logP + k and logE = a logP + b were fitted to the increasing and decreasing parts of each set of data, respectively. The critical noise pixel side length, marked as an intersection between increasing and decreasing least squares lines, was 0.082 and 0.16 at 3 c/deg for the gratings comprising 1 and 64 cycles, respectively. The critical number of noise pixels per grating cycle was 4.1 for the grating comprising 1 cycle and 2.1 for the grating comprising 64 cycles. The theoretical cut-off frequency of noise corresponding to the critical noise pixel size $f_c = 1 / 2p_c$ (See Section 3.1.1) was 2.0 and 1.1 times higher than the spatial frequency of the grating consisting of 1 and 64 cycles.

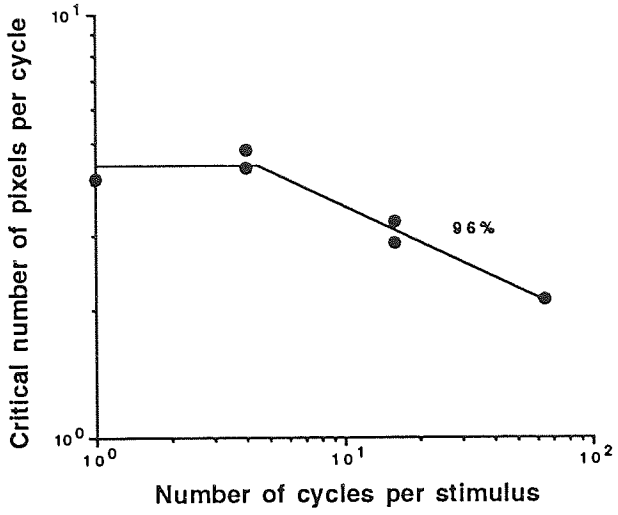

Figure 3.8
The critical number of pixels per grating cycle from Figures 3.4, 3.6, and 3.7 plotted as a function of the number of cycles within the grating area.

In Figure 3.8 the critical number of noise pixels per grating cycle from Figures 3.4, 3.6 and 3.7 is plotted as a function of the number of cycles per grating stimulus. Figure 3.8 shows that for the stimuli consisting of small number of cycles ($C \leq 4$), the minimum i.e. critical number of noise pixels per grating cycle (Y) needed to mimic the effect of white noise in grating detection was approximately constant at 4.4. However, when the number of cycles per stimulus further increased, fewer noise pixels were needed per grating cycle to mimic the effect of white noise. The least squares line obeyed equation $Y = 6.68C^{-0.28}$.

In Figure 3.9 contrast energy thresholds from Figures 3.4, 3.6, and 3.7 were plotted as a function of the spectral density of pixel noise, calculated according to equation (3.4). The data presented in Figure 3.9 was obtained using noise pixels of various sizes below the critical size.

Contrast energy thresholds for all the data in Figure 3.9 increased in direct proportion to the spectral density of pixel noise with a slope of +1. However, there was a vertical shift upwards in contrast energy thresholds with increasing number of grating cycles. When equation $E = kN_0$ was fitted separately to each set of data, the values of the proportionality constant k was found to be 3.2, 13, 35, 340 for gratings comprising 1,

4, 16 and 64 cycles, respectively. Explained variances, calculated as explained in Appendix 1, varied from 96%-99%.

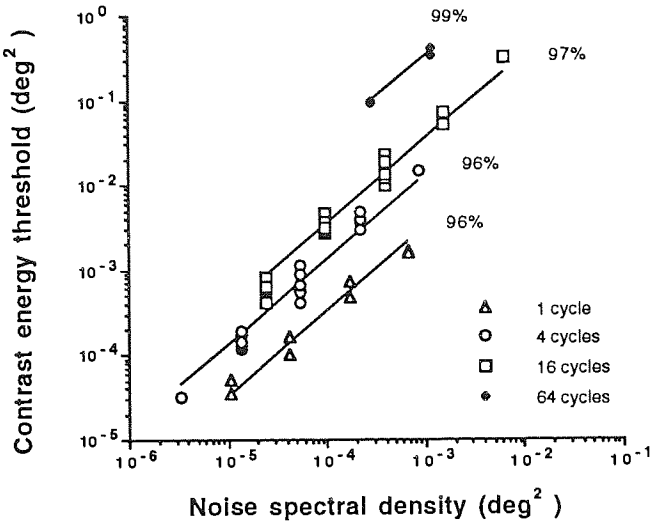

Figure 3.9
Contrast energy thresholds for vertical gratings consisting of 1-64 cycles from Figures 3.4, 3.6 and 3.7 plotted as a function of the spectral density of pixel noise.

3.2.3 Discussion

The experimental results showed that when noise pixels were below the critical size, contrast energy thresholds for cosine gratings were directly proportional to the spectral density of noise calculated as the product of noise pixel area and r.m.s contrast squared: when the spectral density of pixel noise increased with noise pixel size, contrast energy threshold increased in direct proportion to the spectral density, and when the increase in noise pixel size was compensated for by decreasing the r.m.s contrast of noise, contrast energy threshold remained constant. However, when noise pixel exceeded the critical size, contrast energy threshold started to decrease with increasing noise pixel size in both conditions. The result means that pixel noise mimics the effect of white noise in grating detection only when the noise pixel side length is below the critical size. At such pixel sizes contrast energy threshold increases in direct proportion to the spectral density of pixel noise irrespective of the number of cycles within the grating area, but the

level of contrast energy thresholds depended on the number of cycles.

An obvious reason for the decrease in contrast energy threshold when the noise pixel side length exceeded the critical size is the reduction of the spectral density of noise in the vicinity of the spatial frequency of a grating. The decrease in contrast energy thresholds can be explained by the block structure of the noise: When noise pixel size exceeds the critical size, the grating stimulus may still be masked by the edges of the blocks. With growing block size also this effect would then diminish because the number of edges in the stimulus declines and the visual system starts to process each block as a separate stimulus window therefore paying less attention to the edges. The masking effect of the block structure is well-known from the study of Harmon and Julez (1973) who investigated the recognisability of portraits sampled with square blocks of uniform density. They showed that the recognition could be recovered by filtering the high-frequency noise introduced by the edges of the blocks to the range of the spatial frequencies of the original image. On the other hand, Morrone, Burr and Ross (1983), showed that recognition could also be recovered by adding more high-frequency noise which destroys the block structure. Thus, the block structure tends to act as an additional mask in detection.

The critical noise pixel size was inversely proportional to the spatial frequency of the grating. As a result, the critical number of noise pixels per grating cycle, calculated by dividing the length of the grating cycle by the critical side length of the noise pixels, was independent of spatial frequency when the grating consisted of a constant number of cycles i.e. had constant bandwidth in octaves. On the other hand, the narrower the bandwidth of the stimulus the greater the critical noise pixel size and consequently fewer noise pixels per grating cycle were needed to mimic the effect of white noise. The critical number of noise pixels per grating cycle was found to be constant at about 4 for the gratings consisting of 1-4 cycles but it varied between 4 and 2 for the gratings consisting of 4-64 cycles. Accordingly, the cut-off frequency of noise ($f_c = 1/2p_c$) corresponding to the critical pixel size was 2-1 times the spatial frequency of the gratings.

The finding that the critical number of noise pixels still mimicking the effect of

white noise decreased with bandwidth, when the grating comprised more than 4 cycles, means that the gap between the cut-off frequency of the noise and the nominal spatial frequency of the grating decreased. This suggests that the bandwidth of the detection mechanism above the nominal spatial frequency of the grating decreases with decreasing bandwidth of the stimulus. However, the detection mechanism seems to be unable to adjust its bandwidth when the number of cycles increased from 1 to 4.

It is, however, improbable that the critical number of noise pixels per grating cycle would decrease below 2 even if the number of cycles would increase above 64, because two noise pixels per grating cycle means that the spatial frequency of the vertical grating is equal to the theoretical cut-off frequency of noise ($1/2p_c$). It is already difficult to understand how the pixel noise with the pixel size corresponding to the theoretical cut-off frequency of noise can produce contrast energy thresholds proportional to the spectral density of white pixel noise. According to equation (3.2), at the cut-off frequency ($1/2p_c$) the spectral density of pixel noise along the horizontal frequency axis has decreased to 40.5% of the spectral density of white pixel noise, i.e. the value obtained by multiplying pixel area by the square of the r.m.s contrast of noise. This percentage seems to be fairly low to produce the same effect on contrast energy threshold as white pixel noise. One explanation could be that the bandwidth of the detection mechanism increases towards the spatial frequencies below the nominal spatial frequency of the grating, when the bandwidth of the stimulus decreases below a certain limit. Another possibility could be that the visual system uses off-frequency looking (Pelli, 1981). Off-frequency looking was suggested as a method for the visual system to enhance signal detectability in the presence of a narrow-band mask. However, in our case, off-frequency looking would produce a lower signal-to-noise ratio and thus poorer performance at threshold, which is quite opposite to the original idea about the purpose of off-frequency looking.

When contrast energy thresholds for gratings comprising 1-64 cycles were plotted as a function of the spectral density of white pixel noise, contrast energy thresholds were lowest for gratings comprising 1 cycle and highest for gratings comprising 64 cycles. This vertical shift is due to spatial integration in the visual system (e.g. Howell & Hess, 1978;

Virsu & Rovamo, 1979; Rovamo & al., 1993). When a grating consist of a small number of cycles, the visual system is able to integrate contrast information over the whole image area. This produces low energy thresholds. However, when the number of grating bars exceeds the integration area of the visual system, a relatively smaller proportion of the total amount of contrast information is used and therefore contrast energy thresholds increase. We will return to the topic of spatial integration in the visual system in Chapter 5.

We can conclude that in grating detection the masking potency of pixel noise with constant r.m.s contrast can be increased by increasing the size of the noise pixel up to the critical size. In addition, pixel noise mimics the effect of white noise up to the critical size of noise pixels in the sense that contrast energy threshold is proportional to the spectral density of pixel noise, calculated by multiplying pixel area by the square of the r.m.s contrast of noise.

3.3 THE EFFECT OF THE SHAPE OF NOISE PIXELS

The experiments of Section 3.2 showed that when the size of square shaped noise pixels were below a critical size, the masking effect of pixel noise was directly proportional to the spectral density of noise, calculated by multiplying the pixel area by the r.m.s contrast of noise squared. The masking effect of pixel noise with constant r.m.s contrast can thus be increased by increasing the size of the noise pixel up to the critical size.

In further experiments concerning the masking effect of pixel noise, the effect of noise pixel shape was studied. The aim was to find out whether the critical dimensions of noise pixels were different in horizontal and vertical dimensions, when the stimulus was a one-dimensional grating i.e. whether the masking effect of pixel noise could be further increased without compromising the whiteness of noise by increasing the pixel size along the dimension without luminance modulation in the stimulus, that is along the bars of one-dimensional grating. Furthermore, the effect of the shape of noise pixels on the masking properties of pixel noise for one- and two-dimensional stimuli was studied.

The experiments were carried out by using both simple vertical cosine gratings and circular gratings with a radial luminance modulation and varying the shape and extent of rectangular noise pixels. The luminance modulation of the circular grating is two-dimensional and therefore, it served as a suitable control stimulus for the one-dimensional vertical gratings. Again, pixel noise was considered to mimic the effect of white noise when contrast energy threshold was directly proportional to the spectral density of noise, calculated by multiplying the r.m.s contrast of noise squared by pixel area [see equation (3.4)].

3.3.1 Methods

The experimental methods were identical to the experiment performed in Section 3.2 in all other respects except for stimuli and subjects. Therefore, only these parts of the methodology are described here. The reader is asked to refer to the previous Section for other details.

Stimuli

The stimuli consisted of a one-dimensional vertical cosine grating with a horizontal luminance modulation and a two-dimensional circular cosine grating with radial luminance modulation. The sharp-edged square stimulus window was surrounded by an equiluminous field which was limited to a 20 x 20 cm^2 square by placing a black cardboard mask in front of the screen. Spatial frequency was 0.372 c/cm on the screen. Spatial frequencies of 0.75 and 3.0 c/deg were obtained from viewing distances of 116 and 462 cm. Grating area was 10.7 x 10.7 cm^2. All stimuli comprised 4 cycles and thus had a constant spatial frequency bandwidth in octaves.

Stimuli were embedded in two-dimensional pixel noise which was produced by adding to each noise pixel within the grating area a random number drawn independently from a Gaussian distribution. The Gaussian distribution of random numbers had a zero mean and it was truncated at ± 2.5 times the standard deviation. The luminances of the neighbouring noise pixels were uncorrelated. Thus, noise was white up to the cut-off frequency determined by the size of noise pixels (See Section 3.1.1).

Each noise pixel consisted of n x m image pixels. The side length of noise pixels was varied in the horizontal and/or vertical direction between 1 and 256 image pixels. The maximal side length of 256 image pixels was equal to the side length of the stimulus window and thus represented for one-dimensional spatial noise.

The noise spectral density at low spatial frequencies, where it is constant, was

defined as a product of the r.m.s contrast of noise (c_n) squared and the noise pixel area (p_n^2): $N_e = c_n^2 p_n^2$, where the r.m.s contrast is the standard deviation of the local contrasts of noise. The same formula was applied also for one-dimensional noise. The spectral density of noise either increased due to increasing size of the noise pixels or it was kept constant by reducing the noise contrast in proportion to increasing size of noise pixels.

Each trial contained one exposure with a grating plus noise and one with noise only. For the grating plus noise exposure, five different noise plus grating stimuli were computed for each contrast level of the grating. One of them was chosen randomly for each exposure. The total of 20 contrast levels, i.e. 100 signal plus noise samples, was used for each threshold estimation. For the noise only exposure, one noise sample from the set of 20 samples was chosen randomly for each trial.

Subjects

Three subjects, aged 27, 28, and 30 years, served as observers. OU was a corrected non-astigmatic anisotrope (od. +0.75 DS / os. -0.75 DS) with binocular Snellen acuity of 1.5. HK was an uncorrected hyperope (+0.5 DS oa.) with binocular Snellen acuity of 1.5. JM was a corrected astigmatic myope (od. -1.5 DS / os. -0.50/-0.50 x 180) with binocular Snellen acuity of 1.7.

3.3.2 Results

Figure 3.10 displays contrast energy thresholds for vertical cosine gratings as a function of increasing height of noise pixels. Their width was constant at 1 image pixel. Noise pixel side length thus increased only along the grating bars. Thresholds were measured in two different noise conditions: noise spectral density either increased with increasing noise pixel area (Figure 3.10a) or was kept constant by decreasing noise

contrast with increasing noise pixel area (Figure 3.10b). In Figure 3.10a the r.m.s contrast of noise was constant at 0.3 and noise pixel height increased from 1 to 256 image pixels. Two spatial frequencies, 0.75 and 3 c/deg, were obtained from viewing distances of 116 and 462 cm. Noise spectral densities thus varied between 3.87×10^{-5} - 9.89×10^{-3} deg^2 for spatial frequency 0.75 c/deg, and 2.44×10^{-6} - 6.25×10^{-4} deg^2 for spatial frequency 3 c/deg.

As Figure 3.10a shows, contrast energy thresholds for both spatial frequencies increased linearly with increasing noise pixel height in double logarithmic coordinates. The slope of increase was +1. Contrast energy threshold thus increased in direct proportion to the spectral density of noise, calculated as the product of noise pixel area and the r.m.s. contrast squared. Thus, when the noise pixel size increases in the direction perpendicular to the luminance modulation of the stimulus i.e. along the bars of a one-dimensional grating, the increase in the noise pixel size elevates contrast energy threshold monotonically.

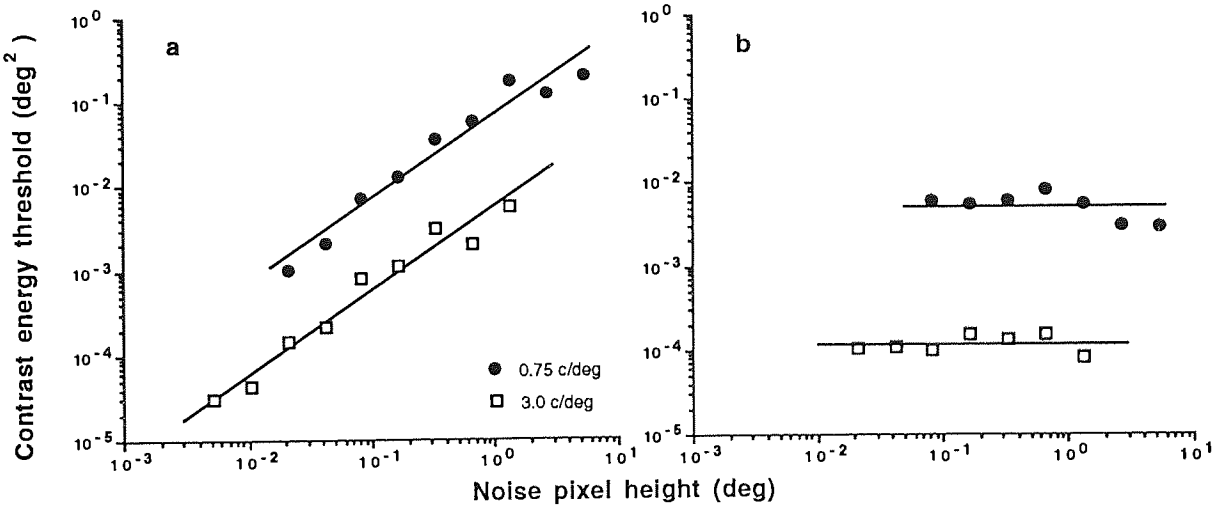

Figure 3.10
Contrast energy thresholds for a vertical cosine grating as a function of the height of noise pixels. The spectral density of pixel noise increased in Figure 3.10a and stayed constant in Figure 3.10b. Subject was JM at 0.75 c/deg and HK at 3 c/deg.

Unlike the experiments of the previous chapter (Figure 3.4), contrast energy thresholds for the two spatial frequencies in Figure 3.10a did not fall on a single

increasing line. In the experiments of Figure 3.10 the side length of the noise pixels increases only in one spatial dimension and thus contrast energy threshold increases with a slope of +1. The decrease in the viewing distance (and thus spatial frequency), on the other hand, increases contrast energy thresholds with a slope of +2. In the previous chapter both factors (the increase in pixels size and the decrease in viewing distance) produced a slope of +2 and the increasing part of the data for all spatial frequencies thus fell on a single increasing line. The vertical shift in Figure 3.10 would disappear if contrast energy thresholds were plotted as a function of the area of noise pixels.

In Figure 3.10b the noise spectral density was kept constant by decreasing the r.m.s contrast of noise from 0.35 to 0.044, when the height of the noise pixels was increased from 4 to 256 image pixels. The spectral density of noise was thus constant at 2.11×10^{-4} from the viewing distance of 116 cm (0.75 c/deg grating) and 1.33×10^{-5} deg^2 from the viewing distance of 462 cm (3 c/deg grating). Figure 3.10b showed that the constant spectral density of noise kept contrast energy thresholds constant for both spatial frequencies. Detection threshold was thus determined by the signal-to-noise ratio, which remained constant.

The result of Figure 3.10 indicates that there is no critical noise pixel size, when the side length of the noise pixels increases only along the direction perpendicular to the luminance modulation of the stimulus i.e. along the bars of one-dimensional grating, because pixel noise mimics the effect of white noise at all pixel heights in the sense than contrast energy threshold is proportional to the spectral density of pixel noise calculated by multiplying the pixel area by the square of the r.m.s contrast of noise.

In the experiment of Figure 3.11 contrast energy thresholds were measured for vertical cosine gratings as a function of the width of the noise pixels (Figures 3.11a and c), and for circular gratings as a function of the height of the noise pixels (Figures 3.11b and d). Along the other direction the noise pixel side length remained constant at 1 image pixel.

In Figures 3.11a and b noise contrast was kept constant when the noise pixel side length increased. In Figure 3.11a stimulus was as in Figure 3.10a, but now the width of

the noise pixels increased across the bars of the vertical grating while their height remained constant at 1 image pixel. In Figure 3.11b, where the stimulus was a circular grating with radial luminance modulation, the height of noise pixels increased from 1 to 256 image pixels while their width remained constant at 1 image pixel. The r.m.s contrast of noise was constant at 0.35. The spectral density of noise thus varied between 5.27×10^{-5} and 1.35×10^{-2} deg^2 and between 3.32×10^{-6} and 8.51×10^{-4} deg^2 at spatial frequencies of 0.75 and 3 c/deg, respectively.

As Figures 3.11a and b show, contrast energy threshold for both vertical and circular gratings first increased with increasing noise pixel side length, but then started to decrease. The increase in contrast energy threshold had a slope of +1 in double logarithmic coordinates. Contrast energy threshold was thus directly proportional to the noise spectral density, calculated by multiplying noise pixel area by the r.m.s contrast of noise squared. However, thereafter, contrast energy threshold for both grating types and spatial frequencies started to decrease despite of the increase of noise spectral density. The reduction of contrast energy threshold with increasing noise pixel side length can be explained by the decrease of the spectral density of noise in the vicinity of the spatial frequency of the grating. This means, that the cut-off frequency of noise had become too low in respect to the spatial frequency of the stimulus in order to mimic the effect of white noise in grating detection.

The critical side length of noise pixels refers to the transition from increase to decrease in the contrast energy thresholds and is here marked as an intersection of increasing and declining least squares lines. They were fitted to the four sets of data in Figures 3.11a and b with the same procedure as in Figure 3.4 of the previous Section: Contrast energy thresholds (E) of both frames were expressed in terms of cm^2 on the screen and plotted as a function of noise pixels side length (P) in cm on the screen. When plotted in this way, the data of Figures 3.11a and b practically superimposed. There was only a small variation in the vertical direction due to the individual and stimulus specific differences in the contrast energy thresholds. A line of least squares $\log E = \log P + k$ with a slope of +1 was fitted to the increasing part of the data. Another line of least

squares logE = a logP + b was fitted to the decreasing part of the data. The solid lines in Figures 3.11a and b were obtained by converting contrast energy thresholds in deg^2 and noise pixel side lengths in deg of the visual field, and multiplying each pair of least squares lines by a suitable constant to take into account the individual and stimulus specific differences in contrast energy thresholds. The constant was determined separately for each pair of lines as a geometric mean of the ratios between the measured and estimated contrast energy thresholds.

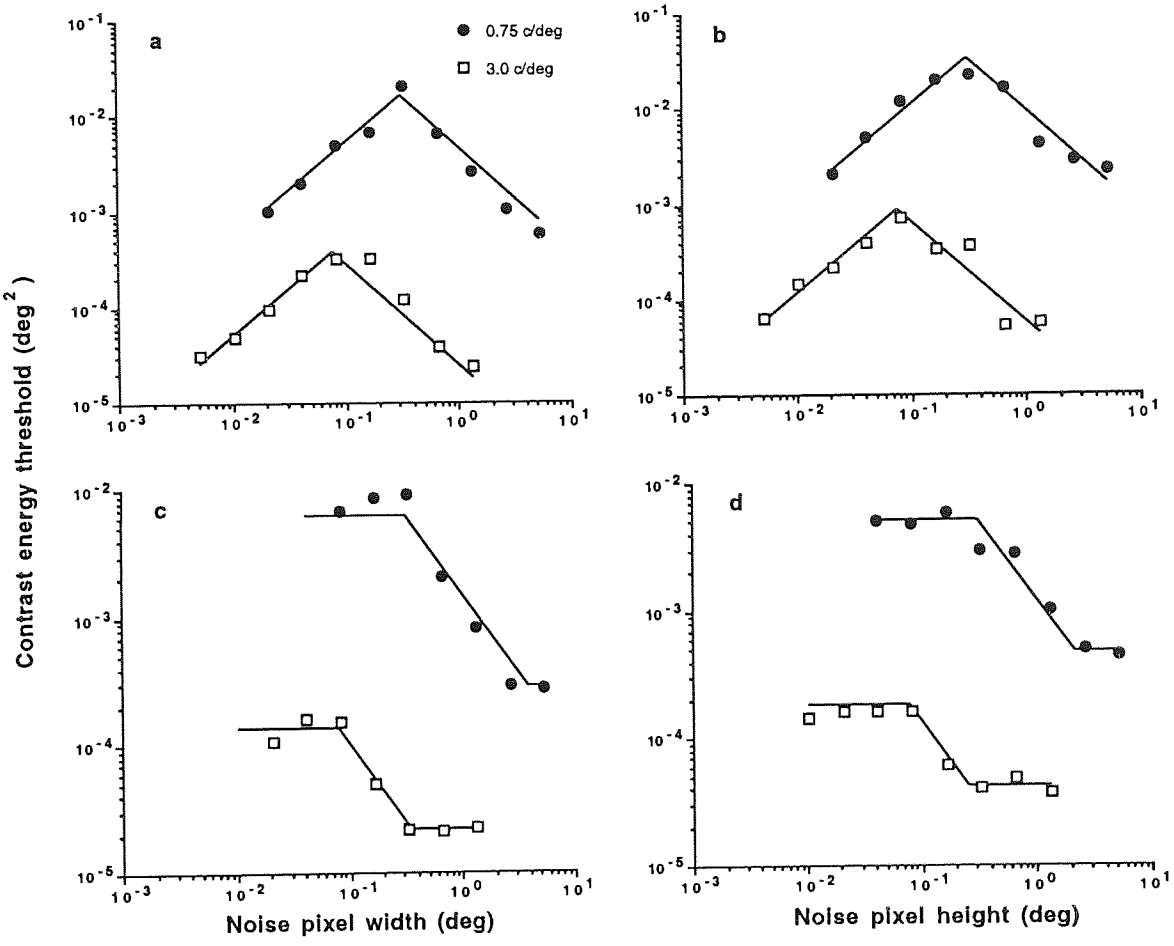

Figure 3.11
Contrast energy thresholds for vertical (a, c) and circular (b, d) cosine gratings plotted as a function of the side length of noise pixels. In Figures 3.11a and b the spectral density of noise increased with increasing side length of noise pixels whereas in Figures 3.11c and d the spectral density of noise remained constant. Subject was HK at 3.0 c/deg, JM for the vertical and OU for the circular grating at 0.75 c/deg.

Irrespective of the grating type, the critical noise pixel side length was found to be 0.31 deg for the spatial frequency of 0.75 c/deg and 0.079 deg for the spatial frequency

of 3 c/deg. The critical noise pixel side length was thus inversely proportional to the spatial frequency of the grating and the corresponding minimum number of noise pixels per grating cycle was constant at 4.2 for all stimuli.

In Figures 3.11c and d the spectral density of pixel noise was kept constant despite of the increasing side length of noise pixels by reducing the r.m.s contrast of noise in inverse proportion to noise pixel area. In Figure 3.11c the stimulus was as in Figure 3.10b; the only difference was the increase of noise pixel width across the bars of the vertical grating. In Figure 3.11d, where the stimulus was a circular grating, only the height of the noise pixels increased, their width remained constant at 1 image pixel. The r.m.s contrast of noise decreased from 0.35 to 0.039 when noise pixel height increased from 2 to 256 image pixels. The noise spectral densities were constant at 1.05×10^{-4} deg^2 for 0.75 c/deg grating and 6.65×10^{-6} deg^2 for 3 c/deg grating.

For both the vertical and circular grating contrast energy thresholds remained first constant and then started to decrease with increasing noise pixel side length. Constant spectral density of noise thus kept contrast energy thresholds constant up to a critical noise pixel side length. Thereafter, contrast energy thresholds decreased until they hit the floor determined by the contrast energy threshold measured without noise. The decrease indicates that the spectral density of pixel noise decreased in the vicinity of the spatial frequency of the grating.

The solid lines in Figures 3.11c and d were fitted to the whole set of data using the same procedure as above: contrast energy thresholds (E) for both frames were first expressed in cm^2 on the screen and plotted as a function of noise pixel side length (P) in cm on the screen. The average of the upper horizontal part of the data was calculated and a least squares line $\log E = a \log P + b$ was fitted to the decreasing part of the data. The solid lines in Figure 3.11c and d were obtained by expressing contrast energy thresholds and pixel side length in the units of the visual field and multiplying each pair of lines with a constant to compensate for the individual and stimulus specific differences in thresholds. The average of the lower horizontal part of the data, indicating the floor determined by the contrast energy threshold without external noise for each subject and

stimulus, was calculated separately for each curve. The critical noise pixel side length refers to the transition from constant contrast energy threshold to decrease in threshold. Irrespective of grating type it was found to be 0.32 deg and 0.080 deg at the spatial frequencies of 0.75 and 3.0 c/deg, respectively. The critical side length of the noise pixels was thus inversely proportional to the spatial frequency of the grating. As a result, the minimum number of noise pixels per grating cycle needed to mimic the effect of white noise was again constant at 4.2 for all grating stimuli.

In Figure 3.12 the spectral density of noise was kept constant by keeping both the size of noise pixels and r.m.s contrast of noise constant. The shape of noise pixels changed from one-dimensional vertical noise pixel to one-dimensional horizontal noise pixel: when noise pixel height reduced from 256 to 1 image pixels, noise pixel width similarly increased from 1 to 256 image pixels; the area and the number of image pixels per each noise pixel thus stayed constant. The r.m.s. contrast of noise was constant at 0.3 and 0.35 for the vertical circular cosine gratings, respectively. Spatial frequencies of 0.75 and 3.0 were obtained from viewing distances of 115 and 462 cm. Noise spectral densities for vertical gratings were 9.89×10^{-3} and 6.25×10^{-4} deg^2 and for circular gratings 1.35×10^{-2} and 8.51×10^{-4} deg^2 at the spatial frequencies of 0.75 and 3.0 c/deg, respectively. Figure 3.13 shows examples of various noise pixel shapes used for both vertical and circular gratings. In Figure 3.12 contrast energy thresholds are plotted as a function of the ratio of the width and height of noise pixels. The solid lines were fitted to the data of each frame using the same procedure as above, but now it was necessary to convert only the contrast energy thresholds to cm^2.

As Figure 3.12a shows, the constant spectral density of noise kept contrast energy threshold constant for the vertical grating when the pixel width/height ratio was equal to or below 1. At these pixel shapes, noise pixels were vertically elongated and their width i.e. side length across grating bars was such that the number of noise pixels per grating cycle was at least 4. The result of Figure 3.13 is thus in agreement with results of Figure 3.11. The result of Figure 3.12a means that pixel noise mimicked the effect of white noise in grating detection irrespective of the shape of noise pixels up to the pixel

width/height ratio of 1. At the pixels width/height ratio of 1, the noise pixels were square shaped. When the pixel width/height ratio exceeded 1, the width of noise pixels across the grating bars exceeded the critical size, and contrast energy threshold started to decrease in accordance with Figure 3.11c.

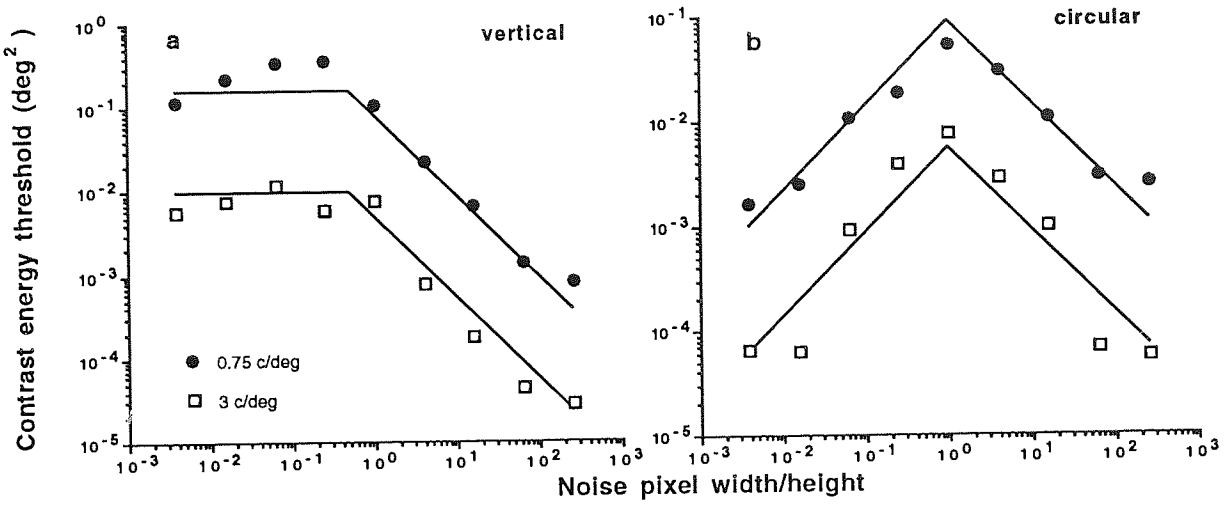

Figure 3.12
Contrast energy threshold for vertical (a) and circular (b) cosine gratings as a function of the ratio between the width and height of the noise pixels. The structure of pixel noise changed from vertical one-dimensional to horizontal one-dimensional pixel noise. Subject was HK at 3.0 c/deg, and JM and OU for the vertical and circular gratings at 0.75 c/deg, respectively.

Figure 3.12b shows that contrast energy threshold for circular gratings first increased and then started to decrease with increasing noise pixel width/height ratio. Contrast energy threshold was at its maximum when the noise pixel width/height ratio was 1 i.e. noise pixels were square-shaped. However, when either width or height of the noise pixels increased, contrast energy threshold started to decrease despite of constant spectral density of noise, calculated by multiplying the noise pixel area by the r.m.s contrast of noise squared. When the noise pixel was square-shaped there was 4 noise pixels per grating cycle both in the horizontal and vertical direction, which equals to the critical number found in Figure 3.11. Therefore, due to the two-dimensional nature of the circular grating stimulus, contrast energy threshold started to decrease when either the vertical or horizontal side length of noise pixels exceeded the critical value.

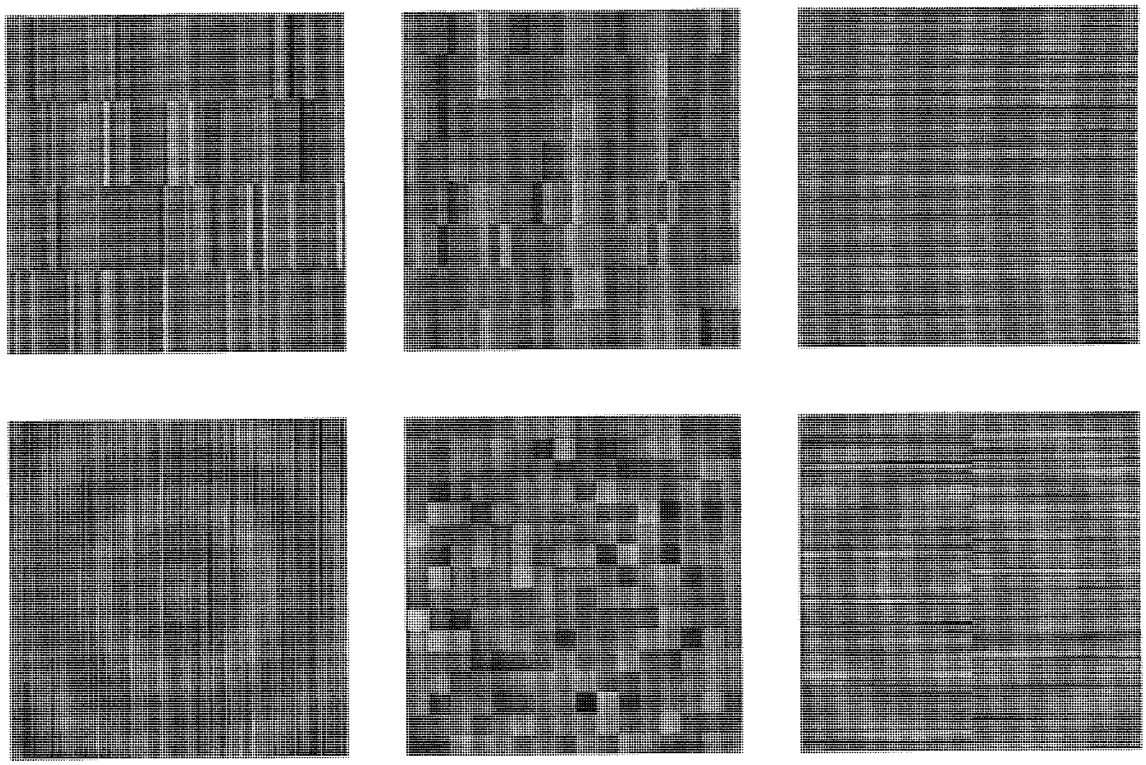

Figure 3.13
Vertical and circular cosine gratings embedded in pixel noise. The area of noise pixels, the r.m.s contrast of noise and thus the spectral density of noise is constant, but the shape of the noise pixel varies. For the vertical grating the noise pixels consist of 4x64, 8x32, and 256x1 image pixels from left to right whereas for the circular grating the noise pixels consist of 1x256, 16x16 and 128x2 image pixels from left to right.

The principal results of Figure 3.12 are demonstrated in Figure 3.13. The r.m.s contrast of the stimuli and noise are constant in all frames. Furthermore, the area of noise pixels remains constant at 256 image pixels, only the shape of noise pixels varies from one frame to another.

As Figure 3.13 shows, the vertical grating is hardly visible, when the noise pixel width is 4 or 8 image pixels, which means that the number of noise pixels per grating cycle across the bars is 16 or 8 i.e. over 4. However, when the width of noise pixels increase further to 256 image pixels, the vertical grating becomes easily visible because the number of noise pixels per grating cycle is now only 0.25. For the circular grating the best masking effect is obtained when the noise pixel size is 16x16 image pixels, which means that the number of noise pixels is 4 both in the vertical and horizontal directions.

When noise pixel side length increases either in the vertical or horizontal direction, the circular grating becomes easier to see, as the noise pixel shapes of 1x256 and 128x2 image pixels demonstrate in Figure 3.13.

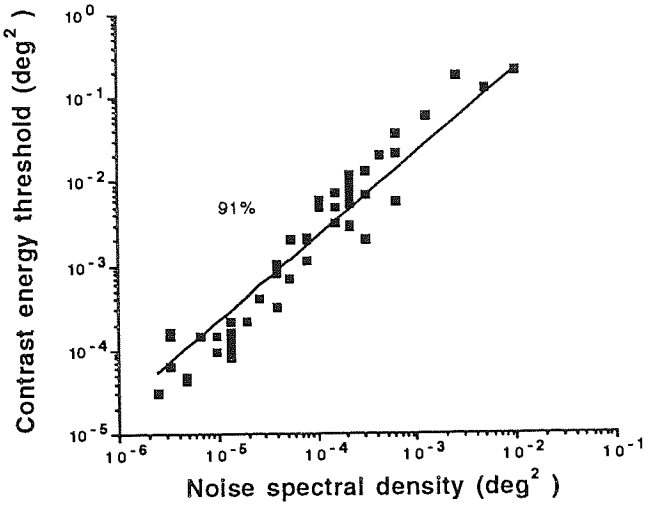

Figure 3.14
Contrast energy thresholds for the vertical and circular gratings from Figures 3.10-3.12 embedded in pixel noise. The side length of the noise pixels were below the critical size both in the vertical and horizontal directions. Noise pixels had various shapes and sizes including one-dimensional noise.

In Figure 3.14 contrast energy thresholds from Figures 3.10-3.12 were plotted as a function of noise spectral density, calculated by multiplying the noise pixel area by the r.m.s contrast of noise squared. Only those datapoints were included where neither the width nor the height of the noise pixels exceed the critical value.

As Figure 3.14 demonstrates, contrast energy thresholds both for circular and vertical gratings increased in direct proportion to the spectral density of pixel noise, calculated by multiplying the noise pixel area by the r.m.s contrast of noise squared. The slope of increase was +1 when plotted in double logarithmic coordinates. Contrast energy thresholds formed a single increasing function irrespective of whether the stimulus was the vertical or circular grating. This suggest that the spatial integration of both stimuli is similar when both kind of gratings comprise four cycles. Furthermore, the increase of contrast energy threshold with the spectral density of noise was independent of pixel shape and similar for one- and two-dimensional noises.

3.3.3 Discussion

The results showed that when the side length of noise pixels increased along the bars of a one-dimensional simple cosine grating, the masking effect of spatial noise rose so that contrast energy threshold increased in direct proportion to the increasing pixel area. The maximal masking effect was obtained when the side length of noise pixels was equal to the length of the grating bars, which made pixel noise one-dimensional. Noise thus mimicked the effect of white noise in grating detection at all pixel heights in the sense that contrast energy threshold was proportional to the spectral density of pixel noise, calculated by multiplying pixel area by the square of the r.m.s contrast of noise. When the side length of noise pixels increased across the bars of the one-dimensional grating or when the stimulus was a circular grating with a radial luminance modulation, there was a critical side length of noise pixels, after which contrast energy threshold was no more proportional to the spectral density of pixel noise but decreased with increasing noise pixel side length. Because the critical side length of noise pixels was inversely proportional to the spatial frequency, the number of noise pixels per grating cycle was constant. It was found to be 4 for the gratings comprising 4 cycles. Furthermore, when both the width and height of the noise pixels were varied simultaneously, the noise pixel shape did not have any effect on contrast energy threshold as long as the width and height of noise pixels were below their critical values. When all contrast energy thresholds corresponding to the pixels below the critical size were plotted as a function of the spectral density of noise the data fell on a single increasing line with a slope of $+1$ in double logarithmic coordinates irrespective of whether noise was one- or two-dimensional.

The result that for the vertical grating contrast energy thresholds were at all pixel heights proportional to the spectral density of noise, calculated by multiplying pixel area by the square of the r.m.s contrast of noise, means that the side length of noise pixels along the bars for the vertical grating has no critical value. The result that pixel noise mimicked the effect of white noise when there was at least 4 pixels per grating wavelength across the bars, i.e. in the direction of luminance modulation in a one-

dimensional grating consisting of four cycles, is in agreement with the results of Section 3.2. The finding that the critical number of noise pixels per grating cycle was 4 also for the circular grating consisting of four cycles suggests that the results of Section 3.2 can also be extended for circular gratings. The spatial frequency of a circular grating is equal along the horizontal and vertical frequency axes of Fourier space. Therefore, the critical noise pixel height and width were equal. However, for a compound grating consisting of two spatial frequencies at orientations of 0 and 90 degrees, the critical number of noise pixels per grating cycle in the horizontal and vertical direction is probably different and depends on the number of cycles in the vertical and horizontal direction. Furthermore, for a simple grating rotated for 45 degrees the critical number of noise pixels per grating cycle should probably be greater than for the vertical or horizontal grating of the same spatial frequency, because (i) the spectral energy of an oblique grating is on the oblique frequency axes of Fourier space and (ii) the spectral density of pixel noise, calculated according to equation (3.2), decreases faster along the diagonal than horizontal and vertical frequency axes. On this basis, the critical number of noise pixels per grating cycle should be greater for circular than vertical grating, because circular grating comprises all orientations, including the oblique ones. It seems, however, that the horizontal and vertical components dominate in determining the critical pixel size for circular grating.

The finding that contrast energy threshold was directly proportional to the spectral density, calculated by multiplying pixel area by the square of the r.m.s contrast of noise, both for one- and two-dimensional spatial noises when the horizontal and vertical dimensions of the noise pixels were smaller than critical, indicates that the spectral density of both one- and two-dimensional noises should be calculated by taking into account both the height and width of the noise pixels. This is in disagreement with Legge et al. (1987), who suggested that the spectral density of one-dimensional noise should be calculated by taking into account only the dimension of the noise pixels across the luminance modulation of the stimulus. However, as the current result shows, the whole pixel area affects the masking power of noise even for stimuli with luminance modulation only along one spatial dimension.

3.4 CONCLUSIONS

The experiments of Chapter 3 have shown that the masking effect of pixel noise can be increased by increasing the size of noise pixels as long as the side length both in the horizontal and vertical directions is below the critical size. The minimum number of noise pixels depends only on the number of bars within the grating area. Therefore, when two-dimensional stimuli are used, the critical i.e. minimum number noise pixels per grating cycle is determined by the number of grating bars in each spatial dimension.

The maximum masking effect is obtained when the pixel size is at the critical size in each spatial direction. For one-dimensional grating there is no critical noise pixel side length along the grating bars and therefore the masking effect increases as the noise pixel height increases up to the height equal to the stimulus height producing one-dimensional noise. Therefore, the spectral density of one-dimensional noise should be calculated as the spectral density of two-dimensional noise.

The result that the critical number of noise pixels per grating cycle depends on the number of cycles within the stimulus area suggests that the detection filter of the visual system is adapted to the spectral bandwidth of the stimulus (at least within the range of 4 to 64 cycles). In spatial terms this would mean that the visual system is able to integrate contrast information over at least 64 grating cycles. On the other hand, the result that the contrast energy thresholds for gratings, when plotted as a function of the spectral density of noise, were the higher the greater the number of grating cycles shows that the integration becomes less efficient with increasing stimulus area. We return to the spatial integration in the visual system in Chapter 5.

4. CONTRAST DETECTION WITH AND WITHOUT EXTERNAL SPATIAL NOISE

4.1 INTRODUCTION

Contrast detection in external noise is limited by the power of noise as described in the previous chapter. This result rests on a well-demonstrated and generally accepted assumption that the effective signal-to-noise ratio is constant at threshold (e.g. Pelli, 1990). Thus, when the masking power of external noise is great enough to be the main determinant of detection threshold, we can control the threshold for detection of a contrast signal by controlling the spectral density of external noise: when the spectral density of external noise is increased, threshold contrast squared increases in proportion, and vice versa.

Any change in threshold contrast thus reflects a change in the effective noise level: if a detection threshold decreases, it indicates that the effective noise level has consequently decreased to produce a constant signal-to-noise ratio at threshold. This assumption leads us to another: contrast thresholds measured without external noise are determined by internal neural noise in the visual system (e.g. Barlow, 1956, 1957, 1977; Nagaraja, 1964; Pollehn & Roehrig, 1970; Van Meeteren & Boogaard, 1972; Pelli, 1981, 1990; Watson, Barlow & Robson, 1983; Ahumada & Watson 1985; Ahumada 1987; Van Meeteren & Valeton, 1988). It follows, that contrast detection in a psychophysical task is actually always a discrimination task between noise-plus-signal and noise alone. Noise, on the other hand, can originate from different sources. Threshold is determined either by combination of noise of various origins or alternatively, when the effective magnitude of one noise source is clearly greater than any other, by the spectral density of the dominant noise.

In a visual detection task quantal fluctuation of light and external image noise are the two main sources of external noise that are of interest in this study. The origins of

internal noise in the visual system are, however, far more ambiguous. One possible classification is provided by George Sperling (1989) who classifies them through various stages of visual processing:

> *Three stages of visual processing determine how internal noise appears to an external observer: light adaptation, contrast gain control and a postsensory/ decision stage. Dark noise occurs prior to adaptation, determines dark-adaptated absolute thresholds and mimics stationary external noise. Sensory noise occurs after dark adaptation, determines contrast thresholds for sine gratings and similar stimuli, and mimics external noise that increases with mean luminance. Postsensory noise incorporates perceptual, decision and mnemonic processes...and mimics external noise that increases with stimulus contrast (multiplicative noise).*

The absolute threshold of the visual system at very low levels of light would thus be limited by "dark" noise intrinsic to the visual system (e.g. Barlow, 1956,1957, 1977). At these luminance levels, a spontaneous activity of the visual receptors in the retina is relatively large in respect to the quanta from the external stimulus reaching the retinal level. This causes an uncertainty on detection performance of the observer as to whether the sensation of light raised from the stimulus or the spontaneous activity of photoreceptors. The amplitude of this noise is thus independent of the light level and results in a constant amplitude threshold as a function of luminance until the quantal fluctuation of light becomes the dominant source of noise. In terms of contrast, the magnitude of "dark" noise decreases in direct proportion to the luminance and detection threshold increases with a slope of +1 as a function of luminance.

As the luminance further increases, quantum noise becomes the dominant source of noise for the visual system. In terms of contrast, the magnitude of quantum noise decreases in direct proportion to the square-root of the luminance. Therefore, when quantum noise is a dominant noise source for the visual system, contrast threshold increases with a slope of + ½ as a function of luminance and results in the DeVries-Rose

law. It has been suggested, however, that the quantum noise is not the only explanation to the square-root relation between detection threshold and background luminance, but it is also partly due to internal neural noise in the visual system (e.g. Laughlin & Lillywhite, 1979; Lillywhite, 1981; see also Graham & Hood, 1992).

Sperling's postsensory noise is equivalent to noise limiting threshold at high retinal illuminances and is thus the source of Weber's law (e.g. Nagaraja, 1964; Van Nes & Bouman, 1967, Pelli, 1990). Constant contrast at detection threshold would result, if the level (in terms of amplitude) of internal noise increased in direct proportion to the luminance of the background. Contrast would thus be constant. Therefore, at high luminance levels an internal noise of some sort is often suggested to limit detection and discrimination threshold as a function of variable of interest (e.g. Nagaraja, 1964; Pollehn & Roehrig, 1970; Van Meeteren & Boogaard, 1972; Pelli, 1981, 1990; Watson & al., 1983; Ahumada & Watson, 1985; Ahumada 1987; Legge & al., 1987; Van Meeteren & Valeton, 1988). Sperling's postsensory noise can thus rise from various sources and levels of signal processing in the visual system causing uncertainty in the visual task.

The concept of constant signal-to-noise ratio at detection threshold allows us to compare detection both with and without noise in terms of signal-plus-noise and noise only discrimination task. If we conduct identical measurements in both conditions (with and without external noise) and keep the physical signal-to-noise properties in the noise condition controlled, we can, by comparing the contrast sensitivities with and without noise, speculate about the effect of internal noise on detection thresholds.

This procedure was previously used by Rovamo & al., (1992) who studied contrast sensitivity both with and without noise as a function of viewing distance (and thus spatial frequency) and eccentricity. They found that when physical signal-to-noise ratio was kept constant, contrast detection in spatial noise was independent of any variable studied as long as contrast sensitivity was lower with noise than without. The independence of contrast sensitivity versus viewing distance and eccentricity in external spatial noise was explained by the fact that the point spread function of the eye's optics (e.g. Deeley & al., 1991; Rovamo & al., 1994a), and sampling limitations of the retina

(e.g. Rovamo & Virsu, 1979; Williams, 1985; Curcio, Sloan, Packer, Hendrickson & Kalina, 1987) attenuate grating and noise contrast similarly at the spatial frequency of the grating. This keeps signal-to-noise ratio constant at moderate viewing distances and small eccentricities, where contrast sensitivity was lower with noise than without.

At longer viewing distances and greater eccentricities the decreasing contrast sensitivity is identical with and without noise (Rovamo & al., 1992). Here the power of the external spatial noise is so much attenuated by the filtering properties of the eye mentioned above that contrast sensitivity becomes predominantly determined by internal neural noise in the visual system. This explains the identical contrast sensitivity with and without external noise.

The purpose of this study was to extend analogous investigations to other parameters influencing detection performance. The detection thresholds were measured for grating stimuli as a function of retinal illuminance, amount of light added onto the screen, exposure time and stimulus area. The study of each of these parameters will be introduced and discussed in a separate section.

4.1.1 General methods

The detailed description of apparatus, stimulus generation, and threshold determination is given in the second chapter of this study. The reader is therefore asked to refer to Chapter 2 for the above details. Apparatus 1 was used in the experiments described here.

Stimuli

The stimuli consisted of vertical cosine gratings of various spatial frequencies as defined in the specific procedures of each experiment. Detection thresholds were

measured both with and without external noise added to the stimulus. Two-dimensional pixel noise was used for the experiments where contrast sensitivities were measured as a function of retinal illuminance or exposure time. One-dimensional noise was used for the experiment investigating the effect of stimulus area.

Two-dimensional noise was produced by adding to each pixel within the grating area a random number drawn independently from an even distribution with zero mean. Neighbouring pixel luminances were uncorrelated. Thus, the two-dimensional noise was white up to a cut-off frequency determined by the pixel density of the display as described in Section 3.1.1 of this thesis.

One-dimensional spatial noise was produced by adding to each vertical row of pixels within the grating area a random number drawn independently from an even distribution with zero mean. The luminances of the neighbouring pixel rows were uncorrelated. Thus, the one-dimensional noise was white up to a cut-off frequency determined by the pixel density of the display (See Section 3.1.1).

Because the stimuli used were vertical gratings, the spectral density of white pixel noise for both one- and two-dimensional case was defined as the product of the r.m.s contrast of noise (c_n) squared and pixel area ($p_x p_y$): $N_e = c_n^2 p_x p_y$, where the r.m.s contrast (c_n) is the standard deviation of the local contrasts of noise. When gratings with noise were used, 5 different noise plus grating stimuli were computed for each contrast level of the grating. One of them was chosen randomly for each exposure. The set of gratings generated for each threshold measurement contained approximately 20 contrast levels. The comparison stimulus was chosen randomly from a set of 20 different noise stimuli. Therefore, the total number of 120 noise samples was available for the threshold estimate.

Procedures

The r.m.s contrast thresholds with or without noise were determined by a forced-choice algorithm described in detail in Section 2.3.1. The inverse of r.m.s. contrast

at threshold gave the r.m.s. contrast sensitivity plotted in the results. All data points shown are based on geometric means of a minimum of three threshold estimates. The two-interval forced-choice procedure was used. Each trial consisted of two exposures, separated by 600 msec and accompanied with a sound signal to indicate the occurrence of exposure. However, only one exposure contained the grating with non-zero contrast; in the other exposure the grating contrast was always zero. The observer indicated which exposure contained the grating by pressing one of two keys on a computer keyboard. An auditory signal followed the subject's response to provide feedback as to whether the subject's responses were correct or not. A new trial began 250 msec after the subject's response. For the experiment of Section 4.3 exposure time varied from 16.7 to 533 msec, corresponding to 1-32 frames. Otherwise exposure time was constant at 500 msec.

The experiments were performed in a dark room; the only light source was the display. A chin-rest was used to stabilize the head. Subjects were asked to look at the centre of the screen. No fixation point was used.

Subjects

Two experienced subjects, aged 25 (KT) and 27 (HK) years, served as observers. Subject KT was a corrected non-astigmatic myope (od. -6.00 DS/os. -4.00 DS) with binocular Snellen acuity of 1.5. HK was an uncorrected hyperope (+0.5 DS oa.) with binocular Snellen acuity of 1.5. Snellen acuity of the dominant eye with optimal refraction was 1.6 for KT and 1.3 for HK.

4.2 THE EFFECT OF LUMINANCE ON CONTRAST SENSITIVITY WITH AND WITHOUT EXTERNAL SPATIAL NOISE

4.2.1 Introduction

In foveal vision contrast sensitivity first increases but then saturates with increasing retinal illuminance (e.g. Van Nes & Bouman, 1967; Van Nes, Koenderink, Nas & Bouman, 1967; Mustonen, Rovamo & Näsänen, 1993). The increase in contrast sensitivity with increasing retinal illuminance obeys DeVries-Rose law (DeVries, 1943; Rose, 1948). For grating stimuli it means that contrast sensitivity is proportional to the square root of the average luminance of the stimulus. Thus, when contrast sensitivity as a function of retinal illuminance is plotted in a double-logarithmic coordinates, the increase in contrast sensitivity has a slope of $+\frac{1}{2}$.

This square-root relation is generally attributed to quantal fluctuation of light (DeVries, 1943; Rose, 1948; Nagaraja, 1964; Van Nes & Bouman, 1967; Van Nes & al., 1967; Barlow, 1977; Pelli, 1990; Mustonen & al., 1993). This means that even with a nominally constant stimulus, the number of quanta collected by the retina in any given area varies from occasion to occasion and is characterised by a Poisson distribution. The variance of Poisson distribution is equal to its mean. The variance normalised by luminance squared is proportional to the spectral density and thus the spectral density of quantum noise changes in inverse proportion to the luminance of visual stimuli. As a result contrast sensitivity increases in proportion to the square-root of luminance. An alternative explanation is that the square-root relation between background luminance and contrast sensitivity holds due to the existence of multiplicative noise within the visual system, as argued by Lillywhite and Laughlin (1979) and Lillywhite (1981). This would correspond to a correlative noise within the visual system, whose magnitude decreases with luminance.

When the retinal illuminance is further increased the dominance of DeVries-Rose law is replaced by Weber's law which results in constant contrast sensitivity as a function of retinal illuminance. The fact that after this transition point detection threshold stays

constant irrespective of retinal illuminance and the noise introduced by quantal fluctuation, the detection is presumably limited by another noise source which is independent of the luminance level. A good candidate is internal neural noise, which has been suggested by numerous studies (e.g. Nagaraja, 1964; Van Meeteren & Boogaard, 1972; Barlow, 1977; Watson & al., 1983; Sperling, 1989; Pelli, 1990). At luminance levels where Weber's law is valid, the internal neural noise is thus believed to be a more significant source of noise than quantal fluctuation of light. As a consequence, the constant ratio between signal contrast energy and the power of internal neural noise means that detection threshold remains constant.

As Van Nes and Bouman (1967) showed, the transition from the DeVries-Rose law to Weber's law for gratings depends on spatial frequency so that the lower the spatial frequency the earlier the transition occurs as a function of retinal illuminance. Van Nes et al. (1967) extended the analysis by showing that the transition luminance is in fact directly proportional to spatial frequency squared. In agreement, Mustonen et al. (1993) confirmed this finding for low spatial frequencies (0.125-4 c/deg) by using gratings containing a constant number of grating periods within a circular stimulus window. They showed that contrast sensitivity for all spatial frequencies studied saturated at a constant "relative retinal illuminance" defined as the retinal illuminance (I) divided by the spatial frequency squared (f^2). Thus, the quantal fluctuation of light on one hand, and the internal neural noise on the other, affects detection threshold similarly at all spatial frequencies.

The experiments introduced in this chapter were performed at a constant level of external noise as a function of retinal illuminance for one spatial frequency in order to compare the detection performance with and without external spatial noise.

4.2.2 Specific procedures

The stimulus consisted of a vertical cosine grating within a sharp-edged circular window. Spatial frequency was 4 c/deg from a viewing distance of 115 cm. Grating area

was constant at 19.4 deg^2 and contained 20 cycles per diameter. The exposure time was constant at 500 msec. The retinal illuminance varied from approximately 0.5 to 5.0 x 10^4 photopic trolands.

Contrast sensitivity was measured both with and without external noise. In the noise condition, the r.m.s. contrast of external noise (c_n) was 0.4. The size of the pixel (p^2) was 4.38 x 10^{-4} deg^2. The spectral density of external noise ($N_e = c_n^2 p^2$) was thus 7.01 x 10^{-5} deg^2.

The grating stimuli at various luminance levels were viewed monocularly. One drop of 0.4% Benoxinate (Oxybuprocaine) hydrochloride USP was installed into the dominant eye of the subject to increase drug absorption. The pupil was thereafter dilated to a diameter of 8 mm with 2 drops of 10% Phenylephrine (Metaoxedrine) hydrochloride BP, which leaves accommodation unaffected. Both drugs were obtained from single use disposable units (Smith & Nephew Pharmaceuticals Ltd, Romford, England).

The average retinal illuminance in photopic trolands is calculated by multiplying the luminance of the screen (L) in cd/m^2 by the pupil area (A) in mm^2. The luminance of the screen was 50 cd/m^2, which thus resulted in the average retinal illuminance of 2510 photopic trolands with the pupil of 8 mm in diameter.

Lower levels of retinal illuminance were obtained by placing a desired number of neutral density filters (Lee Filters Ltd., Hampshire, U.K.) of 0.6 logarithmic units (No 210 ND) on the display screen. Neutral density filters leave the contrast of the stimulus unaffected because the values of local luminances decrease in direct proportion to decreasing mean luminance.

The filters were fixed with black opaque tape that prevented the leakage of light from between the filters and screen. Filters of suitable size were cut from large sheets. Each filter used was calibrated by measuring how much it attenuated the luminance of the screen. After each luminance reduction of 0.6 logarithmic units, the subject adapted to the new screen luminance for 5 minutes.

Higher levels of retinal illuminance were obtained by adding external light to the screen. The light source consisted of two defocussed Liesegang Fantimat 250 AF slide

projectors (Liesegang GmbH, Düsseldorf, Germany) directed obliquely towards the screen and located on both sides of the subject in order to achieve homogenous screen luminance. Different levels of light intensity were produced by using various numbers of neutral density filters of Lee mounted in the slides.

The effect of additional light on the displayed contrast of the grating was taken into account by multiplying the threshold contrasts by $L_o/(L_o+L_i)$, where L_o is the luminance of the screen without additional light and L_i is the amount of light added onto the screen.

4.2.3 Results

In Figure 4.1 monocular r.m.s contrast sensitivity was measured for a vertical 4 c/deg cosine grating as a function of retinal illuminance varied by placing neutral density filters on the display screen as described above.

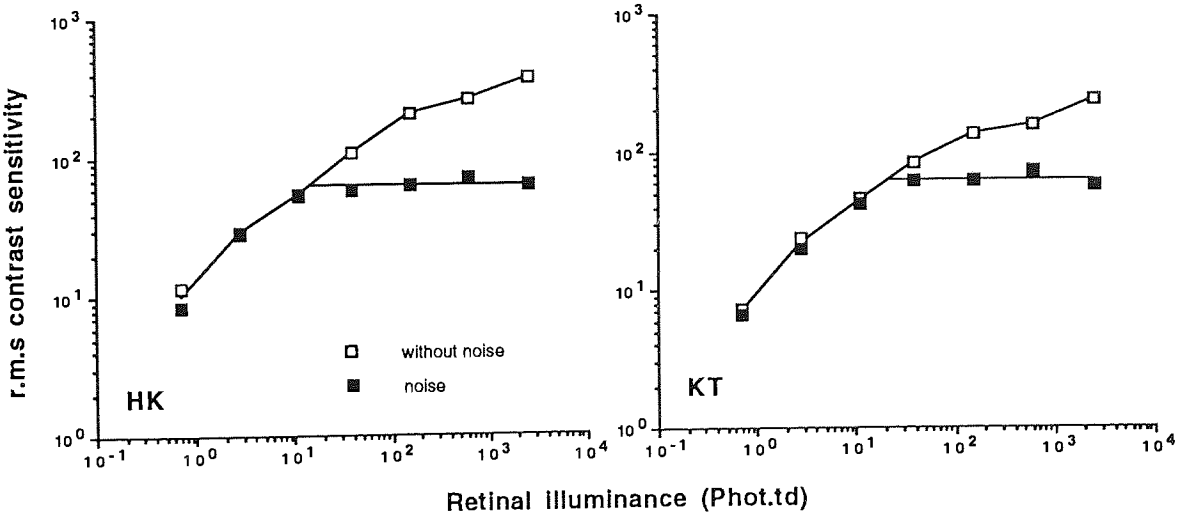

Figure 4.1
Contrast sensitivity for cosine grating as a function of retinal illuminance which was varied by adding neutral density filters on the display screen.

Figure 4.1 shows that contrast sensitivity without external spatial noise increased with retinal illuminance. The slope of increase with luminance was about + ½, obeying DeVries-Rose law up to about 100 photopic trolands.

The increase of contrast sensitivity in external spatial noise, on the other hand, was similar to the increase of contrast sensitivity measured without external noise up to the retinal illuminance of 10 photopic trolands. Above this luminance level contrast sensitivity in external noise was independent of retinal illuminance obeying Weber's law. The transition from the DeVries-Rose to Weber's law thus took place at lower levels of retinal illuminance in external spatial noise.

As Figure 4.1 shows, contrast sensitivity in external spatial noise was independent of retinal illuminance when contrast sensitivity was lower with noise than without. The independence of contrast sensitivity in external spatial noise is in agreement with Pelli (1990) who showed that the differences between contrast thresholds at various luminance levels disappear with increasing spectral density of external spatial noise.

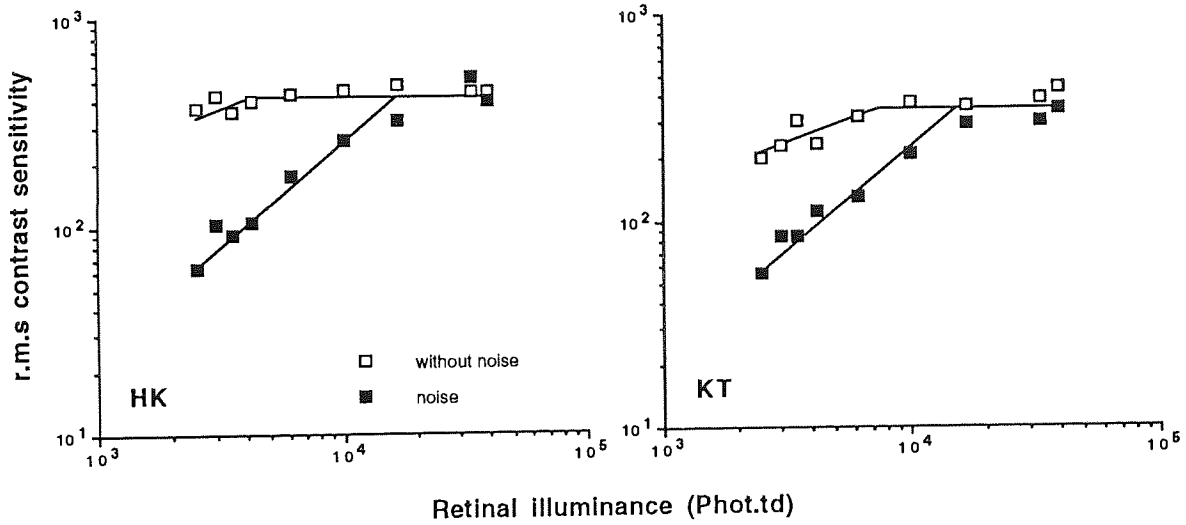

Figure 4.2
Contrast sensitivity for cosine grating as a function of retinal illuminance which was varied by adding light on the display screen.

In Figure 4.2 monocular r.m.s contrast sensitivity was measured for a vertical 4 c/deg cosine grating as a function of retinal illuminance varied by adding light onto the display screen as described above. The effect of additional light on grating contrasts was taken into account by multiplying the threshold contrast by $L_0/(L_0 + L_i)$, where L_0 is the luminance of the screen without additional light and L_i is the amount of light added onto

the screen. The corrected contrast sensitivity is plotted as a function of retinal illuminance.

Figure 4.2 shows that contrast sensitivity without spatial noise first increased with a slope between +½ and +1 indicating the transition from the DeVries-Rose law to Weber's law. After retinal illuminance of 4,000-7,000 photopic trolands contrast sensitivity then became independent of retinal illuminance obeying Weber's law.

Although contrast sensitivity in spatial noise was below contrast sensitivity without spatial noise, it increased as a function of retinal illuminance. The slope of increase was about 1. This result seems, at first, to be in disagreement with the result of Figure 4.1. The reason for this discrepancy, however, is the fact that the additional light also reduced the contrast of external noise whereas in Figure 4.1 neutral density filters did not have any effect on the contrast of the stimulus or noise. In the case of Figure 4.2, the additional light reduced the contrast of external spatial noise in inverse proportion to the increase in retinal illuminance. Noise contrast was thus halved by doubling the retinal illuminance, which explains the slope of 1, if we assume that signal-to-noise ratio is constant at threshold. The increase in contrast sensitivity with external noise continued up to 15,000 photopic trolands, after which it became similar to contrast sensitivity measured without external noise.

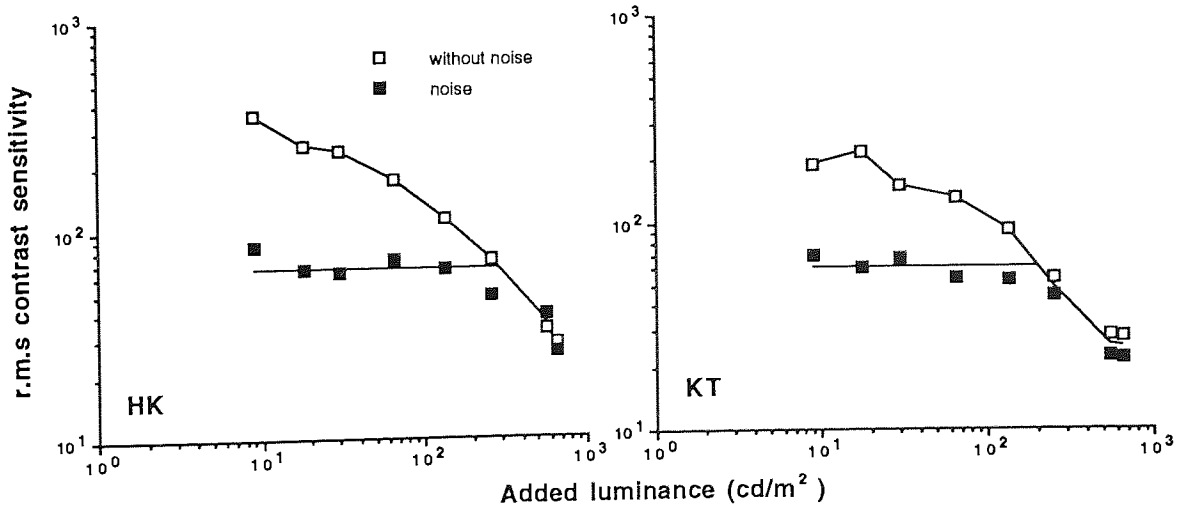

Figure 4.3
Contrast sensitivity for cosine grating as a function of the amount of light added onto the display screen.

In Figure 4.3 the effect of added light is considered as a change in external experimental conditions and its effect on contrast threshold is thus not taken into account. The "uncorrected" contrast sensitivity is plotted as a function of the amount of light added onto the screen. Contrast sensitivity without external spatial noise decreased with increasing amount of light whereas contrast sensitivity with external spatial noise remained practically constant as long as contrast sensitivity was lower with noise than without. Thereafter the decrease of contrast sensitivity was identical with and without spatial noise.

4.2.4 Discussion

The result that contrast sensitivity without external spatial noise increases with a slope of + ½ with increasing retinal illuminance shows that contrast sensitivity is predominantly determined by the quantal fluctuations of light (e.g. DeVries, 1943; Rose, 1948) or light dependent neural noise (Lillywhite & Laughlin, 1979; Lillywhite, 1981). With increasing retinal illuminance the masking effect of quantal fluctuations of light (DeVries, 1943; Rose, 1948) and light dependent neural noise (Lillywhite & Laughlin, 1979; Lillywhite, 1981) decreases. Therefore, at low levels of retinal illuminance (Figure 4.1), where the light-dependent noise is stronger than external spatial noise, contrast sensitivity is identical for gratings presented either with or without spatial noise.

Once the external spatial noise becomes the principal determinant of contrast sensitivity, sensitivity stays constant as a function of retinal illuminance (Figure 4.1). The independence of contrast sensitivity of retinal illuminance in external spatial noise can be explained by the fact that both grating and external spatial noise contrasts remained unchanged when the average luminance of the screen was reduced with neutral density filters. Constant physical signal-to-noise ratio thus kept contrast sensitivity constant.

The saturation of contrast sensitivity with increasing luminance takes place at lower levels of retinal illuminance with spatial noise than without. This is due to the fact

that when external spatial noise is stronger than internal neural noise, less light is needed to reduce light dependent noise so much that external spatial noise becomes the primary determinant of contrast sensitivity. Thus, the transition from DeVries-Rose to Weber's law means that the dominance of light-dependent noise is replaced by light-independent noise.

When higher levels of retinal illuminance were obtained by adding extra light onto the screen (Figure 4.2), contrast sensitivity without external noise first increased with luminance but soon became independent of the amount of light added to the screen. The independence of contrast sensitivity of retinal illuminance means that the effect of light-dependent noise (the quantal fluctuations of light or light-dependent internal neural noise) has become negligible and light-independent internal neural noise is the principal source of noise limiting contrast sensitivity (e.g. Nagaraja, 1964; Pelli, 1990; Watson & al., 1983).

Contrast sensitivity in external spatial noise, on the other hand, increased with a slope of 1 as long as contrast sensitivity was lower with noise than without (Figure 4.2). The increase of contrast sensitivity in external spatial noise can be explained by the fact that additional light reduced the contrast of external spatial noise. Noise contrast decreased in inverse proportion to the increase of retinal illuminance. The increase of contrast sensitivity with decreasing spectral density of external noise continues until the spectral density of external spatial noise is so much reduced by additional light that contrast sensitivity becomes predominantly determined by internal neural noise. This explains why contrast sensitivity is identical with and without external spatial noise above 15,000 photopic trolands.

When contrast sensitivity was not corrected for the amount of light added onto the screen, contrast sensitivity without external spatial noise decreased with increasing additional light. However, contrast sensitivity in external spatial noise was independent of additional light as long as contrast sensitivity was lower with noise than without. Thereafter the decrease of contrast sensitivity was identical with and without external spatial noise. The invariance of contrast sensitivity not corrected for additional light can be explained by the fact that additional light reduces both grating and spatial noise

contrasts similarly. This keeps contrast sensitivity constant until the spectral density of external spatial noise is reduced by the additional light so much that contrast sensitivity becomes predominantly determined by internal neural noise. The dominance of internal noise explains why the decrease of contrast sensitivity with increasing additional luminance is identical with and without spatial noise when there is enough additional light.

4.3 TEMPORAL INTEGRATION WITH AND WITHOUT EXTERNAL SPATIAL NOISE

4.3.1 Introduction

Temporal integration, the improvement of contrast sensitivity with increasing exposure duration, is one of the well demonstrated features of the human visual system. Irrespective of whether the gratings are stationary (e.g. Nachmias, 1967; Arend, 1976; Breitmeyer & Ganz, 1977; Legge, 1978; Rovamo, Leinonen, Laurinen & Virsu, 1984; Harris & Georgeson, 1986) or moving (e.g. Watson, 1979) the contrast sensitivity for foveally presented gratings increases with increasing exposure duration. The same has been shown to be true also for peripherally presented gratings (e.g. Rovamo & al., 1984).

All the studies that have investigated both low and high spatial frequencies, have shown that there is a difference in temporal integration between these two groups of spatial frequencies: the increase in contrast sensitivity with exposure duration saturates at shorter durations for low spatial frequencies than for high spatial frequencies.

Nachmias (1967) studied square-wave gratings at spatial frequencies between 0.44 and 33.2 c/deg and exposure durations between 11 and 500 msec. When temporal integration of spatial frequencies at 0.7 and 17.5 c/deg were compared, he found that contrast sensitivity for 0.7 c/deg grating already saturated at exposure duration approximately 50 msec whereas contrast sensitivity for 17.5 c/deg grating continued improving up to about 250 msec.

Supporting the finding of Nachmias (1967), Breitmeyer and Ganz (1977) and Legge (1978) found similar results for spatial integration of sine-wave gratings: temporal integration continued clearly over longer exposure durations for high spatial frequencies than for low spatial frequencies. Critical exposure duration at which the increase in contrast sensitivity saturated was below 100 msec for low spatial frequencies whereas for higher spatial frequencies temporal integration saturated only after approximately 200 msec exposure durations. The reason for this difference between low and high spatial frequencies is generally attributed to two different temporal mechanisms responding to

low and high spatial frequencies: a transient mechanism which is supposed to respond to stimulus on- and off-set, is most sensitive at low spatial frequencies whereas a sustained mechanism which is able to integrate contrast information over time, is more sensitive at medium and high spatial frequencies. Sustained mechanism is thus believed to cause the more extensive improvement in contrast sensitivity with increasing exposure time for high and medium spatial frequencies.

Rovamo et al. (1984) suggested another kind of explanation. They postulated that the difference between temporal integration of low and high spatial frequencies, respectively, is due to different number of cycles in the stimulus. Temporal integration for various spatial frequencies had been studied using a constant stimulus area in degrees of visual angle, which caused an increase in the number of cycles per stimulus with increasing spatial frequency. They suggested that integration time increases because the number of details increases in the stimulus. Rovamo et al. (1984), however, did not examine the effect of constant number of cycles per stimulus area on temporal integration. This was done later by Harris and Georgeson (1986) and their results disagreed with the suggestion of Rovamo et al. (1984) in favour of the sustained and transient mechanisms.

The purpose of this study was to see whether temporal integration in noise follows the rules found in experiments without external spatial noise. Identical experiments were carried out both with and without external noise. The number of cycles within a circular stimulus area was kept constant when measuring spatial integration at high and low spatial frequencies.

The variable under study was the exposure duration. The studies of Chapter 3 showed that in spatial noise the increase in pixel size along the dimension without contrast modulation increases the masking effect of pixel noise. This suggests that a similar effect should be found in the time domain. Therefore, in theory the third dimension, time, should be taken into account when calculating the spectral density of noise in this experiment. Naturally, the exposure time also affects the contrast energy of the stimulus.

4.3.2 Specific procedures

The stimuli consisted of vertical cosine gratings within a sharp-edged circular field. The spatial frequencies of 0.75 c/deg and 8 c/deg were obtained from viewing distances of 28.6 and 229 cm, respectively. Number of cycles per stimulus diameter was 20 for both stimuli. The grating area was constant at 546 deg^2 at 0.75 c/deg and 4.92 deg^2 at 8 c/deg. The screen luminance was constant at 50 cd/m^2 and viewing was binocular with natural pupils. The exposure duration varied from 16.7 to 533 msec which corresponded to 1-32 frames.

Contrast sensitivities were measured both with and without noise. For 8 c/deg grating the r.m.s. contrast of external noise (c_n) was 0.4 and the pixel area (p^2) 1.10×10^{-4} deg^2. The noise spectral density ($N_e = c_n^2 p^2 t$) thus increased from 2.96×10^{-7} to 9.43×10^{-6} $deg^2 sec$. For 0.75 c/deg grating the r.m.s. contrast of noise was either 0.15 (subject HK) or 0.10 (subject KT). The pixel size was 7.08×10^{-3} deg^2 which resulted in the noise spectral densities of 2.66×10^{-6} - 8.47×10^{-5} $deg^2 sec$ for HK, and 1.18×10^{-6} - 3.77×10^{-5} $deg^2 sec$ for KT.

4.3.3 Results

In Figure 4.4 r.m.s contrast sensitivity is plotted as a function of exposure duration for the spatial frequencies of 0.75 c/deg (Figures 4.4a and b) and 8 c/deg (Figures 4.4c and d), respectively. As Figure 4.4 shows, at the spatial frequency of 0.75 c/deg contrast sensitivity without external spatial noise increased with increasing exposure duration up to 533 msec (the longest exposure duration studied) for subject HK but saturated at around 200 msec for subject KT. At spatial frequency of 8 c/deg, on the other hand, contrast sensitivity without external spatial noise increased with increasing exposure duration up to 533 msec for both subjects.

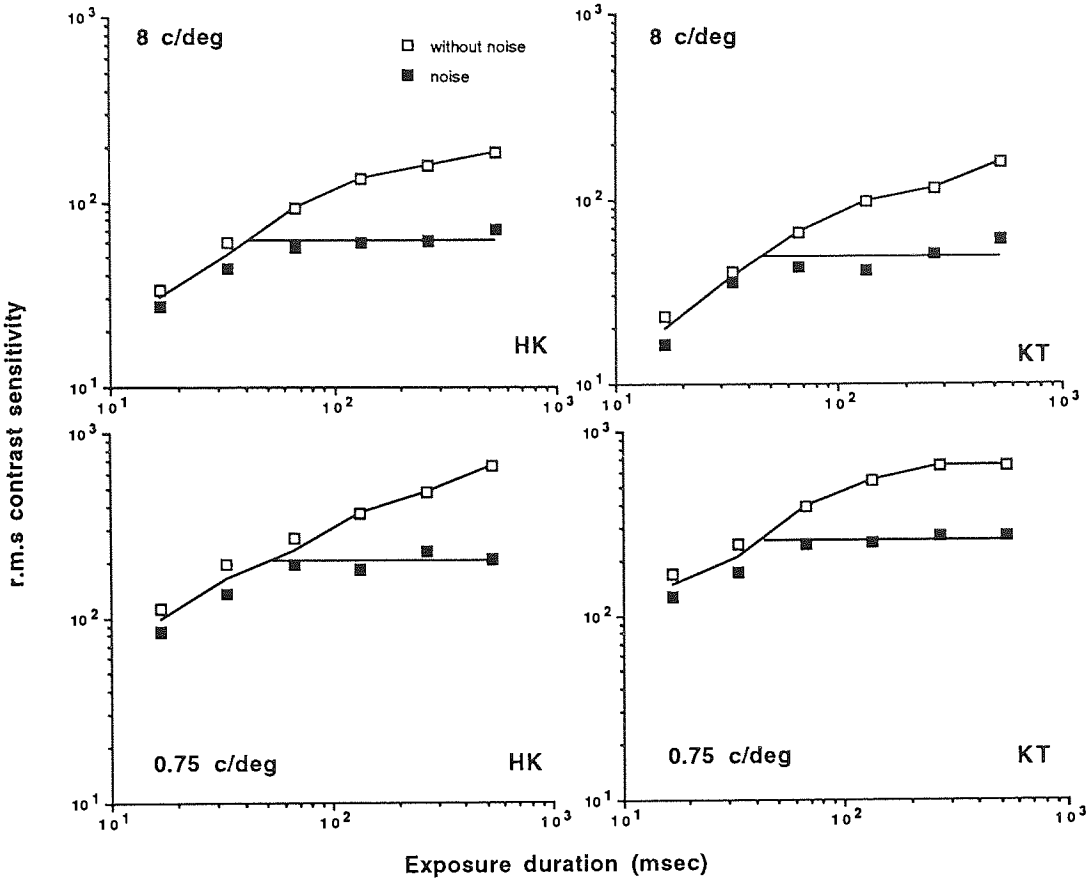

Figure 4.4
Contrast sensitivity for cosine gratings at 0.75 and 8 c/deg as a function of exposure duration.

At short exposure durations the increase of contrast sensitivity was identical with and without noise. Contrast sensitivity in external spatial noise, however, saturated at an exposure duration of 40-50 msec both for the 0.75 and 8 c/deg grating. Contrast sensitivity in spatial noise was constant for exposure durations longer than these. Contrast sensitivity in noise was thus independent of exposure duration when it was lower than contrast sensitivity measured without noise.

4.3.4 Discussion

The results that contrast sensitivity tended to increase as a function of exposure duration longer for the high spatial frequency (8 c/deg) than low spatial frequency (0.75

c/deg) grating is in agreement with studies cited above (Nachmias, 1967; Breitmeyer & Ganz, 1977; Legge, 1978; Harris & Georgeson, 1986) which demonstrated "transient behaviour" for low spatial frequencies and "sustained behaviour" for high spatial frequencies.

Although the result found here does not show as clear a difference between low and high spatial frequencies as the result of Harris and Georgeson (1986) (probably due to maximum exposure duration of only 533 msec), the obtained result supports the view of Harris and Georgeson (1986) and others, that spatial and temporal integration are separable features of the visual system (Rovamo, Luntinen & Näsänen, 1994e) and that temporal integration thus depends only on spatial frequency, not grating area.

The transient-sustained dichotomy of the visual system is thus one plausible explanation of the result. On the other hand, the fact that contrast sensitivity in noise saturated clearly earlier than without noise, and seemed to depend on the spectral density of external noise, suggests the following: if the spectral density were decreased, contrast sensitivity with noise would follow further the contrast sensitivity function measured without noise and thus saturate at longer exposure durations. This would mean that the transient behaviour of the visual system depends on the effective level of spatial noise limiting contrast detection. Therefore, it is interesting to consider alternative explanations of temporal integration in the human visual system by analysing the result obtained with external noise.

At short exposure durations contrast sensitivity increases with exposure duration similarly both with and without external noise. Contrast sensitivity is thus determined by internal neural noise. Sensitivity increases because the signal-to-noise ratio of a stationary grating in a spatio-temporal internal noise is improved by averaging across time.

At longer exposure durations, however, contrast sensitivity saturates. In external spatial noise saturation occurs at shorter exposure durations than without noise because less averaging is needed to reduce the effect of spatiotemporal neural noise so much that external spatial noise becomes the principal determinant of contrast sensitivity. Furthermore, when external spatial noise determines contrast sensitivity, the signal-to-

noise ratio of a stationary grating in stationary external noise cannot be improved by averaging across time and contrast sensitivity thus stays constant as a function of exposure duration.

The saturation of contrast sensitivity without external spatial noise could thus be explained by assuming that internal neural noise has two components: Only the effect of one component can be reduced by averaging across time. The other component, which is independent of exposure duration, becomes the determinant of contrast sensitivity at long exposures. An alternative explanation for saturation is to assume that detection is mediated by a temporal matched filter the sampling efficiency of which decreases with increasing exposure duration.

Furthermore, the constancy of contrast sensitivity in external noise indicates that signal-to-noise ratio remains constant as a function of exposure duration. In theory, this is obtained when the time domain of the stimuli is either ignored or taken into account when calculating both the contrast energy of the stimulus and spectral density of pixel noise. The results of Chapter 3, showed that in spatial domain both height and width of noise pixels has to be taken into account when calculating the spectral density of noise irrespective whether the noise was one- or two-dimensional. This suggests that the same analogy should be applied in time domain and time should thus be taken into account when calculating the spectral density of noise and contrast energy of the stimulus of the current study.

4.4 SPATIAL INTEGRATION WITH AND WITHOUT EXTERNAL SPATIAL NOISE

4.4.1 Introduction

The fact that the human visual system can integrate contrast information over space, i.e. increase its sensitivity with increasing stimulus area, has been demonstrated by numerous studies (e.g. Hoekstra & al., 1974; Savoy & McCann, 1975; Howell & Hess, 1978, Wright, 1982). An extensive review of the literature is presented in chapter 5.1 of this thesis. Therefore, only the main properties of spatial integration will be described here.

The most significant feature of spatial integration is its scale invariance: contrast sensitivity is not determined by the absolute stimulus area in degrees of visual angle, but the significant determinant is the number of details and contour in the stimulus. Contrast sensitivity thus increases with increasing number of grating cycles per stimulus up to a critical number of cycles (Hoekstra & al., 1974; Savoy & McCann, 1975; Howell & Hess, 1978). All spatial frequencies reach their maximum contrast sensitivity at approximately the same number of grating cycles.

Furthermore, Howell and Hess (1978) and Wright (1982) showed that spatial integration operates similarly also along the grating bars. When the number of cycles is kept constant and the height of grating is increased, contrast sensitivity first increases and then saturates. The critical bar length decreases with increasing spatial frequency so that the critical length is approximately constant for all spatial frequencies when it is expressed in terms of number of periods. Scale invariance thus applies also for the grating height.

In this study spatial integration was investigated as a function of grating height. Measurements were carried out both with and without external spatial noise. The physical signal-to-noise ratio was kept constant by using one-dimensional noise whose spectral density increased in direct proportion to increasing contrast energy of the grating as stimulus height was increased.

4.4.2 Specific procedures

The stimuli consisted of vertical cosine gratings within a sharp-edged rectangular field. Spatial frequency of 4 c/deg was obtained from a viewing distance of 115 cm. The width of the rectangular grating area was constant at 8 deg but its height was either 0.25, 0.5, 1, 2, 4, or 8 deg. The increase of grating area thus took place only along the grating bars. The number of cycles per grating width was constant at 32 but the height of the grating expressed in terms of the number of periods increased from 1 to 32 grating periods. The screen luminance was constant at 50 cd/m^2 and viewing was binocular with natural pupils. The exposure duration was constant at 533 msec.

Gratings were presented either without external spatial noise or had white one-dimensional spatial noise added to them. The luminance variation caused by one-dimensional noise took place only horizontally across the grating bars. The r.m.s. contrast of noise was 0.01 and pixel width 0.021 deg. Pixel height increased from 0.25 deg to 8 deg. The noise spectral density ($N_e = p_x p_y c_n^2$) thus increased in proportion to stimulus height from 5.25×10^{-7} to 1.68×10^{-5} deg^2. Because the width of the stimulus field remained constant, contrast energy of the stimulus ($E = c_{r.m.s}^2 A$; see Section 2.4) also increased in proportion to stimulus height and the signal-to-noise ratio in external spatial noise thus stayed constant as a function of stimulus area.

4.4.3 Results

In Figure 4.5 r.m.s. contrast sensitivity for the vertical cosine grating is plotted as a function of grating area.

As Figure 4.5 shows, contrast sensitivity without external spatial noise increased with the bar height and grating area. Contrast sensitivity in one-dimensional external spatial noise, on the other hand, first followed the contrast sensitivity measured without external noise, but saturated earlier. Contrast sensitivity in external noise was constant for

areas larger than 4-8 deg^2 and thus independent of grating area when contrast sensitivity was lower with noise than without.

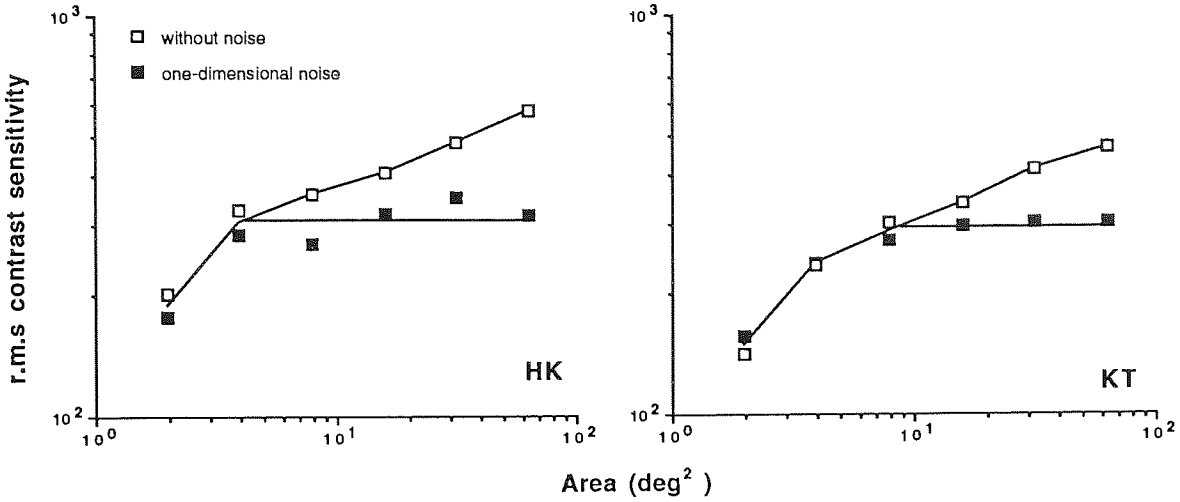

Figure 4.5
Contrast sensitivity for a cosine grating as a function of stimulus area.

4.4.4 Discussion

The result that contrast sensitivity increases with stimulus height is in agreement with Howell and Hess (1978) and Wright (1982). The fact that at small grating areas contrast sensitivity was similar for gratings both with and without external noise shows that contrast sensitivity was determined by spatio-temporal internal neural noise. With increasing grating height the signal-to-noise ratio could be improved by averaging neural noise along the grating bars. Contrast sensitivity thus increases with increasing grating height.

Contrast sensitivity in external one-dimensional noise saturates at a grating height where the averaging of spatio-temporal neural noise along the grating bars has reduced the effect of internal noise so much that external spatial noise becomes the principal determinant of contrast sensitivity. Thereafter, the signal-to-noise ratio of a cosine grating in external spatial noise cannot be improved by averaging along bars because the

luminance variation caused by the one-dimensional noise takes place only across the grating bars. Thus, the physical signal-to-noise ratio and contrast sensitivity both stay constant.

The fact that contrast sensitivity without external noise saturates with increasing grating height can be explained by assuming that internal neural noise has two components and only the effect of one component can be reduced by averaging across space. The other component, which is independent of stimulus area, then becomes the determinant of contrast sensitivity at large areas. An alternative explanation for saturation is to assume that detection is mediated by a matched filter the sampling efficiency of which decreases with increasing grating area.

4.5 CONCLUSIONS

Contrast sensitivity was measured with and without external spatial noise as a function of retinal illuminance, exposure duration, and grating area. The result showed that contrast sensitivity first increased similarly both with and without external noise as a function of the variable under study. However, for all the variables studied, contrast sensitivity with noise saturated earlier than contrast sensitivity without noise. After saturation contrast sensitivity with noise stayed constant and independent of the variable under study. We can thus conclude that when contrast sensitivity is determined by external spatial noise, it is independent of the variable under study, if the physical signal-to-noise ratio remains constant. Contrast sensitivity thus depends only on the signal-to-noise ratio.

As showed by the experiments of Chapter 3, the spectral density of one-dimensional noise has to be calculated by taking into account the whole pixel area, rather than its width (in case of vertical one-dimensional noise) only. Section 4.4 of this chapter confirms this result: When contrast thresholds were determined by external noise (i.e. they were lower with than without noise), the one-dimensional spatial noise kept contrast thresholds constant as a function of stimulus height. This suggests, that signal-to-noise ratio remained constant. However, the physical signal-to-noise ratio stayed constant as a function of grating height only when both the spectral density of pixels noise and the contrast energy of the stimulus increased similarly as a function of stimulus height. Similarly, the third dimension, time, should be taken into account when calculating the spectral density of noise. This was done in the experiments of Section 4.3, where the variable under study was time. Naturally, the time domain has to be taken into account also when calculating contrast energy thresholds for gratings. For other experiments of this Chapter the time dimension could be ignored as it was constant; unless, of course, the dependence of contrast energy threshold on spectral density of noise was to be compared between various experimental conditions. It seems that we should understand

noise pixels as three dimensional "blocks" in order to understand the masking effect of spatial noise for the visual system.

The results obtained with noise allow us to speculate about the role of internal noise as a limiting factor of contrast sensitivity. In agreement with the studies cited in the introduction, contrast sensitivity without external noise can be assumed to be limited by internal neural noise. It is generally believed that the saturation of contrast sensitivity as a function of retinal illuminance (Weber's law) is due to the fact that light-dependent noise (the quantal fluctuation of light or light-dependent neural noise) is overpowered by light-independent neural noise in the visual system. Thus, without external spatial noise the saturation of contrast sensitivity with increasing stimulus area and exposure duration could also reflect the effect of internal neural noise and/or limited areal/temporal integration.

The idea of limited extent of integration in the visual system is in agreement with the studies suggesting that the collection of information in the visual system is limited to a window of attention (e.g. van Essen & al., 1991) or sampling aperture (e.g. Burgess, 1990), and that the span of attention in each glimpse is limited to a relatively small amount of information (e.g. Verghese & Pelli, 1992). This assumption in the spatial domain is further studied in the last Chapter of this thesis by using spatial stimuli of various spatial structures. An analogous explanation could be possible for the time domain. This, however, needs further experimental work and is not under the scope of this study.

5 SPATIAL INTEGRATION IN CONTRAST DETECTION

5.1 INTRODUCTION

Spatial integration refers to the ability of the visual system to integrate visual information over space in order to improve its performance. The fact that the visual system can spatially combine information over space in order to reach a threshold decision is well known in certain particular conditions: Ricco's law defines the critical summation area within which an increasing area of a light spot produces a corresponding increase in sensitivity (e.g. Graham & al., 1939; Baumgardt, 1972). When the area of a light spot further increases, sensitivity starts to increase in proportion to the square root of the area following so called Piper's law, until sensitivity saturates as the size of the spot exceeds the maximum summation area. The vernier offset threshold, on the other hand, depends on the spatial dimensions of the stimulus (e.g. Westheimer & McKee, 1977a, b). Threshold for detection of misalignment of two vertical lines is dependent on the length of lines. Threshold decreases up to a critical line length, after which it stays constant.

In grating detection, as opposed to light spots, the increase in the absolute stimulus area is not the critical attribute determining contrast sensitivity for gratings. Instead, contrast sensitivity to a grating is determined by an increase in the number of grating bars irrespective of the stimulus area in square degrees of the visual field: contrast threshold for grating stimuli decreases as the number of bars in the stimulus, or their length, increases (Findlay, 1969; Hoekstra & al., 1974; McCann & al., 1974; Savoy & McCann, 1975; Estévez & Cavonius, 1976; Howell & Hess, 1978; Robson & Graham, 1981; Virsu & Rovamo, 1979; Rovamo & al., 1993). Accordingly, if the number of grating bars and stimulus shape is kept constant by decreasing spatial frequency while increasing the grating area, contrast sensitivity stays constant. This property of the visual system to integrate contrast information across space is here called spatial integration.

5.1.1 Spatial integration of foveal grating stimuli

Several studies have investigated spatial integration of foveally presented grating stimuli. Findlay (1969) studied the effect of the grating size on contrast at detection threshold for gratings at spatial frequency of 30 c/deg. He showed that there was a 30-40% decrease in threshold contrast when the number of grating bars increased from 6 to 28. He concluded that the visual system could integrate information up to about 12 cycles at spatial frequency of 30 c/deg.

Some other studies have extended the investigations over a larger range of spatial frequencies. Hoekstra et al. (1974), McCann et al. (1974), and Savoy and McCann (1975) concentrated to low spatial frequencies and concluded that the number of grating bars played a dominant role in determining the threshold for low spatial frequencies.

Hoekstra et al. (1974) investigated the relationship between luminance and the minimum number of cycles necessary for maximum sensitivity. They studied the range of spatial frequencies from 2 to 7 c/deg at high luminance level (165 cd/m^2) and found that contrast sensitivity saturated for all spatial frequencies when the number of cycles exceeded 8 cycles. In addition they studied spatial integration of the grating at 2 c/deg using luminance levels of 2-600 cd/m^2 and concluded that the critical number of grating bars increased with increasing luminance approximately from 3 to 8 cycles. However, a contradicting result was recently obtained by Rovamo et al. (1994c) who showed that contrast sensitivities for grating stimuli with spatial frequencies from 0.5 to 32 c/deg saturated at a constant number of grating cycles irrespective of the retinal illuminance which varied over 8 logarithmic units. This result suggests that spatial integration is similar at all luminance levels.

McCann et al. (1974) and Savoy and McCann (1975) examined the effects of the luminance of the surround of the grating, viewing distance, and the observers task. They found that irrespective of the parameters mentioned above, the number of grating bars in the stimulus was the critical determinant of contrast sensitivity.

Furthermore, Hoekstra et al. (1974), and Savoy and McCann (1975) showed that there was no low-frequency drop in contrast sensitivity function when the stimulus contained at least the critical number of cycles. They concluded that the low frequency drop of contrast sensitivity function is entirely due to a decrease in the number of cycles used. Estévez and Cavonius (1976) and later on other studies using extensive number of cycles in the grating stimuli (Howell and Hess, 1978; Robson & Graham, 1981; Virsu & Rovamo, 1979; Rovamo & al., 1993) showed that this conclusion was too hasty. As a result, it was recognised that even when the number of grating cycles is sufficient, there is a small decrease in contrast sensitivity at low spatial frequencies possibly due to the neural interactions (lateral inhibition) in the visual system.

In spite of the original motive of these early studies concerning the effect of the number of cycles on the grating visibility at low spatial frequencies, they raised a more general question of the basis of the relationship between spatial extent of the grating and its detection threshold. Howell & Hess (1978) investigated the functional area of the foveal visual field over which the spatial integration at threshold occurs by using stimuli with various numbers of grating cycles and various grating bar lengths. They found that detection sensitivity for gratings with various spatial frequencies and constant bar length increased until the critical number of 10 grating cycles was achieved. Furthermore, they results showed that the critical length of the grating bars also varied with spatial frequency. When the bar length was plotted as a relative measure, indicating their length as a number of grating periods, the critical length seemed to vary between 10 to 16 grating periods for all spatial frequencies studied. Similar result was later obtained by Wright (1982), who found a critical bar length of 7-14 sinusoidal periods.

5.1.2 Spatial integration in peripheral vision

The obvious question that rises when contrast sensitivity is studied as a function of increasing stimulus area is how the results are affected by the contribution of the

extrafoveal areas of the visual field. It is a well established fact that contrast sensitivity and visual acuity decreases as a function of eccentricity (e.g. Harvey & Pöppel, 1972; Pöppel & Harvey, 1973) but only a couple of studies have addressed the question of spatial integration in the periphery of the visual field (Robson & Graham, 1981; Pointer & Hess, 1989 and 1990).

Robson and Graham (1981) compared spatial integration of gratings in various parts of the visual field to the overall contrast sensitivity on these areas. They used Gaussian windowed grating patches consisting of a constant number of cycles and spatial frequencies of 3-24 c/deg. When a grating patch was moved away from the fovea in a vertical direction by an amount equal to 0-32 grating periods, they found that contrast threshold was first constant and then gradually increased. However, when the location of a grating patch was changed along a horizontal line situated 42 grating periods above the fixation, contrast threshold stayed approximately constant over the range of eccentricities studied. At corresponding retinal locations the extent of spatial integration was determined from these results: in the near periphery contrast sensitivity first increased with increasing number of grating cycles but then saturated. In the far periphery spatial integration did not saturate at all but seemed to operate over the maximum number of cycles used. The critical number of cycles in the fovea was about 8 cycles.

In accordance, Pointer and Hess (1989, 1990) showed that contrast sensitivity decreased as a function of eccentricity across all main meridians (horizontal, vertical and oblique) linearly when the eccentricity was expressed in terms of number of grating cycle. However, the slope of the decrease depended on spatial frequency being greater the higher the spatial frequency even when the eccentricity was expressed in relative units (i.e. grating periods). Furthermore, in disagreement with Robson and Graham (1981), their experiments showed that spatial integration saturated at the same number of grating cycles (3-4 cycles) both in fovea and in the far periphery (20-50 deg) for the spatial frequencies studied (3.2 and 0.8 c/deg). Similar result has been reported by Rovamo et al. (1993), who compared spatial integration of 0.5 c/deg grating at the fovea and at the eccentricity of 30 deg.

5.1.3 Scale invariance of spatial integration

According to the studies above, detection of a stationary spatial stimulus has two main properties in fovea and probably also in periphery: scale invariance and limited spatial integration. Limited spatial integration is reflected by the fact that with increasing stimulus area contrast sensitivity first increases but then saturates. Scale invariance, on the other hand, is demonstrated by the fact that it is not the absolute stimulus area in degrees of visual angle, but the number of cycles (or the amount of contour and detail) in the image, that determines detection threshold. This means that neither magnification nor the viewing distance affects the detectability of the grating (as long as the effect of the eye's optics and sampling limitations of the retina are negligible).

Virsu and Rovamo (1979) introduced a measure of grating area which captured the property of scale invariance: a square cycle. A square cycle refers to a unit area of grating in which each side is equal to the length of one spatial period. When Virsu and Rovamo (1979) plotted contrast sensitivity as a function of the number of square cycles it increased similarly for all spatial frequencies (1-32 c/deg) and saturated at an approximately constant number (144) of square cycles corresponding to an area of 12 grating cycles in height and width. Approximately similar result was later achieved by Rovamo et al. (1993) showing that the critical number of square cycles was 114 (about 11 grating cycles) for spatial frequencies from 0.65 to 32 c/deg.

The number of square cycles in a grating having an area A and spatial frequency f is calculated by multiplying area with the spatial frequency squared (Af^2). When the number of square cycles in a grating is constant, the grating is large in area at low spatial frequencies and small in area at high spatial frequencies, but in both cases the grating contains the same amount of detail and contour.

The number of square cycles does not depend on the unit of measurement. For a grating in a square window, the number of square cycles equals to the squared number of cycles per stimulus. A number of square cycles increases with increasing number of grating bars. In addition, the viewing distance or magnification of a stimulus does not

affect the number of square cycles: when a grating is viewed further away, the magnification of the stimulus and stimulus area decreases, but the corresponding increase of spatial frequency keeps the number of square cycles constant.

The concept of the number of square cycles has also an advantage over the number of cycles because it takes into account the height of the stimulus. As Howell and Hess (1978), and Wright (1982) showed, both the width and the height of the grating stimuli had an effect on its detection threshold. The number of square cycles increases irrespective of whether the stimulus area is increased in horizontal or vertical direction. Consequently, two grating stimuli consisting of an equal number of square cycles might differ in shape: stimulus window might be a square or a circular in shape, or the grating consisting of only a few long bars can have a same number of square cycles than one consisting of several short bars.

According to Rovamo (1993; personal communication), however, the spatial integration of strongly elongated stimuli does not quite follow the integration function measured using square shaped grating stimuli. Spatial integration of elongated stimuli seems to extend over a larger area than simple circularly symmetric area of spatial integration would predict. The area of spatial integration can thus be adaptive in shape depending on the stimulus characteristics.

According to the studies cited above, spatial integration of stationary grating stimuli at threshold seems to be limited to a square area of about 10 grating cycles per side. In terms of contrast detection this means that detection threshold decreases when stimulus size is increased up to about 10 grating cycles of width or height, after which the decrease ceases. Scale invariance and limited spatial integration has also been found at suprathreshold contrasts. Jamar and Koenderink (1983) measured detection of amplitude and frequency modulation of carrier gratings having contrast eight times their threshold contrast. The detection threshold for amplitude and frequency modulation decreased as a function of the number of cycles of the carrier frequency up to 16 cycles irrespective of the number of modulation cycles within the grating area.

5.1.4 Areal integration in spatial noise

It is generally believed that the signal-to-noise ratio at the detection threshold is constant (e.g. Cornsweet, 1970, see also chapter 3). When this approach is applied to spatial integration, it suggests that because the signal-to-noise ratio of a regular pattern, such as a grating, will increase as the size of a pattern is increased (contrast energy of the stimulus increases whereas the spectral density of spatiotemporal internal neural noise stays constant), it results in a decrease in the detection threshold.

On the other hand, contrast sensitivity to grating stimuli is not affected by viewing distance (e.g. Savoy & McCann, 1975; McCann, 1978; Rovamo & al., 1992) provided that spatial frequency is not so high that detection is attenuated by the point spread function of the eye's optics (e.g. Deeley & al., 1991) or sampling limitations of the retina (e.g. Curcio & al., 1987). This suggests that the signal-to-noise ratio at detection threshold is not affected by the stimulus area when the number of details in the stimulus is constant.

Rovamo et al. (1992) have pointed out that contrast sensitivity for gratings both with and without external two-dimensional spatial noise behaves similarly as a function of viewing distance: Contrast sensitivity for a grating without spatial noise is first constant and then decreases. Accordingly, in external noise contrast sensitivity stays constant irrespective of viewing distance as long as sensitivity is lower with noise than without. After this point, due to the optical filtering of the eye, contrast sensitivity decreases similarly for stimuli both with and without noise. The independence of contrast sensitivity of viewing distance in noise suggest, that also in spatial noise spatial integration of gratings is dependent on the number of grating cycles.

The results of Coltman and Anderson (1960) support this result by showing that detection threshold for a grating pattern in white noise did not change over a large range of viewing distances. Furthermore, they showed that the number of cycles determines spatial integration also in external noise: the critical number of 7 cycles, suggested by

Coltman and Anderson (1960), is in good agreement with the studies performed without spatial noise.

Using a somewhat different approach, Van Meeteren and Barlow (1981) measured detection efficiency for gratings created by modulating the density of random dots and found that spatial integration extended up to a grating width of 5 cycles. Detection efficiency indicates "how well" a human observer performs when compared to the ideal observer (this will be explained in more detail in Section 5.2). Constant detection efficiency as a function of stimulus area therefore means complete spatial integration. Best efficiencies for gratings were found with only one cycle, but there was only a small difference between 1 and 5 cycles. For 15 cycles the efficiency was much lower, however.

The study of Kersten (1984) showed that in one-dimensional spatio-temporal noise spatial integration of vertical cosine gratings (with Gaussian temporal and horizontal spatial window) extended only up to one cycle whereas without external noise integration saturated at about 4 - 8 cycles. The disagreement of this result with others obtained might be due to the fact that noise varied only in one spatial dimension. In no noise condition detection threshold is determined by two-dimensional spatiotemporal internal neural noise and therefore comparison between noise and no-noise condition may not be straightforward.

The study of Luntinen et al. (1994) is the most comprehensive investigation of spatial integration of gratings in two-dimensional noise. They measured areal integration for spatial frequencies of 0.125 - 16 c/deg using several levels of noise spectral density. According to their results the spatial integration saturated approximately at the same number of cycles (about 8.5 cycles) irrespective of the spectral density of external noise. This suggests that spatial integration operates similarly irrespective of whether external noise is added or not - the dominance of internal neural noise, which limits detection without external spatial noise, is just replaced by the dominance of external spatial noise in the noise condition. The detection threshold in the presence of external noise is in fact limited both by internal and external noise (external noise does not "eat" internal neural

noise away), but when the masking power of the external noise is great enough the effect of internal noise is negligible and the detection threshold seems to be determined by external noise added to the stimulus.

5.1.5 Spatial integration of complex patterns

There are only very few studies concerning spatial integration of complex spatial patterns. One study investigating spatial integration of compound grating stimuli was done by Rovamo et al. (1994d). They studied spatial integration of compound gratings consisting of various numbers of simple gratings of the same spatial frequency and phase but of different orientation. The orientation difference between grating components (simple cosine gratings) was 180/n where n was the number of components and varied from 1 to 16. When the number of orientation components increased from one to six, the critical area decreased due to increasing complexity of stimulus structure. However, with more than six orientation components, the critical area started to increase although the number of components increased. This was suggested to be due to the fact that when the number of components exceeded six, the compound grating started to resemble a circular grating in the middle of the stimulus, the area of which increased with increasing number of components, thus making the stimulus simpler and more regular in structure. Therefore, their findings supported the view that the area of spatial integration is determined by the amount of contour and detail within a stimulus (Virsu & Rovamo, 1979).

The problem that will be faced with stimuli more complex than simple gratings is the definition of the amount of contour and detail. For gratings, it can be defined in terms of grating bars, or like Virsu and Rovamo (1979) suggested, in terms of the number of square cycles. However, such a measure might be problematic to define for more complex stimuli with broad spatial frequency bandwidth and ambiguous stimulus area. The purpose of this last chapter of my thesis is to study spatial integration when more complex stimuli

are used and develop new measures for the amount of contour and detail (image complexity).

When detection of complex images are studied, we have to solve the problem of how to take into account the filtering properties of the human visual system: the optical and neural filtering does not affect all the stimulus components similarly especially if the stimulus consists of a large variety of spatial frequencies.

A way to overcome this problem is to use sufficient external noise in the detection task: When the external noise used is great enough in comparison to the internal noise in the human visual system (See Chapter 3), detection threshold of the observer is determined by the ratio of signal's energy and the spectral density of external noise. The effect of the human optical and neural transfer functions can be omitted when using external noise, because the filtering properties of the visual system have the same effect on both the signal and noise at each spatial frequency. For example, for a compound grating consisting spatial frequencies of 0.5 and 6 c/deg, the optical and neural filtering of the visual system affects the two components differently. However, if the compound grating is presented in external visual noise, the filtering affects the spatial frequency components of both grating and noise similarly and therefore, the signal-to-noise ratio, which determines the threshold, is similar before and after filtering. As a result, the signal-to-noise ratio stays constant across the spatial frequency spectrum of the image and the detection threshold is not affected by the filtering.

Another advantage obtained by using external noise is that we know the magnitude of the noise that limits the performance of human observer and a theoretical ideal detector. Therefore, human performance can be compared with the ideal one and this sets the baseline for human performance.

5.2 MEASURING HUMAN EFFICIENCY IN DETECTION TASK

5.2.1 Ideal performance in a signal-known-exactly task

Ideal performance (or detector) serves as an absolute standard of reference by which human performance can be evaluated. In other words, it sets the maximum limit to the performance.

There is no single ideal detector: in any visual task the ideal performance depends in a complex way on the signal and noise properties, the nature of the task and the amount of a priori information about signal parameters (Green & Swets, 1966). The simplest case of definition of an ideal performance is the one where signal is known exactly. My introduction to the ideal performance will concentrate on this specific case because it was applied to the analysis of the data of this thesis. All the data was collected using an experimental procedure that minimised the subject's uncertainty of the signal: each threshold determination began at a clear suprathreshold contrast, usually the model stimulus was provided simultaneously with the stimulus, the place were the stimulus was to appear was clearly indicated, and so forth. (See chapter 2.3).

An ideal performance in a pattern detection task, where the signal is known exactly and signal is presented in white noise, is to cross-correlate the signal plus noise with the copy of the signal (Tanner & Birdsall, 1958). Because there is no uncertainty as to the signal to be detected or where the signal will appear, cross-correlation gives the best possible signal-to-noise ratio and thus ideal performance in this particular condition. When the signal is cross-correlated using a copy of itself, all the signal energy is collected whilst noise is only collected within the signal bandwidth.

According to the *Signal detection theory* the detection threshold for any detector is determined by the signal-to-noise ratio, which is believed to be constant at threshold. In the case of ideal detector, which has no intrinsic noise, threshold is only limited by the external noise added to the stimulus. Visual noise is composed of random values of

luminance in one or two spatial dimensions, as in my thesis, and/or time. When the random luminance variation of noise has a Gaussian distribution, noise is called Gaussian noise.

The definition of ideal performance in *Signal detection theory* is based on the Gaussian nature of the noise that limits the performance of the ideal detector (Green & Swets, 1966). Therefore, in order to be able to compare the ideal and human performances, we have to try to ensure that the external noise presented in the detection task has a Gaussian nature also after filtering and pooling in the visual system. According to the central limit theorem, the sampling distribution of the mean will be Gaussian regardless of the sample size, when the population is itself Gaussian. Therefore, Gaussian distributed external noise remains Gaussian distributed regardless of the filtering properties of the visual system.

In this thesis the noise used was two-dimensional static noise with a Gaussian distribution and zero mean which means that noise did not change the mean luminance of the stimulus. There was random luminance variation in both spatial dimensions but no variation in time. External noise (N_e) is characterised by its spectral density. For white noise the spectral density is calculated by multiplying the squared r.m.s. contrast of noise with the pixel area (i.e. the area of one noise sample) (Legge & al., 1987; see also chapter 3.1.2).

According to the above, the ideal detector in the experiments presented in this thesis is the Matched Filter (Green & Swets, 1966; Hauske, Wolf & Lupp, 1976) which performs cross-correlation of the signal plus noise with a copy of the signal. Response (R) of a detecting filter is given by

$$R = \int\int m(x,y)\, s(x,y)\, dx\, dy, \qquad (5.1)$$

where m(x,y) is the detection filter and s(x,y) is the signal. In the case of the Matched Filter, the detection filter equals to the signal. Therefore equation (5.1) can be presented in the form

$$R = \int\int s^2(x,y)\,dx\,dy, \tag{5.2}$$

which equals the energy of the signal (E).

External noise causes variance in the response of a detector. The spectral density of external noise (N_e), on the other hand, represents the variance of the random luminance values at each spatial frequency (See Section 3.1). For the Matched Filter the variance in the response (σ_n^2) caused by external noise takes place at the spatial frequencies within the filter (i.e. equal to the signal). The variance is thus

$$\sigma_n^2 = N_e \int\int |M(u,v)|^2\,du\,dv, \tag{5.3}$$

where M(u,v) is a Fourier transform of the detection filter. Because the Matched Filter equals the signal, its Fourier transform can be replaced by the Fourier transform of the signal [S(u,v)]

$$\sigma_n^2 = N_e \int\int |S(u,v)|^2\,du\,dv. \tag{5.4}$$

According to Parceval's Theorem

$$\int\int |S(u,v)|^2\,du\,dv = \int\int s^2(x,y)\,dx\,dy. \tag{5.5}$$

We therefore get

$$\sigma_n^2 = N_e \int\int s^2(x,y)\,dx\,dy = N_e E. \tag{5.6}$$

The signal-to-noise ratio at threshold for the ideal detector in the signal-known-exactly task is therefore

$$\frac{R^2}{\sigma_n^2} = \frac{E^2}{N_e E} = \frac{E}{N_e} = d'^2, \tag{5.7}$$

where E is the energy of the signal and thus the energy threshold for the ideal detector (E_{ideal}), N_e is the two-sided spectral density (consisting of both positive and negative frequencies) of external white Gaussian noise, calculated by multiplying the squared r.m.s

contrast of noise by the size of noise pixel. d' is the detectability index (Tanner and Birdsall, 1958). The energy threshold for the ideal detector is thus given by

$$E_{ideal} = d'^2 N_e. \tag{5.8}$$

The value of the detectability index (d') depends on the nature of the task (Elliot, 1964) and its calculation is based on the probability level at which ideal detector performs the given task. The threshold estimation algorithm used in this thesis gives threshold estimates at the probability level of 0.84 of correct responses in a two-alternative forced-choice task. From Elliot's (1964) forced-choice tables, the value for d' is 1.4. Thus d' squared is 2. The energy threshold for an ideal detector in this study was thus

$$E_{ideal} = 2 N_e \tag{5.9}$$

5.2.2 Human detection efficiency

The human performance in a signal-known-exactly task is limited by the total noise spectral density within the spatial frequency range of the stimulus. It consists of internal (N_i) and external (N_e) noise. Because the signal-to-noise ratio at detection threshold is, however, possibly signal dependent, the energy threshold (E_{human}) is equal to the sum of internal (N_i) and external (N_e) two-sided noise spectral densities weighted by a stimulus dependent parameter (k) (e.g. Legge & al., 1987):

$$E_{human} = k(N_i + N_e) = kN_i + kN_e. \tag{5.10}$$

Spectral densities N_i and N_e are the variances of internal (when back-projected into the visual field) and external noises per unit of spatial frequency, respectively. They are additive because the variance of the sum of two independent random variables is equal to the sum of their variances (Variance sum law). The constant k, on the other hand, is related to the efficiency with which the observer samples the available stimulus

information. For the time being, let us ignore the implication of the constant k, and return to it later in this Section.

If there is no external noise, the threshold energy is equal to kN_i. The term kN_i can thus be replaced by the energy threshold measured without external noise (E_0):

$$E_{human} = E_0 + kN_e. \tag{5.11}$$

If the effect of external noise is large compared with the effect of internal noise and thus $kN_e >> E_0$ we can write

$$E_{human} = kN_e. \tag{5.12}$$

In this thesis, where the notation of detection efficiency is used, the r.m.s. contrast threshold in noise was always at least 3 times the r.m.s. contrast threshold without noise. Then, the contrast energy being a squared value of r.m.s. contrast (see chapter 2.4 of this thesis), the contrast energy threshold with noise (E_{human}) was at least 9 times the energy threshold without noise (E_0). Hence, the contribution of internal noise in the equation (5.11), and the error in equation (5.12) is less than 11%.

The efficiency (η) of the observer compared with the ideal detector is given by the ratio of energy thresholds for the ideal detector and the real detector (Tanner and Birdsall, 1958). Thus,

$$\eta = \frac{E_{ideal}}{E_{human}}, \tag{5.13}$$

where E_{ideal} and E_{human} are the energy thresholds for the ideal and human detectors in the presence of external noise N_e. From the previous Section (5.2.1) we get $E_{ideal} = 2\ N_e$. Thus, in these experiments

$$\eta = \frac{2N_e}{E_{human}}, \tag{5.14}$$

where E_{human} is the energy threshold measured experimentally in the presence of excessive external noise N_e.

Let us now return to the implications of the constant k in the equation (5.10). When there is no external noise limiting the performance, then $N_e = 0$ and

$$k = \frac{E_{human}}{N_i}, \tag{5.15}$$

from which we obtain

$$\frac{k}{d'^2} = \frac{E_{human}}{d'^2 N_i} = \frac{1}{\eta}. \tag{5.16}$$

Thus

$$\eta = \frac{d'^2}{k}. \tag{5.17}$$

Hence, the greater the value of k the lower the efficiency which here reflects a failure by the observer to collect all the available information. Note that k is always equal or greater than d'^2 because the maximum efficiency is 1.

5.3 SPATIAL INTEGRATION OF COMPLEX IMAGES WITH A SIMPLE SPATIAL FREQUENCY SPECTRUM

As explained above, the main determinant of contrast sensitivity with increasing stimulus area is a relative rather than an absolute area of the stimulus (e.g. Hoekstra & al., 1974; Howell & Hess, 1978; Robson & Graham, 1981; Virsu & Rovamo, 1979; Rovamo & al., 1993). For grating stimuli this means that in order to keep the effect of spatial integration constant at detection threshold the number of grating bars and stimulus shape has to be constant.

Virsu and Rovamo (1979) first introduced a scale invariant formula for relative stimulus area for grating stimuli - a square cycle (Af^2). A square cycle is a square shaped area, the side length of which equals to the wavelength of a grating. It is obtained by multiplying stimulus area (A) with spatial frequency squared (f^2). The measure of square cycles does not depend on the unit of measurement, magnification of the stimulus or the viewing distance used.

In this study the concept of square cycles was tested with a more complicated stimulus structure than a simple grating. The stimulus used had a single radial spatial frequency and a randomised phase. Although the stimulus structure is very complex, the notion of spatial frequency and stimulus area is straightforward, and therefore, the number of square cycles is applicable.

5.3.1 Methods

The apparatus, stimulus generation, and threshold determination is explained in detail in the second chapter of this thesis. Therefore, the reader is asked to refer Chapter 2 for description of the above. Apparatus 2 was used in this experiment.

Stimuli

Horizontal cosine gratings were used as control stimuli for more complicated two-dimensional narrow-band random stimuli with the same radial spatial frequency. The spatial frequencies of the cosine gratings and the radial spatial frequencies of the random stimuli were 0.186, 0.372, 0.744, 1.49 and 2.98 c/cm on the screen. From viewing distances of 77, 154, and 308 cm the spatial frequencies studied ranged from 0.25 to 16 c/deg. The size of the square shaped stimulus window was 5.38 x 5.38 cm^2 for both stimuli. The number of cycles per stimulus were thus 1, 2, 4, 8, and 16 and the number of square cycles 1, 4, 16, 64, and 256, respectively.

The random stimuli were produced by using the inverse of the two-dimensional discrete Fourier transform of a very narrow-band annular amplitude spectrum. The annular amplitude spectrum consisted of discrete samples of a cosine function of one cycle width along the radial spatial frequency. The radial spatial frequency is $f_r = (f_x^2 + f_y^2)^{1/2}$, where f_x and f_y are the spatial frequencies along the horizontal and vertical frequency axes, respectively. An example of the Fourier spectra of a cosine grating and a corresponding random image are shown in Figure 5.1.

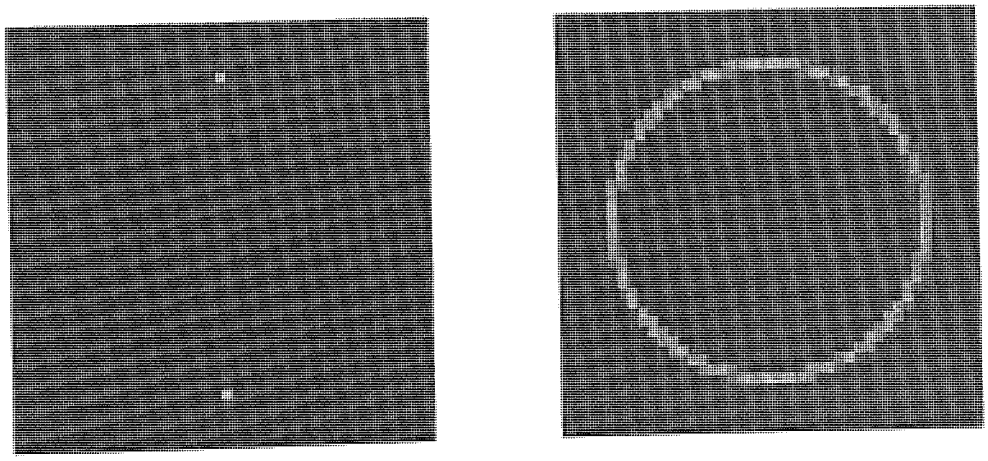

Figure 5.1
Fourier spectra of a cosine grating and a random image used in the study.

The phase spectrum of the random stimuli were obtained from a phase spectrum of a noise waveform. Noise waveform was produced by adding a random number with zero mean to each picture element. Random stimuli thus consisted of one spatial frequency, all orientations and random phase. Figure 5.2 shows grating and random stimuli with 1, 16, and 256 square cycles.

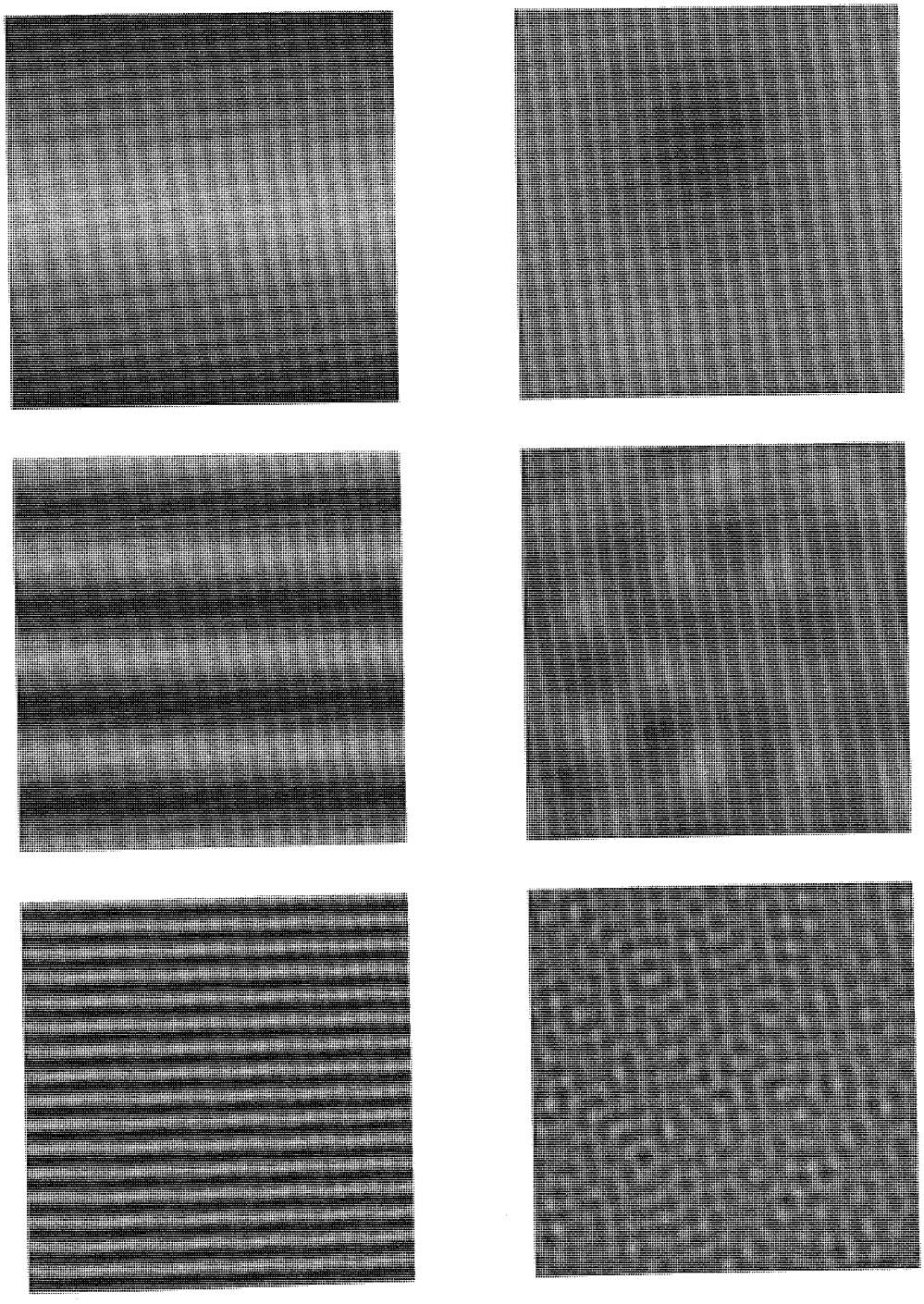

Figure 5.2
Horizontal gratings and random stimuli consisting of 1, 16, and 256 square cycles.

Contrast energy thresholds were measured in two-dimensional, white spatial noise. Noise was produced by adding a normally distributed random number with zero mean to each picture element. The Gaussian distribution of random numbers was truncated at 2.5 times the standard deviation on both sides of zero. The values of the random numbers in the neighbouring pixels were uncorrelated. Thus, the two-dimensional pixel noise was white up to the cut-off frequency determined by the pixel size. The pixel size on the screen was 0.042 x 0.042 cm^2 resulting in the cut-off frequency of 11.9 c/cm on the screen (f_c = 1/2p; See Section 3.1.1 for more details). Hence, noise was white in the frequency range of our stimuli.

The spectral density of white pixel noise is the product of noise r.m.s. contrast (c_n) squared and the pixel area (p^2): $N_e = c_n^2 p^2$, where the r.m.s. contrast (c_n) is the standard deviation of the local contrasts of noise (Section 3.1.2). In our experiments the r.m.s. contrast of noise was 0.3. The pixel area varied from 9.77 x 10^{-4} to 6.10 x 10^{-5} deg^2 depending on the viewing distances used. Thus, the noise spectral density (N_e) varied from 8.79 x 10^{-5} to 5.49 x 10^{-6} deg^2. Control experiments confirmed that the external noise added to the stimulus produced at least three-fold reduction of contrast sensitivity in comparison to the no-noise condition. The noise spectral density was thus great enough to ensure that external noise was in practice the only noise source limiting visual performance.

Each trial during the experiments consisted of three rectangular stimulus windows shown simultaneously side by side. The size of each window was 5.38 x 5.38 cm^2 (128 x 128 image pixels) and their inter-centre distance was 7 cm. The stimulus windows were surrounded by an equiluminous homogenous field. An example of the screen in one experimental trial is shown in Figure 5.3.

The window in the middle of the screen contained a copy of the signal without noise. This model signal was used to minimise the observer's uncertainty of the stimulus to be detected. On both sides of the model there was a window containing noise. One of the noise windows also contained the signal to be detected. The contrast of the model

signal was always twice the contrast of the signal in noise. This ensured that the model signal was clearly visible even at the threshold of the signal to be detected.

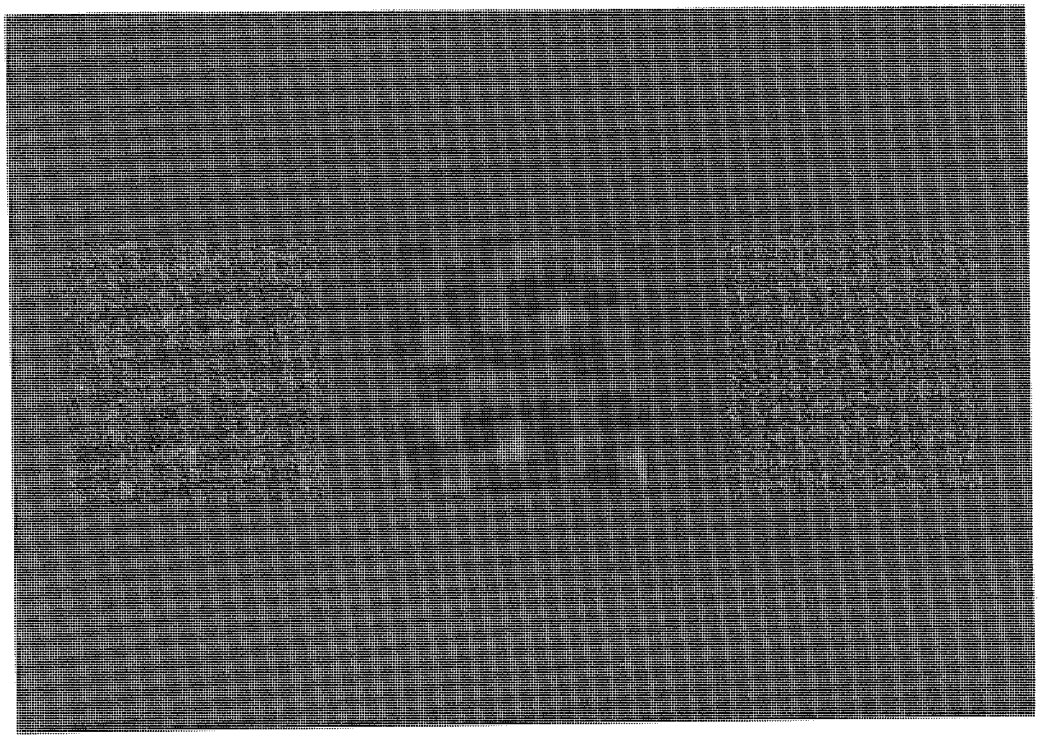

Figure 5.3
A stimulus of one experimental trial in a two-alternative forced-choice task of the study.

The stimuli were computed and stored on a hard disk. There were ten stimuli with different noise samples at each contrast level. In five of them the signal was on the left side and in the other five on the right side. For each trial one of the ten stimuli was chosen at random for presentation. A different set of ten noise sample pairs (2 noise windows in each stimulus) had been generated for each contrast level. In the experiment about 15 contrast levels were used for measuring a single threshold. Thus, the total number of different noise samples available was about 300 per threshold.

In the experiments we measured contrast energy thresholds with a probability level of 0.84 using the two-alternative forced-choice algorithm. Results are expressed both

in terms of contrast energy thresholds and detection efficiencies. For detailed descriptions refer to Sections 2.4 and 5.2.

Procedure

Detection thresholds were determined by using a standard two-alternative forced-choice procedure: The stimuli were viewed binocularly with natural pupils (diameter 5-6 mm). The observer had an unlimited viewing time to indicate in which of the two noise windows the stimulus was. The response terminated the presentation and started a new trial. An auditory feedback was given to indicate the incorrectness of the response. For more details, please refer to the Section 2.3.

Subjects

Two experienced subjects (HK and RN) served as observers. HK (aged 28 years) was an uncorrected hyperope (+0.5 DS oa.) with binocular Snellen acuity of 1.5 and RN (aged 41 years) was a corrected myope (-4.25 DS oa.) with binocular Snellen acuity of 2.0.

5.3.2 Results

In Figure 5.4 contrast energy sensitivity, reciprocal of contrast energy at threshold, is plotted as a function of the number of square cycles (Af^2) for the horizontal gratings (5.4a) and random stimuli (5.4b) of various sizes. The various stimulus areas were obtained by using the viewing distances of 77, 154 and 308 cm. The range of spatial frequencies measured is indicated at the end of each curve. Both figures show the

results for two observers. Each data point is a geometric mean of three threshold estimates measured with different sets of noise samples.

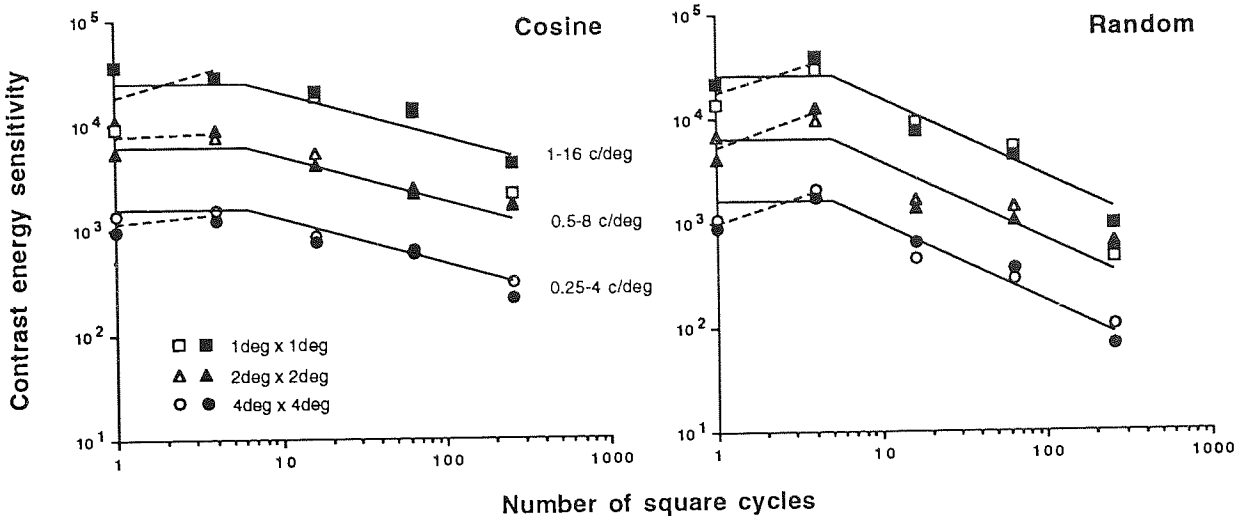

Figure 5.4
Contrast energy sensitivity as a function of the number of square cycles for cosine gratings and random stimuli for two subjects. Solid and open symbols refer to RN and HK, respectively.

The results for the two observers are almost identical. The solid lines were fitted to the whole data of each frame of Figure 5.4: when contrast energy thresholds were expressed in terms of cm^2 on the screen and sensitivities (S) were then plotted as a function of the number of square cycles (N), the data for each frame practically superimposed. Horizontal line corresponds to average of the horizontal part of the data. Least squares line of the form $\log S = a \log N + b$ was fitted to the decreasing part of the data. The solid lines in each frame of Figure 5.4 were obtained by converting contrast energy sensitivities back to the units of the visual field. The dotted lines from one square cycle to four square cycles were drawn on the basis of the geometric means of two observers for each curve separately.

Figure 5.4 shows that for all stimulus sizes and spatial structures of the stimuli (simple grating or random stimulus), contrast energy sensitivity as a function of the number of square cycles had the same shape irrespective of the spatial frequency. Contrast energy sensitivity curves were vertically separate because the stimulus area in

deg^2 of the visual field varied due to changes in the viewing distance from one curve to another, and this affects the value of contrast energy sensitivity when expressed in the units of the visual field (See Section 2.4).

As the dotted lines in Figure 5.4 show, contrast energy sensitivity for both kinds of stimuli slightly increased from one to four square cycles. This is probably an artefact caused by a small size of the equiluminous surround (in respect to a cycle length) for 1 square cycles stimuli (Howell & Hess, 1978), as numerous studies have shown that contrast energy sensitivity (and detection efficiency) remains constant for small stimulus sizes when the equiluminous surround is large enough (e.g. Kersten, 1984; Burgess, 1990; Luntinen & al., 1994). Therefore, I have approximated energy sensitivity to be constant for gratings up to about 7 square cycles and for random stimuli up to 5 square cycles (solid lines). The constancy of contrast energy sensitivity indicates complete spatial integration; in other words, the relative stimulus area was still well below the limit of spatial integration area of the visual system and the whole stimulus area was used for detection. After 5-7 square cycles contrast energy sensitivity started to decrease for both kinds of stimuli. For gratings, sensitivity decreased with a slope of -0.43. For random stimuli the slope was -0.75. The slope of -1 would indicate the saturation of spatial integration. Therefore, the result shows that spatial integration in the visual system had not completely saturated even at the maximum number of 256 square cycles, used in the study.

Figure 5.5a shows detection efficiencies as a function of the number of square cycles for the observer HK and Figure 5.5b for the observer RN. The horizontal solid lines correspond to the geometric average of the horizontal part of the data of each frame. The decreasing dashed lines were fitted to the data corresponding to cosine gratings and the decreasing solid lines to the data corresponding to random stimuli for each frame separately. Decreasing lines are of the form $\log\eta = a \log N + b$. Because detection efficiency is proportional to contrast energy sensitivity, the functions have approximately the same shape as in Figure 5.4.

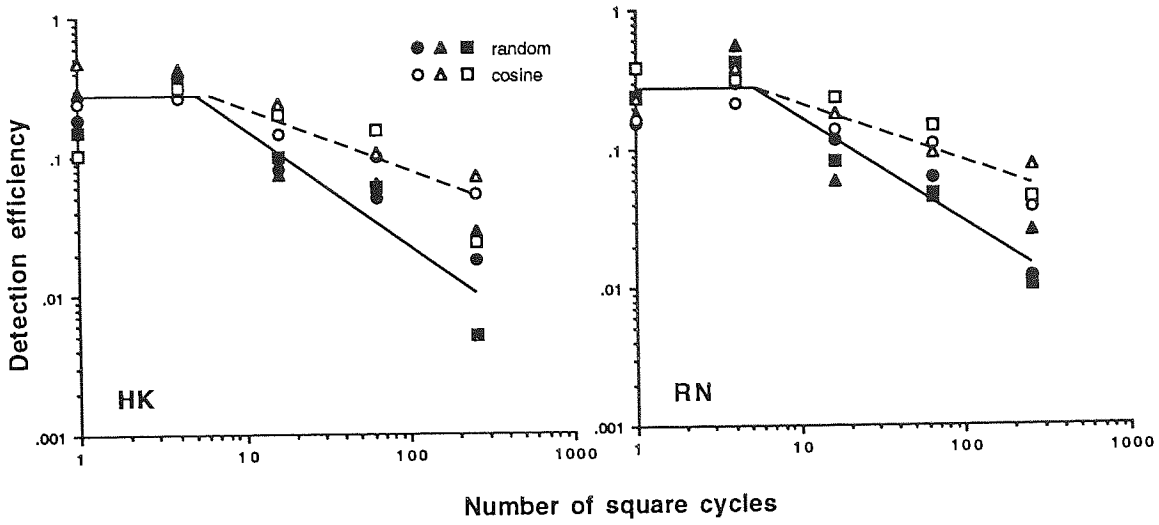

Figure 5.5
Detection efficiency for two subjects as a function of the number of square cycles for cosine gratings and random stimuli.

When the number of square cycles was small (1-4) the detection efficiencies for both kind of stimuli are nearly equal and stay almost constant. The constancy of the detection efficiency means that the efficiency of the collection of contrast information stays constant across the corresponding stimulus area, i.e. remains proportional to the amount of contrast information available.

With increasing number of square cycles (>4) the detection efficiencies for both kind of stimuli started to decrease. However, the decrease in detection efficiency for the random stimuli was steeper than for cosine gratings. The slope of the decrease for the cosine gratings is -0.45 and -0.41 for subjects HK and RN, respectively. For the random images the slope is -0.74 and -0.75 for HK and RN.

5.3.3 Discussion

The result that detection performance at small numbers of square cycles was so similar irrespective of the stimulus structure shows that when the stimulus contains only few details spatial integration in the visual system is similar irrespective of the spatial frequency, orientation range and phase spectrum of the stimulus.

The slope of -1 for the detection efficiency as a function of stimulus area or the number of square cycles would mean that spatial integration has saturated, i.e. the maximum amount of spatial contrast information that the visual system can collect is used for detection and increasing the amount of information does not improve the stimulus visibility. This results in a decrease of detection efficiency: When the stimulus area exceeds the area of spatial integration of the visual system, the human observer is able to use only a fixed amount of the contrast information available and the contrast energy threshold starts to increase with increasing number of details and contour in the stimulus. An ideal observer, on the other hand, is able to use all the information available and therefore, with increasing stimulus complexity, the energy threshold for an ideal observer stays constant. As a result, the ratio (E_{ideal}/E_{human}) of the contrast energy thresholds for the ideal (E_{ideal}) and human (E_{human}) detectors, i.e. detection efficiency, starts to decrease. It implies that the steeper the slope of the decrease in detection efficiency, the poorer is the collection of contrast information in the visual system.

The slope of -1, i.e. the saturation of spatial integration, is absent in the data. Neither simple grating stimuli nor random stimuli reach the number of square cycles, at which integration is completely saturated. However, the slope of decrease of detection efficiency is steeper for random stimuli, which suggests that spatial integration of stimuli with simple spatial structure, i.e. gratings, might operate over a larger area than integration of stimuli with complex structure, i.e. random images. The difference may be explained by the fact that an irregular random stimulus is more complex than a cosine grating, which makes the comparison of the model and noisy stimulus in the detection task more difficult and possibly inaccurate at a large number of square cycles.

The applicability of the concept of the number of square cycles to the complex random images used in this study shows that the spatial integration of complex images in noise is also limited by the number of details in the image. This suggests that spatial integration of any spatial pattern is scale invariant. However, as already stated, it seems that irregularity of the image has an effect on the saturation point of spatial integration. In order to find out, whether the difference in detection efficiency was due to the complex

spatial frequency content or irregular structure of the random image, the next study investigated spatial integration of natural patterns, the spatial frequency content of which was complex but the phase spectra was ordered. Stimuli were thus not irregular but highly ordered in appearance.

5.4 SPATIAL INTEGRATION OF BAND-PASS FILTERED SYMBOLS

The first study pointed out that the measure of square cycles was applicable for stimuli which comprised a single spatial frequency even though the structure of the stimulus was complex. The results are in agreement with grating studies showing the scale invariance of spatial integration (e.g. Hoekstra & al., 1974; Howell & Hess, 1978; Robson & Graham, 1981; Virsu & Rovamo, 1979; Rovamo & al., 1993): the integration is determined by the amount of details and contour in the image.

The results obtained suggested that integration of stimuli with complex structure operates over a smaller area than integration of simple grating. However, as our complex stimuli was produced by randomising the phase spectra of a relatively simple stimulus, the reason for a decrease in the detection efficiency might have been due to the irregularity of the stimulus produced by random phases.

In this study the purpose was to find out how the visual system integrates stimuli with complex spectra comprising different spatial frequencies and orientations, but having an ordered phase spectra and thus highly ordered appearance. Three Sloan letters (K, H, O) and a plus symbol (+) were used as the stimuli. To vary the extent of the amplitude spectra, they were band-pass filtered with various bandwidths and centre-frequencies. Figure 5.6 shows the original, unfiltered stimulus patterns and their Fourier spectra.

Another question addressed was whether the notion of square cycles could be generalised to the stimuli with more complex amplitude spectra. A measure, analogous to the number of square cycles, was developed and tested.

5.4.1 Methods

The apparatus, procedure and subjects were identical to the previous chapter. Please, refer to the previous chapter and Chapter 2 for the detailed description.

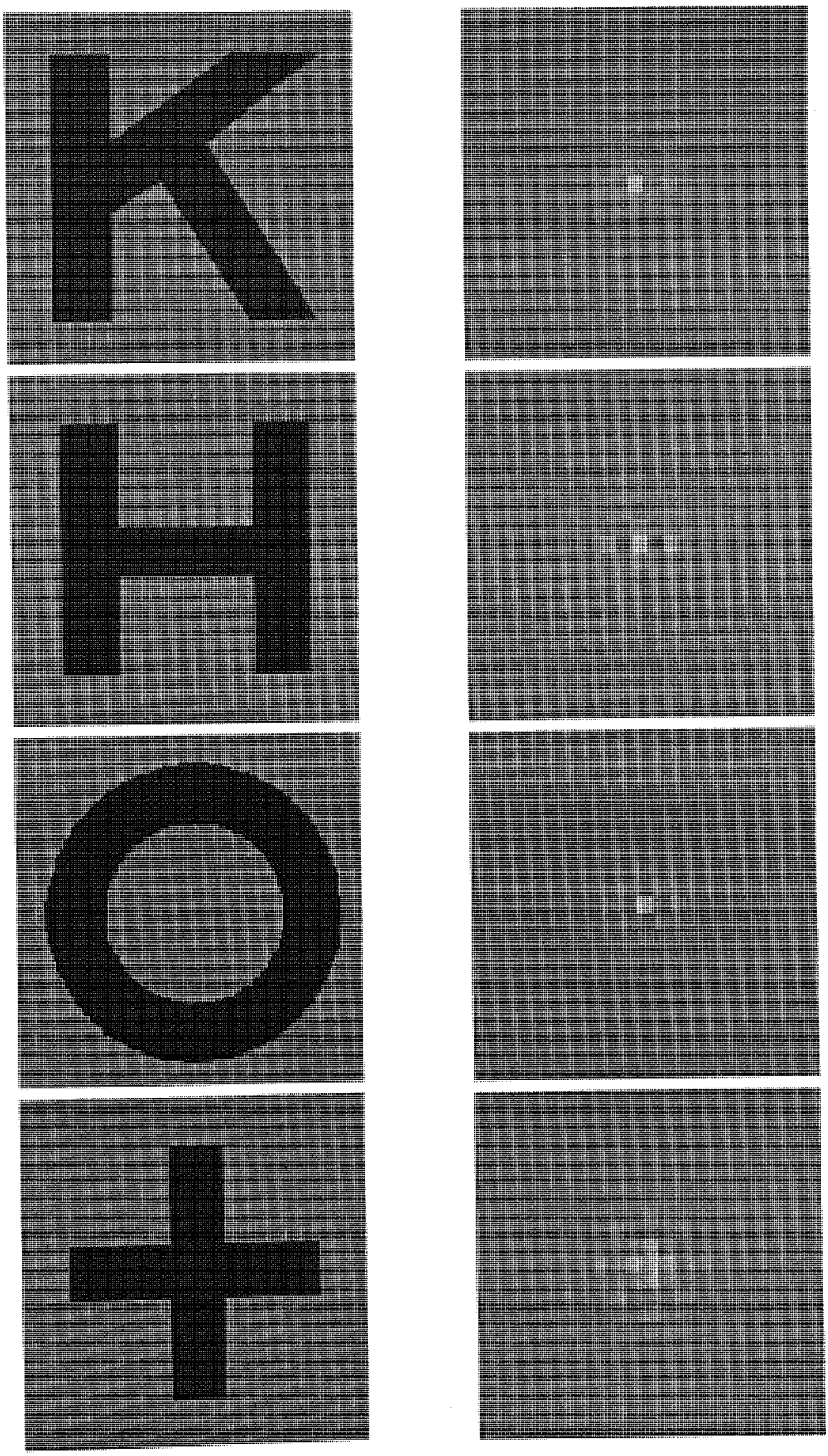

Figure 5.6
Letter stimuli used in the experiment and their Fourier spectra presented as an intensity function.

Stimuli

Two set of stimuli were generated for the experiments. The basic stimuli in both sets were Sloan letters H, K, and O, and a plus pattern (+). The stimuli were band-pass filtered using a circularly symmetric log-Gaussian transfer function:

$$MTF(f) = e^{-\ln^2(f/f_c)/b^2\ln(2)} \tag{5.18}$$

where f is radial spatial frequency ($f=(f_x^2+f_y^2)^{1/2}$), f_x and f_y are the spatial frequencies along the horizontal and vertical frequency axes, f_c is radial centre frequency, and b is half of the spectral bandwidth at half height in octaves. The log-Gaussian transfer function has the advantage over a Gaussian transfer function that it always filters out the zero frequency component. Furthermore, the band-width of the log-Gaussian transfer function is symmetrical in octaves around the centre frequency.

Two-dimensional discrete Fourier transforms (G(u,v)) of the basic stimuli (g(x,y)) were multiplied by the MTF(f). The inverse Fourier transform of this product gave the filtered stimuli (g'(x,y)) used in the experiments:

$$G(u,v) = \frac{1}{n^2}\sum\sum g(x,y)\, e^{-j2\pi(ux+vy)/n} \tag{5.19}$$

$$g'(x,y) = \sum\sum [MTF(u,v)\, G(u,v)]\, e^{j2\pi(ux+vy)/n} \tag{5.20}$$

The Fast Fourier Transform algorithm was used to compute the Fourier transforms. The first set of stimuli were filtered at various centre frequencies using a constant bandwidth. Figure 5.7 shows the stimuli with various centre frequencies.

In Figure 5.7, the bandwidth of the filter was one octave and the centre frequencies used were 1, 2, 4, 8, and 16 c/deg from the viewing distance of 154 cm. With increasing centre frequency the blurry shape of the stimulus changes to a sharp outline figure. The higher the stimulus centre frequency the smaller the area under which contrast energy deviates from zero.

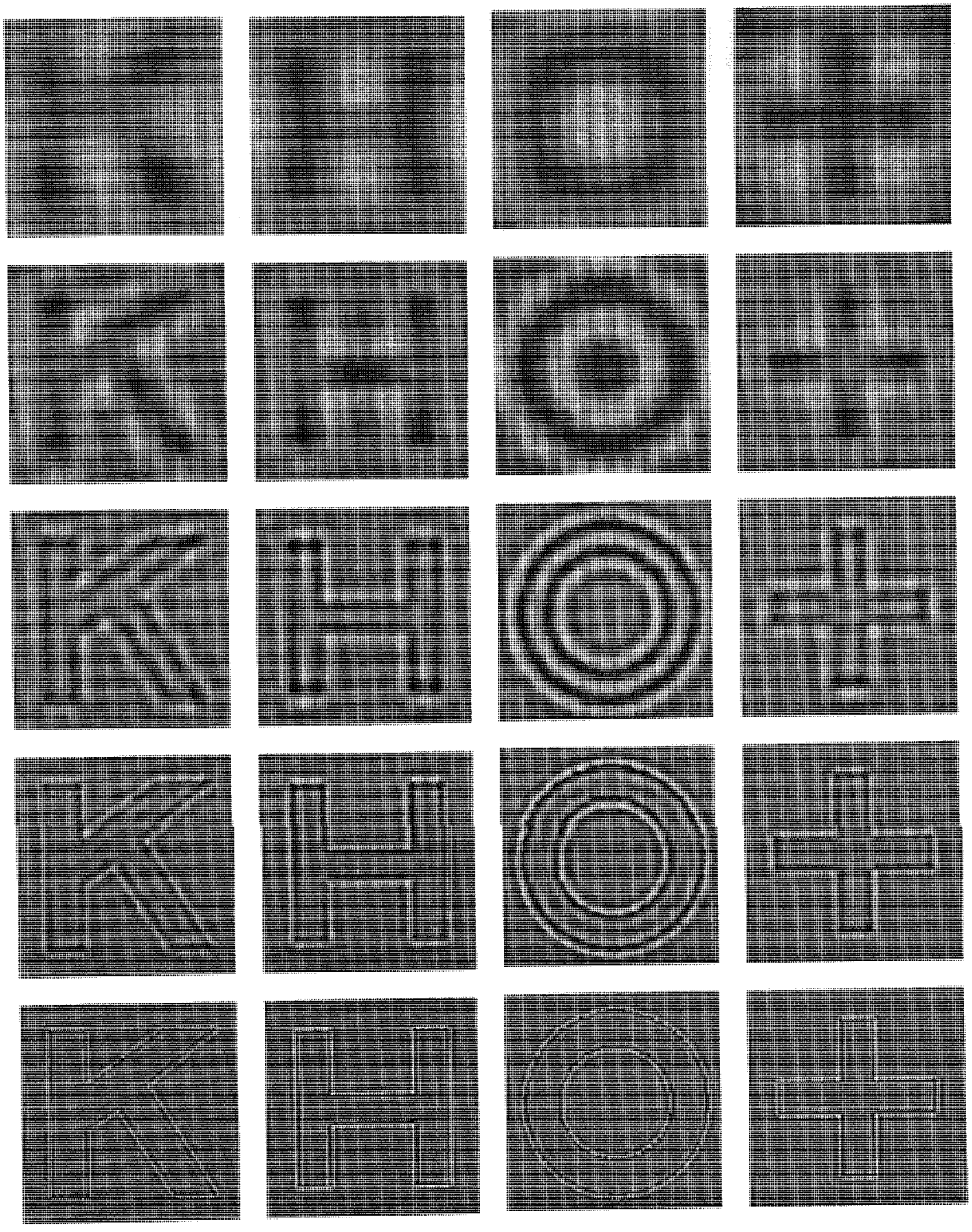

Figure 5.7
Letter stimuli filtered using various centre frequencies (1-16 c/deg) and a bandwidth of 1 octave. The centre frequency of the band-pass filter increases from the top to the bottom.

The second set of stimuli, shown in Figure 5.8, was obtained by using various filter bandwidths at a fixed centre frequency. The bandwidths of the filters used were 0.25, 0.5, 1, 2, and 4 octaves. The centre frequency was constant at 4 c/deg. The stimuli with the narrowest bandwidth contain many fine details and the structure of the original

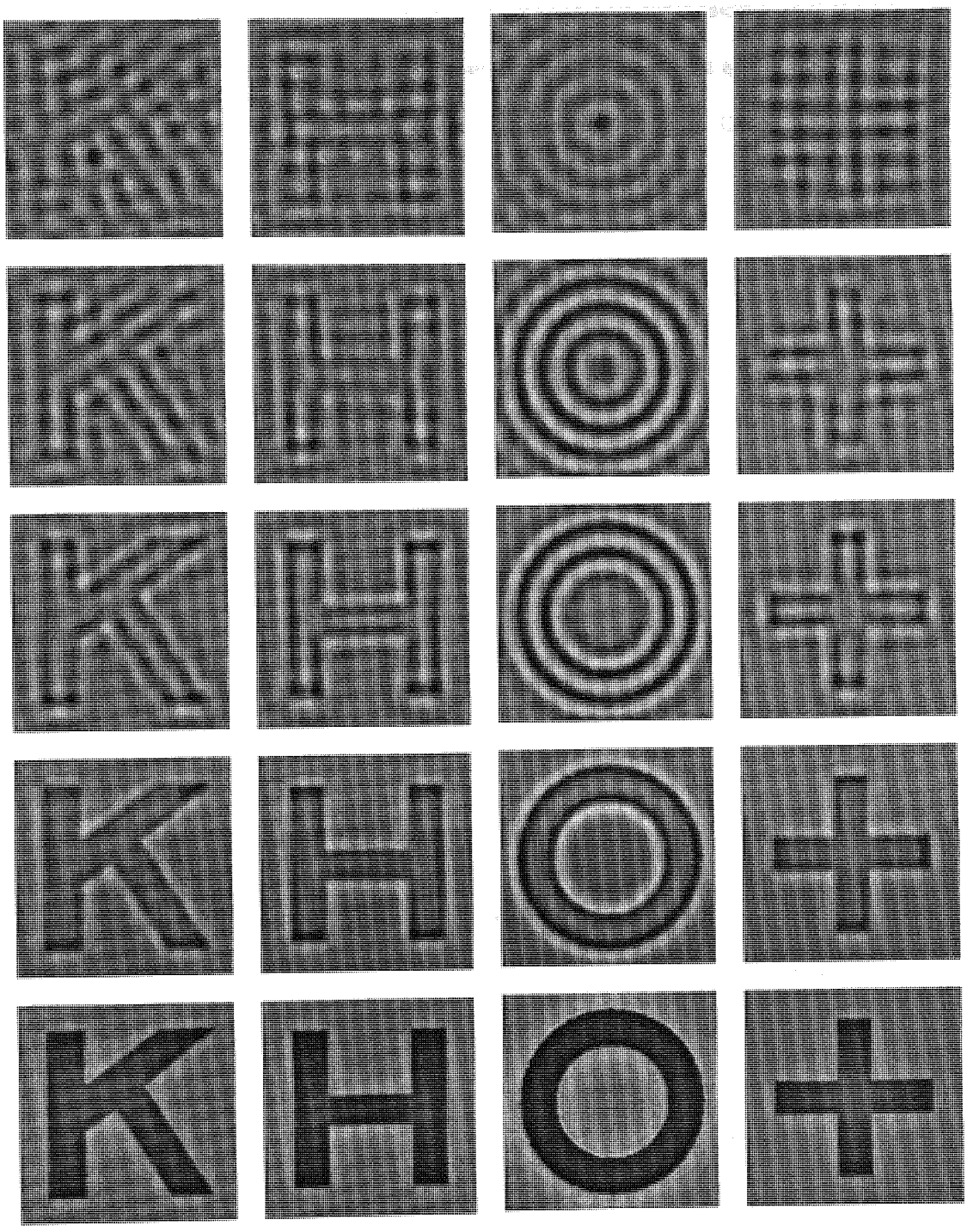

Figure 5.8
Letter stimuli filtered using various filter bandwidths (0.25-4 octaves) and a centre spatial frequency of 4 c/deg. The bandwidth increases from the top to the bottom.

stimulus is difficult to perceive. Contrast energy is almost evenly distributed across the stimulus area when the bandwidth is very narrow. With increasing bandwidth the area under which the local contrast energy deviates from zero decreases and the original stimulus shape becomes apparent.

Contrast energy thresholds were measured in two-dimensional spatial noise using the same procedure as in the previous experiment. Each stimulus consisted of three windows shown simultaneously side by side as explained above. Only one viewing distance, 154 cm, was used. Noise spectral density was 2.2×10^{-5} deg^2.

5.4.2 Results

Detection efficiencies for four different stimulus patterns (H, K, O, and +) band-pass filtered using various centre frequencies are shown in Figure 5.9. The stimuli were filtered using a fixed 1 octave filter bandwidth and the centre frequency of 1 - 16 c/deg. The results are also expressed in terms of contrast energy sensitivity on the right vertical axis. On the basis of the definition of detection efficiency (equation 5.14, Section 5.2.2) we can express contrast energy threshold as

$$E_{human} = \frac{2N_e}{\eta} \qquad (5.21)$$

which gives us also the relation between detection efficiency (η) and human contrast energy sensitivity (S_{human}), because contrast energy sensitivity is the inverse of contrast energy threshold. Hence, S_{human} in this experiment equals to $22.7\eta \times 10^3$.

As Figure 5.9 shows, detection efficiencies were approximately similar for all the stimulus patterns measured: efficiencies decreased with increasing centre frequency of the band-pass filter. The efficiencies were 20 - 50% at 1 c/deg and 1 - 7% at 16 c/deg. The slope of the decrease is approximately -1.

This could be explained by assuming that integration area in deg^2 decreases with increasing spatial frequency, as is the case with gratings (see Introduction). This relationship is an indication that a measure analogous to the number of square cycles is the critical determinant of stimulus visibility.

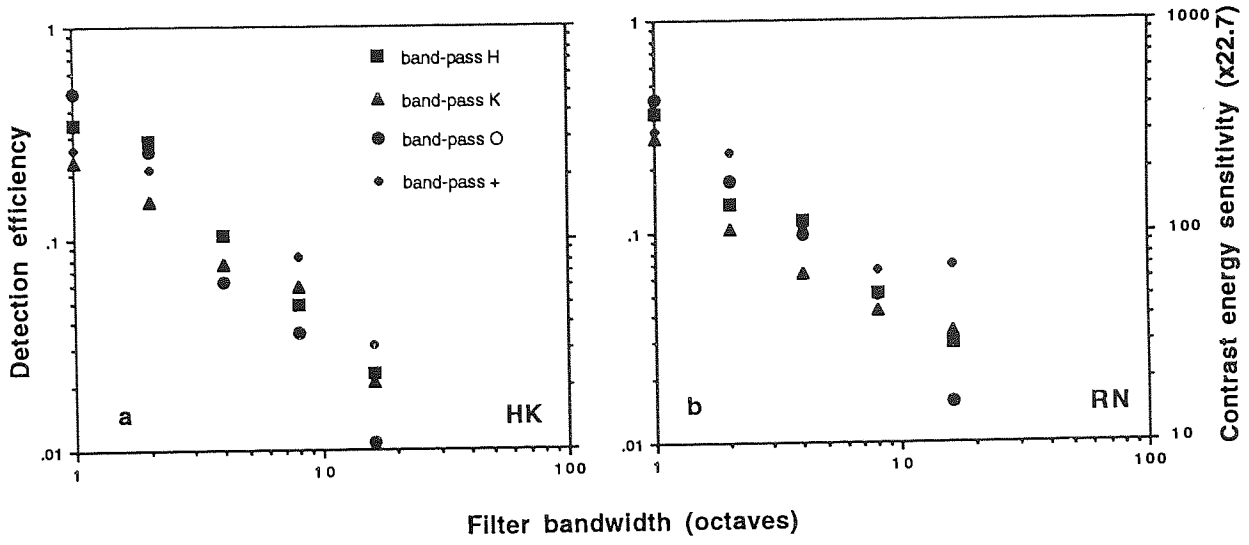

Figure 5.9
Detection efficiencies for band-pass filtered letter stimuli as a function of the centre frequency of the filter. Stimuli are shown in Figure 5.7.

The detection efficiencies plotted in Figure 5.10 were obtained using a fixed 4 c/deg centre frequency. The filter bandwidth increased from 0.25 to 4 octaves. The corresponding contrast energy sensitivities are again plotted on the right vertical axis.

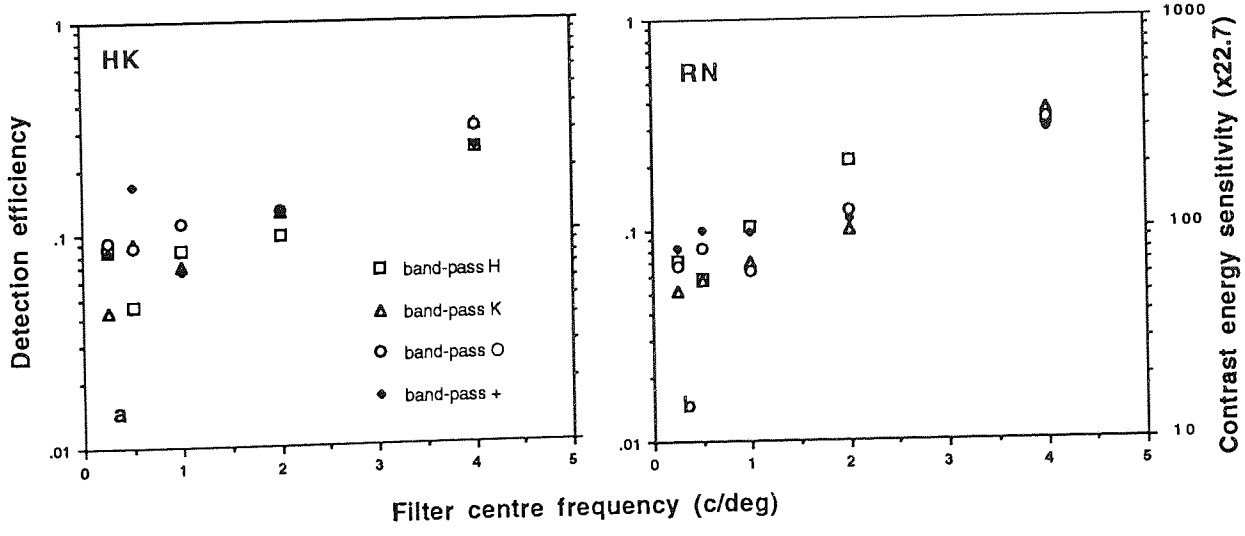

Figure 5.10
Detection efficiencies for band-pass stimuli as a function of the filter bandwidth. Stimuli are shown in Figure 5.8.

As Figure 5.10 shows, efficiency and energy sensitivity increased with filter bandwidth. The efficiencies were 4 - 10% at 0.25 octaves and 25 - 40% at 4 octaves. The results can be explained by the fact that the area in which the local contrast energy deviates from zero becomes smaller with increasing bandwidth. This results in a decrease in the amount of details and contour in the stimulus (See Figure 5.8). As a result a larger proportion of the absolute image area displayed is integrated in detection.

The decrease of efficiency as a function of filter centre frequency in Figure 5.9, and the increase in efficiency as a function of filter bandwidth in Figure 5.10 indicates that neither the centre frequency nor the bandwidth of the signal can alone explain the changes in detection efficiency and energy sensitivity. Instead, it has to be their combination that determines detection efficiency

If we go back to the Figures 5.7 and 5.8, we will see that the filtered stimuli used in the experiments became more complex and the number of details increased with increasing filter centre frequency or decreasing filter bandwidth. On the other hand, as Figures 5.9 and 5.10 show, also detection efficiency decreases with increasing filter centre frequency and decreasing bandwidth. We could therefore assume, that an increasing number of details in the stimuli used in this experiment produces the same effect as an increasing number of square cycles in gratings. Hence, a measure similar to the number of square cycles could be suitable for describing spatial integration of the complex stimuli of this study.

Relative image area - a measure of the number of details in complex images

In order to apply the concept of the number of square cycles (Af^2), obtained by multiplying spatial frequency squared (f^2) by the stimulus area (A), for our filtered patterns, image spectrum should be described by a single spatial frequency and stimulus area should be redefined. Neither for the spatial frequency of the stimulus nor for the

stimulus area is there a straightforward measure in the case of band-pass filtered patterns used in this study.

Possible measures of spatial frequency for describing complex stimuli could be the spatial frequency corresponding to the peak value of the amplitude spectrum or the radial median spatial frequency. However, because the contrast energy of each stimulus is distributed over a range of spatial frequencies and orientations and may have many peak values, the radial median spatial frequency (f_m) of the contrast energy spectrum was considered to be a suitable measure of spatial frequency when calculating the relative image area of the filtered stimuli. This means that 50% of the stimulus contrast energy was above and below the radial spatial frequency chosen.

Although the stimulus window size was constant for all stimulus patterns used, the actual area where contrast energy deviated markedly from zero varied greatly from one pattern to the other. The filtering of stimuli affected the area under which the contrast energy deviated from zero. This area tended to become larger when the signal bandwidth became narrower or the median spatial frequency became lower. To take this into account, the area for each stimulus image was determined by calculating the number of pixels for which the square of the contrast signal was greater than a minimum deviation from zero. The minimum deviation was chosen so that the resulting area (A_{95}) comprised 95% of the total image energy.

The relative image area was then obtained by multiplying the square of the radial median spatial frequency (f_m) of the image energy spectrum by the image area (A_{95}). The relative image area ($A_{95}f_m^2$) can be regarded as a descriptor of stimulus complexity in the sense that its value increases with the number of details in the image.

In the Figure 5.11 the detection efficiencies for both sets of stimuli are plotted as a function of relative image area defined above. The detection efficiencies for the grating and random stimuli from the previous chapter are also plotted in Figure 5.11. The relative image area for the gratings and random stimuli were calculated by using the same technique as for the other stimuli.

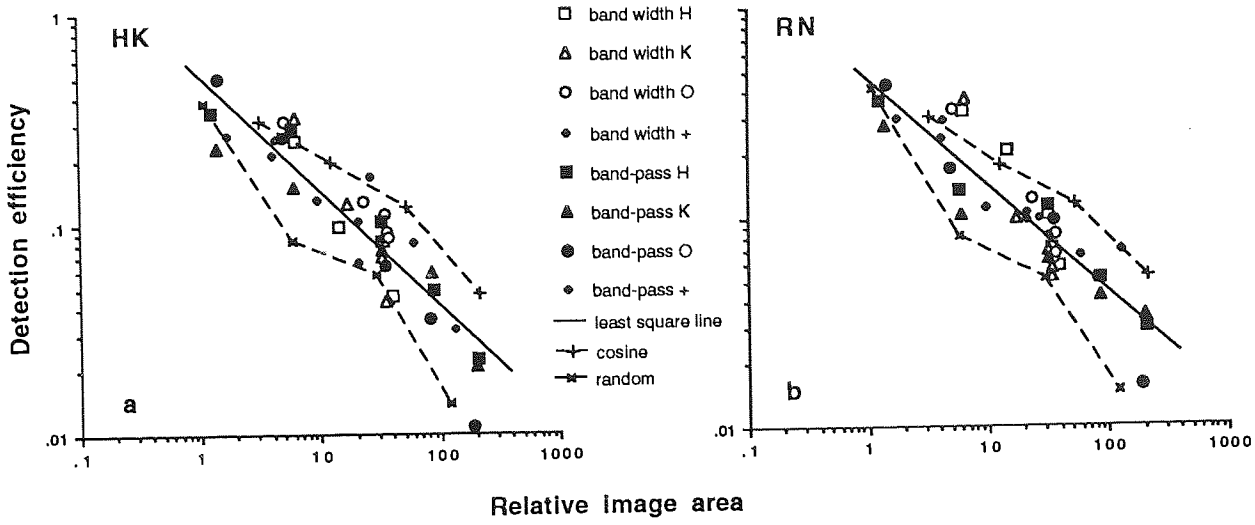

Figure 5.11
Detection efficiencies for band-pass filtered letters as a function of the relative stimulus area expressed as a product of the square of the median spatial frequency (f_m) of the image energy spectrum and the image area (A_{95}).

The efficiencies for all stimulus patterns decreased linearly as a function of relative image area when plotted in double logarithmic coordinates. The least square line fitted to the data explained 91% of the data for both subject. The explained variance was calculated according to Appendix 1. It is interesting to note, that cosine grating on the one hand and random stimuli on the other approximately define the upper and lower limits of the range within which efficiencies for band-pass filtered patterns varied.

The least square line fitted to the data has a slope of -0.49 for subject HK and -0.54 for RN. As mentioned earlier the slope of -1 for detection efficiency means a complete lack of spatial integration. In terms of r.m.s. contrast sensitivity, it indicates the saturation of a contrast sensitivity function. The slope of -0.5 for efficiency corresponds to a positive slope of 0.25 for the contrast sensitivity function.

5.4.3 Discussion

The result that detection efficiency decreased with increasing filter centre frequency but increased with filter bandwidth shows that neither of these factors alone

determine detection efficiency. Instead, the comparison of stimulus images and detection efficiencies measured showed that it is the number of details in the image rather than its spatial frequency content that defines the spatial area that the visual system can employ in order to enhance detection performance. This is in good agreement with grating studies (e.g. Hoekstra & al., 1974; Howell & Hess, 1978; Robson & Graham, 1981; Virsu & Rovamo, 1979; Rovamo & al., 1993).

A modified version of the measure of the number of square cycles, relative stimulus area, was developed and applied to the letter stimuli. Detection efficiencies for all kinds of stimuli studied followed a single decreasing function when plotted as a function of relative stimulus area. This shows that the measure of relative image area successfully described the efficiency of spatial integration also for more complex images than simple gratings. It indicates that when the number of details in the image increases, detection efficiency decreases similarly for various kinds of stimulus patterns.

Therefore, although the spatial frequency bandwidth of the stimulus affects the spatial frequency bandwidth that the detection mechanism used by the visual system, the bandwidth and complexity of the spatial frequency spectrum is not the determinant of decreasing efficiency of spatial integration. According to current results, the critical determinant seems to be the spatial structure of the stimulus.

5.5. THE EFFECT OF SPATIAL SPREAD OF CONTRAST ENERGY WITHIN THE STIMULUS AREA

The first two spatial integration experiments described here, together with number of grating studies done elsewhere (e.g. Howell & Hess, 1978; Virsu & Rovamo, 1979; Robson & Graham, 1981), suggest that the number of details in the image is a critical determinant of the area of spatial integration. Detection efficiency decreases when the number of details - the number of square cycles for grating stimuli and the amount of details and contour for complex stimuli - increases.

However, none of the studies cited above show whether the decrease in efficiency or the saturation of contrast sensitivity is due to the increase in the total amount of contrast information within the retinal area stimulated or due to the increasing distance between the furthermost parts in the stimulus, i.e. the spread of the stimulus parts over the stimulus area. In other words, it has not been investigated, whether the reason for the decreasing ability to use spatial information with increasing area is due to the actual amount of information available within the stimulus window or due to the spatial spread of this information.

In order to separate the two factors mentioned above, detection efficiencies were measured for the two kinds of grating stimuli: One being a conventional rectangular cosine grating with constant spatial frequency but increasing stimulus area, and thus having an increasing number of square cycles (the uniform grating). The other consisting of nine grating patches of one square cycle each spread over the area equal to the area of the conventional grating (the patched grating). Thus, the number of square cycles for the patched stimulus stayed constant whereas the spread of the furthermost parts in the stimulus increased similarly for both kinds of stimuli.

5.5.1 Methods

The apparatus used in this experiment was the apparatus 1 described in Section 2.1.1. Subjects were the same but the procedure, which is described below, differed slightly.

Stimuli

Two kinds of stimuli were used: conventional uniform cosine gratings with increasing stimulus area and constant spatial frequency of 2 c/cm, and a patched grating consisting of a rectangular array of nine (3 x 3) small grating patches of one square cycle each having the same spatial frequency as the uniform grating. The distance between the grating patches increased so that the area defined by the outline of the rectangular array of grating patches was equal to the area of the uniform cosine grating.

The spatial frequency for both kinds of gratings was 4 c/deg from the viewing distance of 115 cm. The area subtended 0.8 x 0.8, 1.8 x 1.8, 2.8 x 2.8, and 4.8 x 4.8 deg^2. With increasing area the inter-centre distances between the grating patches were 1, 3, 5, and 9 cycles, the smallest thus being a uniform grating.

The stimuli were embedded into white two-dimensional spatial noise. Its root-mean-square contrast ($c_{r.m.s.}$) was 0.3 and spectral density (N_e), calculated as the product of the pixel area and the contrast squared, was 3.94×10^{-5} deg^2 from the viewing distance of 115 cm. The noise window extended uniformly across the stimulus window for both kinds of grating stimuli. Examples of the stimuli embedded in two-dimensional spatial noise are shown in Figure 5.12.

Procedure

Contrast energy thresholds were determined by using a two-interval forced-choice algorithm with a staircase method described in detail in the chapter 2.3. The probability

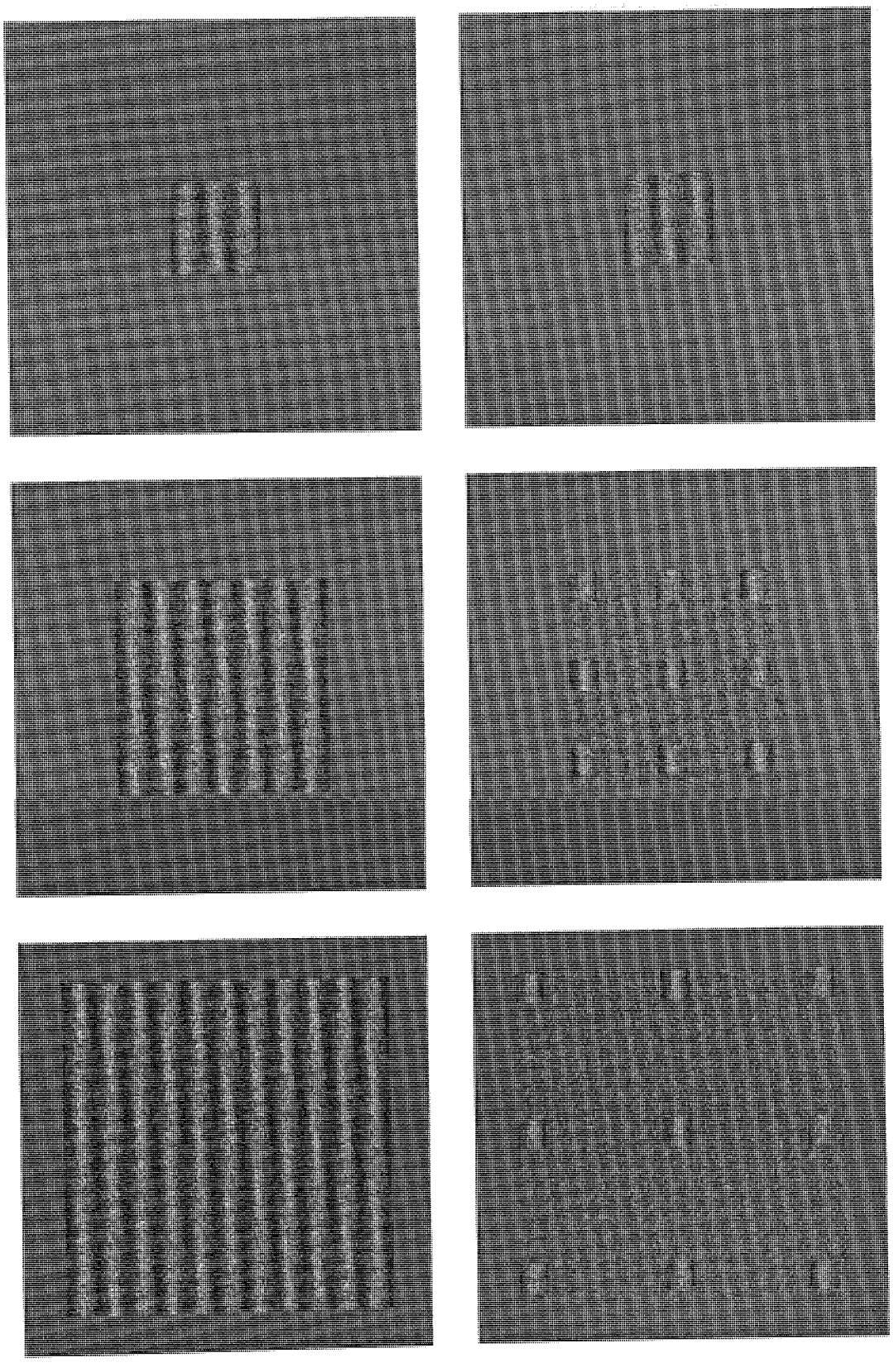

Figure 5.12
Examples of the stimuli used: uniform and patched vertical cosine gratings embedded in two-dimensional pixel noise. The inter-centre distances between the grating patches are 1, 3, and 5 cycles.

level of correct responses was 0.84. Each trial consisted of two successive exposures, one of which contained stimulus plus noise and the other noise alone. The optimal duration of the exposure (a further increase in exposure time did not increase the detection efficiency) was separately determined for each subject by a pilot experiment. It was found to be 500 ms and 1000 ms for observers HK and RN, respectively. By means of one of the two keys on the computer keyboard, the observer indicated which one of the exposures contained the stimulus.

There were 5 noise samples at each contrast level. The number of contrast levels used in the experiment was about 20. Thus the total number of noise samples used in determining one threshold was 100 plus 21 noise samples used for the noise presentation only.

Detection efficiencies were calculated with equation (5.13) from the contrast energy thresholds measured. There were, however, certain methodological differences between the experiments conducted in the earlier chapters: viewing time was restricted to a limited period of time, each trial consisted of two instead of one exposure, and no model stimulus was available for the observer. These differences could have resulted in reduced efficiencies in comparison to the efficiencies measured with model stimulus and unlimited viewing time. In Figure 5.13 detection efficiencies for the horizontal grating from the experiments of Section 5.3 are plotted together with detection efficiencies for vertical grating of this study.

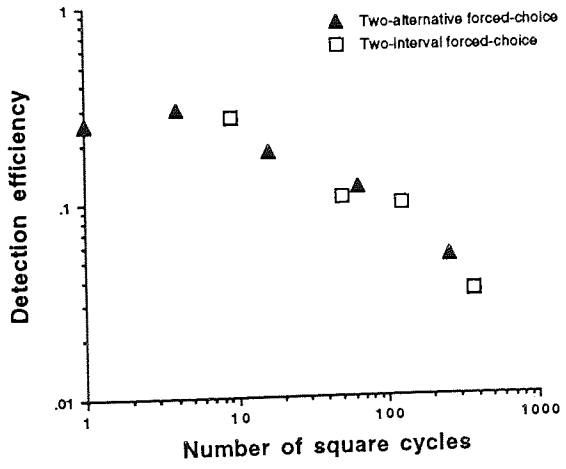

Figure 5.13
Detection efficiencies obtained either by the two-alternative or two-interval forced- choice method for cosine gratings as a function of the number of square cycles.

As Figure 5.13 shows, the detection efficiencies obtained by the two methods applied in Section 5.3 and the current study plotted as a function of the number of square cycles yielded very similar results. Therefore, any differences in detection efficiencies of this and other studies introduced in this chapter are not due to differences in experimental methods.

5.5.2 Results

Detection efficiencies for the uniform cosine gratings within rectangular windows and rectangular arrays of grating patches are shown as a function of stimulus area in Figure 5.14. For the patched grating the stimulus area is the area of the square drawn along the outline of the array. Contrast energy sensitivity is plotted on the right vertical axis.

Figure 5.14 shows that detection efficiencies for both patched and uniform gratings decreased as the function of stimulus area. However, the total area stimulated on the retina differs greatly for the two kinds of stimuli: the retinal area covered by the uniform grating increases with increasing stimulus area whereas the retinal area covered by the patched gratings stays constant despite increasing stimulus area plotted on the horizontal axis in Figure 5.14. Since the detection efficiencies for both kinds of stimuli are similar, the reason for decreasing efficiency with area for a spatial stimulus must be the increasing distance between local contrasts rather than an increase in the absolute retinal area stimulated.

The result implies that contrast information from different parts of a stimulus is combined less efficiently as the distances between the parts increase. The increase in the number of details in the stimulus alone is therefore not enough to explain the decrease in efficiency.

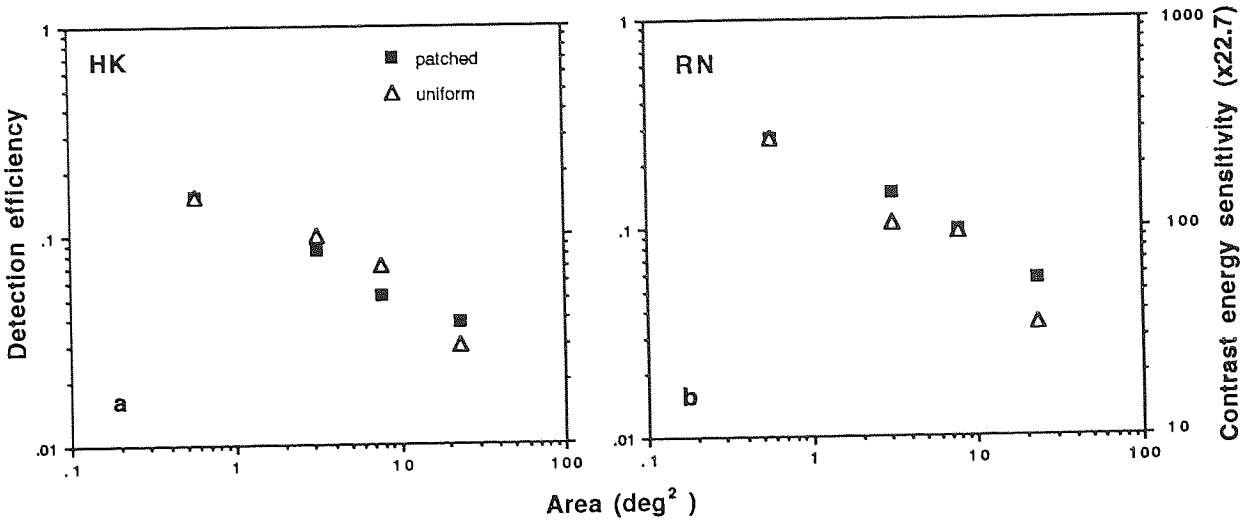

Figure 5.14
Detection efficiencies for uniform and patched gratings as a function of stimulus area. For the patched grating the stimulus area is the area of the square drawn along the outline of the array.

The present result also suggests that the measure of image area should be based on the distances between different parts of the stimulus, and it should express the extent of the spread of contrast energy across the stimulus. For this reason the measure of image area used in Section 5.4 that comprised 95% of image energy (A_{95}) is not a suitable measure. Area measures based on a constant percentage of the total contrast energy of the stimulus cannot explain the decrease in detection efficiency with increasing distance between grating patches. In such cases A_{95}, for example, would indicate the sum of the areas that each grating patch occupies and thus would not change with increasing distance between the patches.

In the following, a new measure of image complexity, related to the number of square cycles and the relative image area of Section 5.4, is introduced. The main difference is the way of calculating the area of the stimulus. This new measure is based on the hypothesis that the human observer would place hers/his centre of attention to a centre of gravity calculated on the basis of contrast distribution in the image. Even if there were no contrast energy at the centre of the stimulus but only at the edges, the most economic way to detect a short-lasting stimulus would still be to focus the attention to the centre of gravity. The measure of stimulus area is thus based on the spread of spatial

information within the stimulus area rather than on the area over which the stimulus energy is concentrated.

A measure of image complexity

The distribution of contrast patches across the stimulus field was here described using the notion of centre of gravity of the image both in the spatial and spectral dimensions. The centre of gravity in the spatial dimension defines the assumed centre of attention of the observer and it takes into account the distribution of local contrasts in the image. The measure of spatial spread (α) then expresses how contrast energy of the stimulus is distributed around the centre of gravity. The centre of gravity in spectral dimension, on the other hand, defines the spatial frequency that affects the dominant detail size in the image. From these two measures, a measure of image complexity, related to the original number of square cycles, could be derived: the measure of image complexity was defined as a product of the spatial spread (α) of contrast energy and the square of radial centre spatial frequency (f_c) of the image energy spectrum ($Z = \alpha f_c^2$). The spatial spread (α) of contrast energy is given:

$$\alpha = \pi \frac{\int\int r^2(x,y)c^2(x,y)\ dxdy}{\int\int c^2(x,y)\ dxdy}, \qquad (5.23)$$

where r(x,y) is the distance of point (x,y) from the centre of gravity (x_g,y_g) of the stimulus, and c(x,y) is the contrast waveform of the image. The numerator in the equation computes the weighted sum of the distances (r(x,y)) squared using the square of contrast signal as a weight. The denominator computes the sum of weights, which in this case is the same as the total contrast energy of the image. The quotient in equation (5.23) thus gives us a squared radius based on a kind of weighted variance of the distances in the image. Therefore, spatial spread is a measure of area which refers to a circular area the radius of which is based on the weighted variance of the contrast energy. It can also be

recognised as a radial moment which can be used for the normalisation of image scale in invariant pattern recognition (e.g. Sheng & Arsenault).

The centre of gravity in equation (5.23) is defined by:

$$x_g = \frac{\int\int x c^2(x,y)\ dxdy}{\int\int c^2(x,y)\ dxdy} \tag{5.24}$$

and

$$y_g = \frac{\int\int y c^2(x,y)\ dxdy}{\int\int c^2(x,y)\ dxdy} \tag{5.25}$$

for horizontal and vertical dimensions, respectively. The distance r(x,y) is

$$r(x,y) = \sqrt{(x-x_g)^2+(y-y_g)^2}. \tag{5.26}$$

The radial centre spatial frequency (f_c) of the image energy spectrum is computed from a logarithmic polar-coordinate transformation ($|F(u,\phi)|^2$) of the contrast energy spectrum of the image:

$$f_c = \exp\left(\frac{\int\int u^2 |F(u,\phi)|^2\ du d\phi}{\int\int |F(u,\phi)|^2\ du d\phi}\right)^{1/2} \tag{5.27}$$

where $u = \ln\sqrt{(f_x^2 + f_y^2)}$, f_x and f_y are horizontal and vertical spatial frequencies, respectively. Orientation (ϕ) is $\arctan(f_y/f_x)$. The logarithmic polar-coordinate representation of the spectrum has the property that a scale or an orientation change of the image only results in a translation in the (u,ϕ) -plane. Figure 5.15 shows a diagram of the logarithmic polar-coordinate transformation of the Fourier space.

In a linear Fourier space the orientation within each discrete orientation sample (sector) is constant irrespective of the spatial frequency, i.e. distance from the origin. The size of each orientation sample was 0.28 degrees. When, on the other hand, we move along a radial spatial frequency axis within each orientation sector, the gratings are just scaled versions of each other. The sample size along the spatial frequency axis always

doubled with increasing spatial frequency. This resulted in a constant step size in logarithmic coordinates. The spatial frequency step size was 0.005 octaves.

The Fourier space

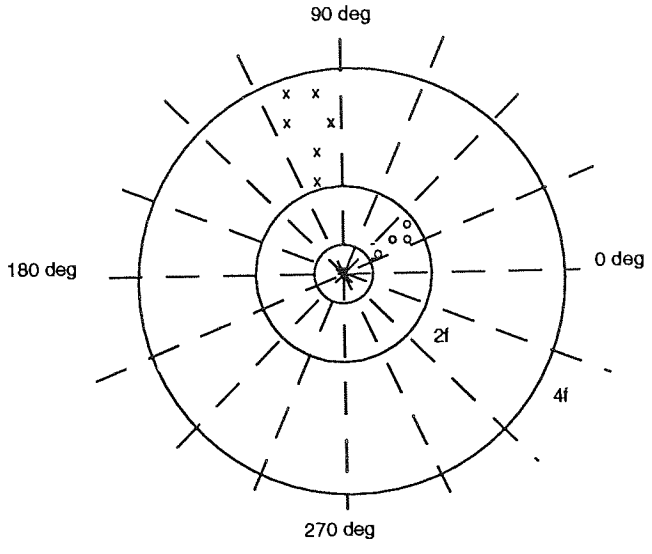

The logarithmic polar-coordinate transformation of the Fourier space

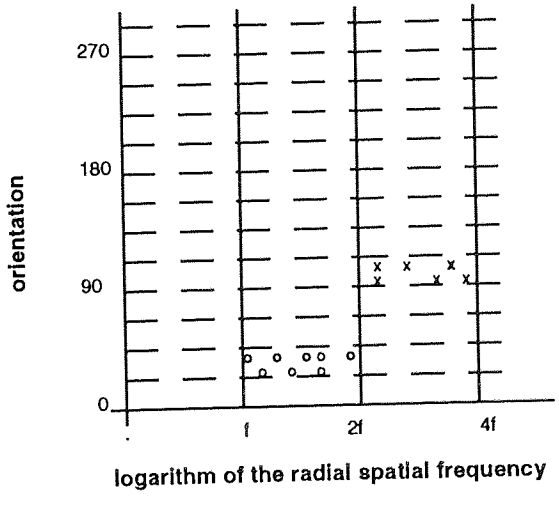

Figure 5.15
The logarithmic polar-coordinate transformation of the Fourier space.

This invariance is in agreement with the fact that at low spatial frequencies contrast detection is independent of orientation (Campbell, Kulikowski & Levinson, 1966) and spatial scale (Savoy & McCann, 1975; McCann, 1978; Rovamo & al., 1992).

It is worth noting that the measure of image complexity introduced here is scale invariant like the earlier measures developed. However, now the spread of contrast information over the image area is calculated rather than taking into account the whole image area. For a cosine grating in a square window the value of image complexity is approximately equal to half of the number of square cycles calculated by multiplying grating area by spatial frequency squared.

In the Figure 5.16 detection efficiencies for the uniform and patched gratings are plotted as a function of image complexity calculated as above. In addition, detection efficiencies for cosine gratings and random images from Section 5.3 and band-pass filtered patterns from Section 5.4 are plotted in Figure 5.16.

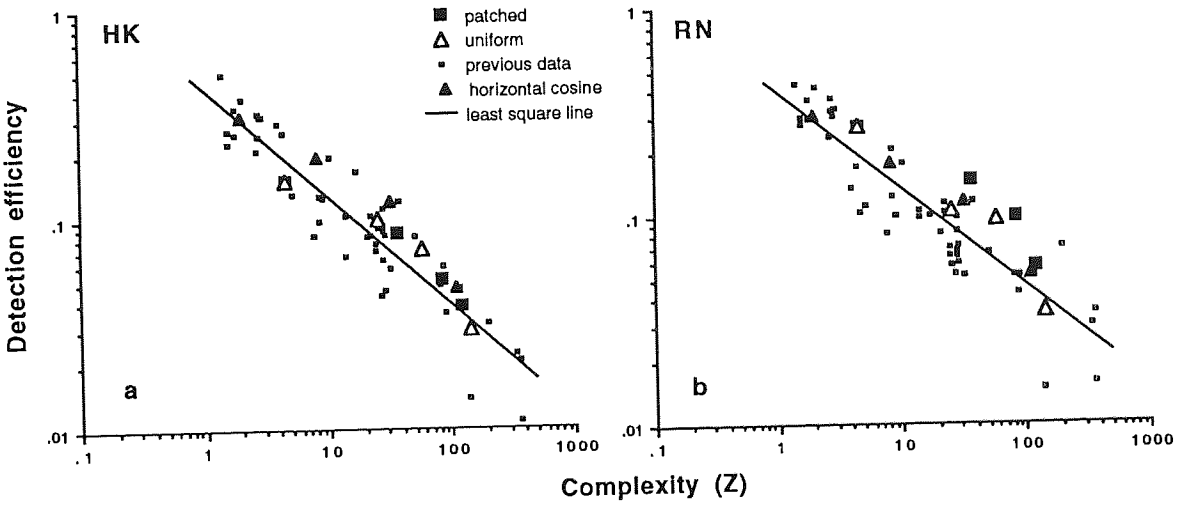

Figure 5.16
Detection efficiencies for the uniform and patched gratings, and for the stimuli of the previous Sections of this Chapter plotted as a function of image complexity.

Detection efficiencies for the uniform and patched gratings and for the stimuli from Sections 5.3-5.4 followed a single decreasing linear function of image complexity when plotted in double-logarithmic coordinates. The slope of decrease was -0.52 and -0.47 for the subjects HK and RN, respectively. Explained variance of the least squares lines shown in Figure 5.16 was 86% for subject HK and 80% for RN. Explained variances were calculated according to Appendix 1.

5.5.3 Discussion

The result showed that detection efficiency decreases similarly for both uniform and patched grating when the area across which the contrast information is distributed was similar. Therefore, neither the stimulated area on the retina nor a straightforward measure of the number of details in the image is enough to define the area of spatial integration in the visual system. Rather, the amount of contrast information used in detection seems to decrease as the spatial spread of contrast information increases.

A new measure of image complexity, which was based on the spatial spread of contrast information and the average size of the details in the image, was developed. Again, the measure is related to the number of square cycles, calculated as a product of grating area and the spatial frequency squared and originally introduced by Virsu and Rovamo (1979). However, in the new measure the stimulus area is replaced by the spread of contrast energy, which described the stimulus area on a basis of a kind of weighted variance of the distances in the image. Therefore, the total contrast energy within the stimulus area does not affect the measure of spatial spread.

Detection efficiencies both for patched and uniform gratings as well as random images (Section 5.3) and band-pass filtered symbols (Section 5.4) decreased similarly as a function of the new measure of image complexity. The efficiency of spatial integration therefore, seems to be determined both by the number of details in the image, and the distance of how the contrast information has spread around the centre of gravity.

5.6 THE EFFECT OF SPECTRAL BANDWIDTH AND STIMULUS IRREGULARITY

An increase in grating area makes the amplitude spectrum of the stimulus narrower in Fourier space. Therefore, the purpose of this last study concerning spatial integration of complex patterns in noise was to find out whether the decrease in detection efficiency with increasing area of spatial stimuli follows from the decreasing bandwidth of the amplitude spectrum.

One way to increase the area of a two-dimensional, spatially limited image, such as a band-pass filtered point stimulus, without affecting its amplitude spectrum, is to modify its phase spectrum. Each spatial frequency component of an image has its specific phase in Fourier space. Thus, the phase spectrum of the image defines the spatial relationship between its frequency components. When the phase spectrum of a band-pass filtered point stimulus is modified, for example, by adding a random number to the phase of each spatial frequency component, the stimulus area will increase but its bandwidth remains unchanged.

Another question addressed was whether the increasing stimulus irregularity introduced by randomising the phase spectrum has a further effect on stimulus detectability. The study carried out in Section 5.3 suggested, that spatial integration of images with randomised phase spectra operates over a smaller area than simple gratings. However, in those experiments the spectral bandwidth of the stimulus varied with increasing area and image complexity.

The basic stimuli used were band-pass filtered point stimuli with various bandwidths and a circular cosine grating with a radial luminance modulation. Their amplitude spectrum bandwidth was kept constant while their area and complexity were increased by modifying their phase spectra. The basic stimuli had all their spatial frequency components in zero phase. The image area of band-pass filtered point stimuli was changed by distributing the phase spectra of the stimuli randomly within various ranges. For a circular grating the randomisation of the phase spectrum did not affect

stimulus area but only increased stimulus irregularity. The circular grating, therefore, served as a control stimulus.

5.6.1 Methods

The Apparatus 1 described in Section 2.1.1 was used in the experiments. The procedure is identical to the one used in experiments of Sections 5.3 and 5.4 of this thesis. Subjects HK and RN served as observers (For details about the procedure see Section 5.3).

Stimuli

Band-pass filtered points of different bandwidths and a circular grating were used as basic stimuli for the experiments. All the basic stimuli had their spatial frequency components in zero phase. From each of them four new stimuli were produced by randomly distributing the stimulus phase spectrum within 90, 180, 270, and 360 degrees.

Band-pass filtered points were obtained from an impulse stimulus with a white amplitude spectrum. In practice, the local contrast of only one bright pixel in the middle of the image was different from zero. The two-dimensional discrete Fourier transform of an impulse stimulus was computed by the Fast Fourier Transform algorithm and multiplied by a circularly symmetric log-Gaussian transfer function:

$$MTF(f) = e^{-\ln^2(f/f_c)/(b^2 \ln 2)} \tag{5.28}$$

where f is radial spatial frequency, f_c is radial centre frequency, and b is half of the spectral bandwidth at half-height in octaves. In our experiments radial centre frequency was always 4 c/deg. Bandwidths at half height of the filter were 0.25, 0.5, 1 and 2 octaves.

After filtering, the phase spectrum of each band-pass filtered impulse stimulus was modified by adding an evenly distributed random number with zero mean and a range of 90, 180, 270 or 360 deg to the phase value of each spatial frequency component (f_x, f_y). Corresponding randomization of stimulus phase spectrum was carried out in the Fourier transform of a circular cosine grating, which had a radial spatial frequency of 4 c/deg. Following the phase randomization procedure, the inverse Fourier transforms gave the stimuli used in the experiments.

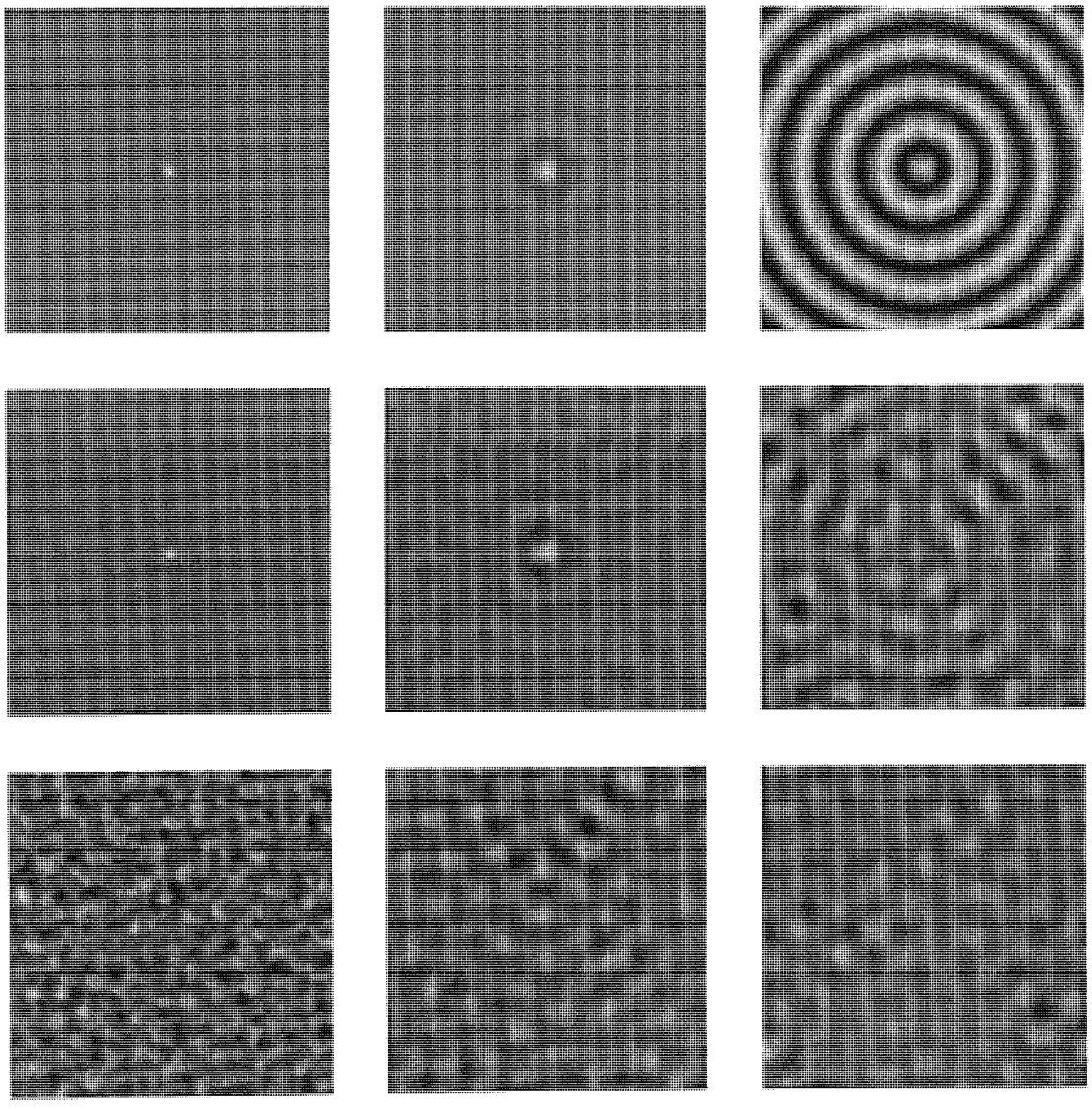

Figure 5.17
Examples of the stimuli used in the experiments. The left column shows band-pass filtered point stimuli with 2 octaves bandwidth. In the middle the bandwidth is 0.5 octaves. The right-most columns shows the circular grating. For all stimuli the range of phase randomisation is 0, 180, and 360 degrees from top to bottom.

Examples of the stimuli are shown in Figure 5.17. As it shows, the narrower the bandwidth of the point stimulus the larger was the area to which most of the contrast energy was confined. In the point stimulus with the original zero phase and 2 octaves bandwidth practically all the contrast information was concentrated at the centre of the stimulus whereas in the stimulus with 0.5 octaves bandwidth considerably more contrast energy was also spread into the surrounding.

In addition, for all point stimuli the increase in phase range resulted in an increase in stimulus area. When the phase was completely randomised (phase range of 360 deg), the point stimuli filled the whole stimulus window irrespective of the stimulus bandwidth. For the circular grating the area did not increase with phase modification; only the stimulus structure was changed.

The increase in phase range also degraded the image structure. For a phase range of 180 degrees the structure in all the stimuli was still partially visible, but it was completely destroyed when a phase range was 360 degrees. In the latter case the phase spectrum is completely random and the grain of image is finer the wider the stimulus bandwidth.

Contrast energy thresholds were measured in two-dimensional spatial noise by using the same procedure as in experiments of Sections 5.3 and 5.4. Each stimulus consisted of three stimulus windows shown simultaneously side by side as explained above (See Section 5.3). From the viewing distance of 154 cm noise spectral density was 22.0×10^{-6} deg^2.

5.6.2 Results

In Figure 5.18 detection efficiencies and contrast energy sensitivities are shown for two subjects as a function of phase range within which the phase value of each spatial frequency component of the stimulus varied. The solid lines are drawn through the geometric means of the two observer.

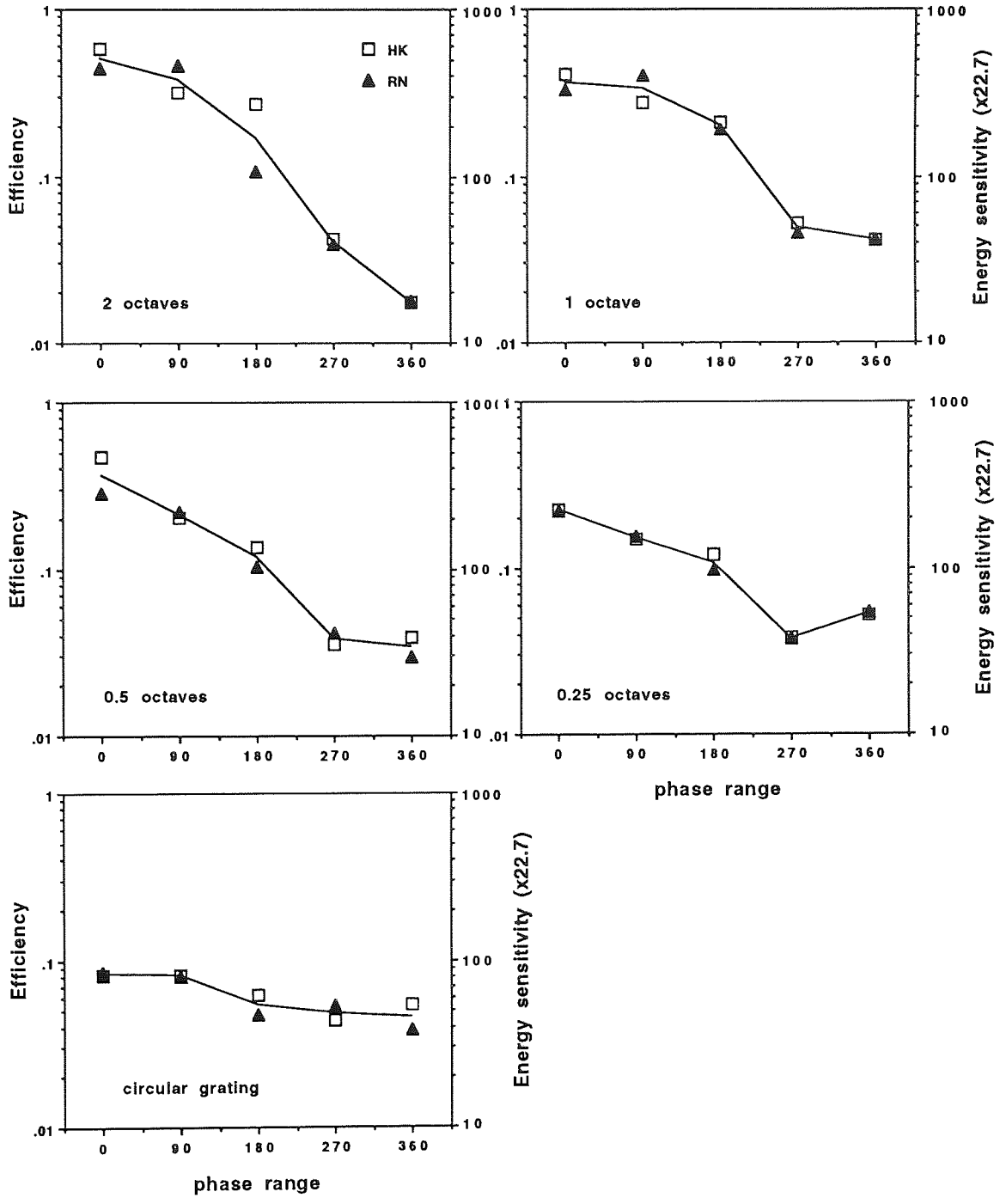

Figure 5.18
Detection efficiency for the band-pass filtered point stimuli and circular grating as a function of phase randomisation.

As Figure 5.18 shows, efficiency and energy sensitivity decreased with increasing phase range for all point stimuli. However, the effect of increasing phase range on efficiency reduced with decreasing stimulus bandwidth. Comparison with Figure 5.17 reveals that in fact, the effect of phase range on efficiency seemed to depend on the

change in the stimulus area: For the stimulus with 2 octaves bandwidth efficiency decreased from approximately 50% to 1.5% whereas for the stimulus with narrow, 0.25 octaves bandwidth, efficiency decreased from about 20% to 4%. In accordance, the area to which most of the contrast energy was confined increased more with increasing phase range for stimuli with large bandwidths (1-2 octaves) than for stimuli with narrow bandwidths (0.25-0.5 octaves). Between 270 and 360 degrees of phase range the decrease in efficiency slowed down and even reversed with decreasing stimulus bandwidth.

When the stimulus area was kept constant by using the homogenous circular grating, the increase of the phase range had only a small effect on detection efficiency. Efficiency decreased from 8% to 4.5% with increasing phase range.

In order to show the dependence of detection efficiency on the stimulus area, detection efficiencies of Figure 5.18 were plotted as a function of the spatial spread of contrast energy (α) in Figure 5.19. The spatial spread of contrast energy (α) is an area measure introduced in the previous section. It is a kind of variance of distances weighted by local contrast squared and normalised by the total contrast energy of the image (See section 5.5.2). The advantage of the spatial spread of contrast energy is that it takes into account the increasing area across which the contrast energy has spread, even in a case where the area is not evenly "filled" with contrast energy, as is the case with patched gratings, for example. The spatial spread of contrast energy is thus a better measure for stimulus area than, for example, a measure of stimulus area that comprises a certain percentage of stimulus energy (e.g. A_{95}) which would not be, in the case of patched grating, affected by the area across which grating patches have spread.

Figure 5.18 shows that efficiency decreased approximately linearly in semi-logarithmic coordinates as a function of stimulus area expressed in terms of the spatial spread of contrast energy (α). The least squares line of the form $\eta = \eta_0 \times e^{k\alpha}$ fitted to the efficiency data explained 84% and 86% of the total variance for subjects HK and RN, respectively. The value of constant η_0 was -1.1 for both subjects and the value of

constant k was 0.47 and 0.42 for subjects HK and RN, respectively. The explained variance was calculated for the logarithmic values as described in Appendix 1.

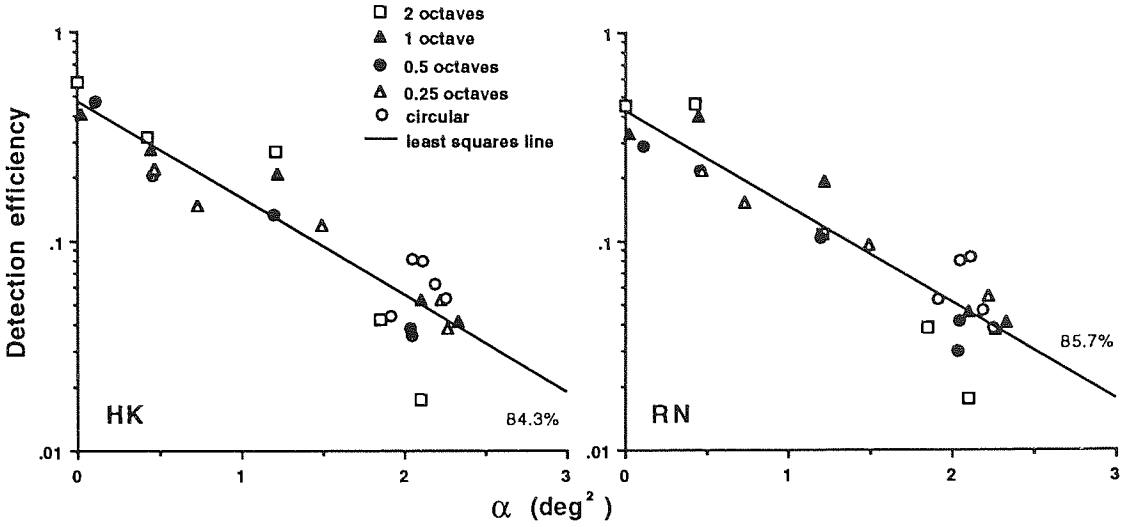

Figure 5.19
Detection efficiency for band-pass filtered point stimuli and circular grating as a function of the spatial spread of contrast energy for the subjects HK and RN.

For point stimuli the spatial spread of contrast energy increased as a function of phase randomisation whereas for the circular grating the spatial spread of contrast energy stayed approximately constant irrespective of the phase range. As a result, all the efficiency data for the circular grating were clustered within a small part of the decreasing function.

Although an increase in the spatial spread of contrast energy due to increase in area clearly results in a decrease in detection efficiency, the other studies of spatial integration of complex image described in Sections 5.3-5.5 of this thesis as well as all the grating studies reviewed in Introduction have pointed out that it is the number of details in the image that determines detection efficiency rather than the stimulus area: variation in grating area only affects detection efficiency if image complexity changes. Therefore, in Figure 5.20 detection efficiencies for our point stimuli have been plotted as a function of image complexity - the measure of the amount of details and contour in the image introduced in Section 5.5.2.

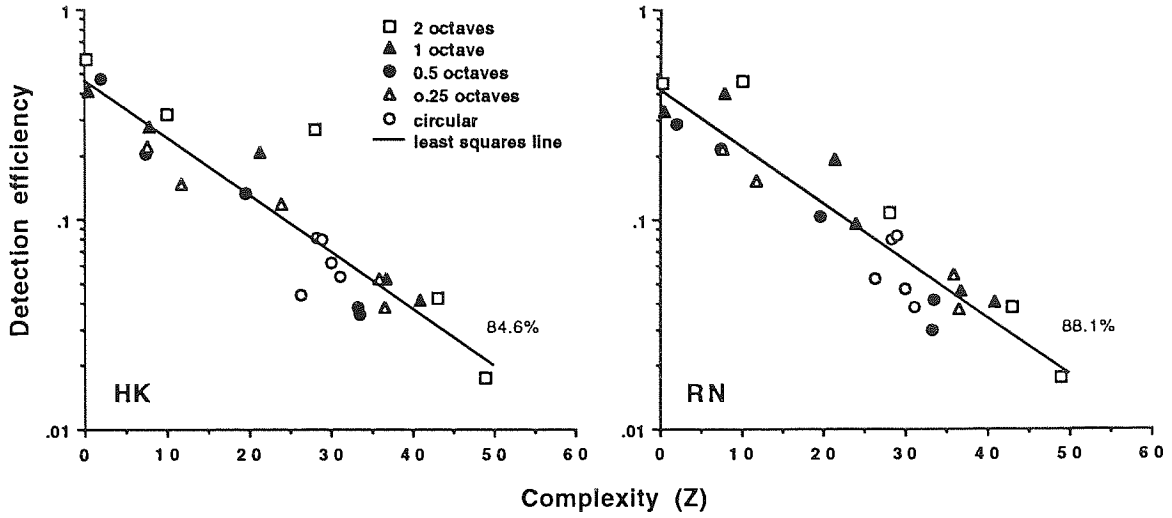

Figure 5.20
Detection efficiencies for the band-pass filtered point stimuli and circular grating as a function of image complexity for subjects HK and RN.

The range of phase modification affected image complexity (Z) in the same way as it affected the spread of contrast energy (α). This, of course, can be expected as the image complexity ($Z = \alpha f_c^2$) was defined as the product of the spatial spread (α) of contrast energy and the square of centre spatial frequency (f_c) of the image energy spectrum. In this experiment the centre frequency of the stimuli stayed approximately constant (3.7-4.8 c/deg) and thus the resulting values of image complexity were almost equal to the spatial spread of contrast energy multiplied by a constant.

Figure 5.20 shows that detection efficiency decreased again linearly in semi-logarithmic coordinates as a function of image complexity. The least squares line of the form $\eta = \eta_0 \times e^{kZ}$ fitted to the efficiency data explained 85% and 88% of the variance (See appendix 1) for subjects HK and RN, respectively. A marginally better explained variance was thus obtained when efficiencies were plotted as a function of image complexity instead of the spatial spread of contrast energy. The value of constant k was -0.06 for both subjects and the value of constant η_0 was 0.46 and 0.42 for subjects HK and RN, respectively. Again, the data for circular grating clustered within a small part of the decreasing function.

Finally, in Figure 5.21 efficiency data from the studies described earlier in this Chapter (plus symbol) are plotted together with the data of this experiment (open circles for points, closed circles for circular grating) as a function of stimulus complexity in double-logarithmic coordinates. The data for random stimuli from Section 5.3 is plotted with another symbol (closed squares).The least-squares curve of the form $\eta = \eta_0 \times Z^k$ fitted to the previous efficiency data from Sections 5.3-5.5 explained 88% and 82% of the data of subjects HK and RN, respectively. The values of constants η_0 and k were 0.41 and -0.50 for HK and 0.38 and -0.44 for RN.

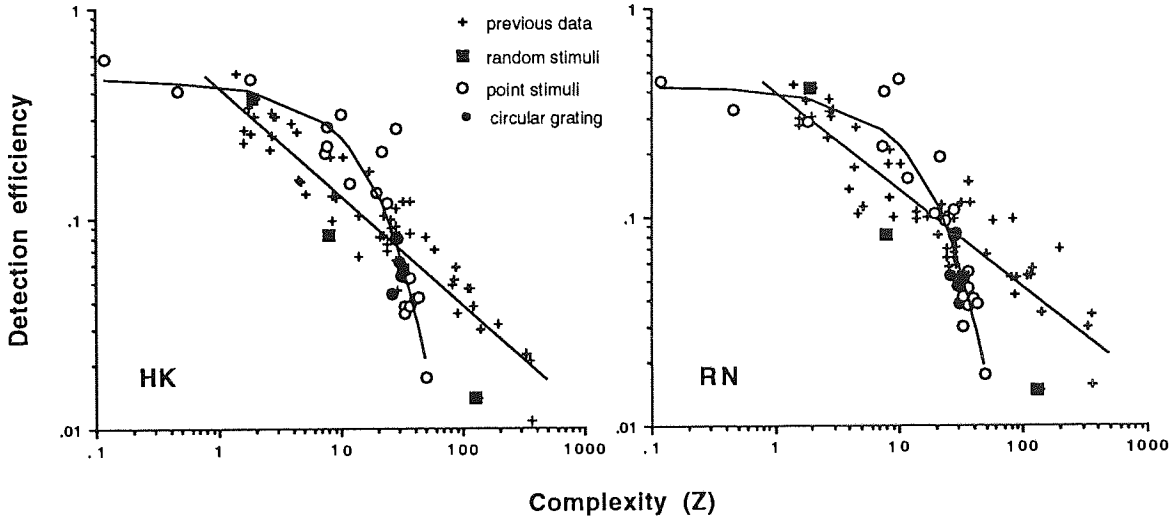

Figure 5.21
Detection efficiencies for the band-pass filtered point stimuli and circular grating of the current experiment as well as for the stimuli from the previous experiments described in Sections 5.3-5.5.

The detection efficiency curve for the point stimuli clearly differs from the data obtained using stimuli with ordered phase spectra (band-pass filtered letters, uniform and patched gratings). Detection efficiency at medium values of image complexity tended to be higher for point stimuli than for other stimuli. On the other hand, at higher values of image complexity detection efficiency dropped more rapidly for point stimuli with randomised phase spectra than for regular patterns from the studies of Sections 5.3-5.5, where the stimuli had ordered phase spectra at all image complexities. The point stimuli and circular grating with the largest image complexities (270 and 360 degrees of phase

randomisation) looked more like irregular texture or noise. As our experiments were performed in external spatial noise, it is quite possible that the detection task for stimuli with large ranges of phase randomisation changed its nature from pattern detection in noise to discrimination of noise texture in the presence of another.

The efficiency for random stimuli from Section 5.3 of this chapter was equal to the efficiency of all the other stimuli at low image complexities. This is in agreement with the result of Section 5.3 showing that at small image complexities spatial integration is similar for gratings and random images. At these low values of image complexity, any stimuli would contain little detail and contour and thus the spatial structure of these few details does not affect detection efficiency. At medium and high image complexities detection efficiency for the random stimuli form Section 5.3 decreased approximately linearly as a function of image complexity in double-logarithmic coordinates, but remained lower than the detection efficiencies for the stimuli of the previous studies. It seems thus that spatial integration for stimuli with random structure saturates at smaller image complexities than for stimuli with ordered structure (gratings, letter stimuli). The fact that detection efficiencies for the point stimuli were first relatively high but then suddenly decreased also supports this view as the phase range for the point stimuli increased gradually from ordered phase spectra to completely random phase as a function of image complexity.

5.6.3 Discussion

Detection efficiencies for the band-pass filtered point stimuli with various bandwidths and for the circular grating with a radial luminance modulation were found to decrease with increasing phase range produced by randomising the original zero phase of each spatial frequency component of the stimulus within various ranges. For the point stimuli an increase in phase range increased stimulus area and reduced efficiency although the amplitude spectrum of the stimulus was left unchanged. On the other hand, a change

in the bandwidth of the band-pass filtered point stimuli affected efficiency only when it was accompanied by a change in stimulus area, too. Thus, the decrease in detection efficiency in this study was primarily due to the increase in stimulus area expressed as the spatial spread of contrast energy (α).

When the spatial spread of contrast energy was kept constant by using the circular grating, the increase of phase range had only a small effect on detection efficiency. Efficiency decreased from 8% to 4.5% with increasing phase range. The phase randomisation produced an increase in the irregularity of the circular grating, which could be a contributing factor for a slight decrease in efficiency.

Although an increase in stimulus area (α) explained the decrease of detection efficiency for the point stimuli used in the current experiment, there is clear evidence that the primary determinant of detection efficiency is the number of details in the image, supporting the view that spatial integration is scale invariant (see Sections 5.1-5.5 of this Chapter). For the point stimuli and circular grating, however, image complexity (αf_c^2) and spatial spread of contrast energy (α) were equally good determinants of efficiency, because the centre spatial frequency for all the stimuli used was approximately constant (3.7-4.8 c/deg).

On the other hand, when comparing the shapes of the detection efficiency curves as a function of image complexity for point stimuli and for the stimuli of the previous studies (Sections 5.3-5.5), I found that they differed from each other. At higher values of image complexity efficiency decreased faster for the point stimuli of the present study than for the stimuli of the previous studies. The main difference between the stimuli of previous studies and the point stimuli of the current study is that as the complexity of point stimuli increased their spatial structure became increasingly random and looked more like irregular texture or band-pass filtered noise whereas all the other stimuli used so far remained spatially ordered although the number of details increased with increasing complexity. Therefore, detection efficiencies for the most randomised stimuli of the current study (phase range of 270-360 degrees) might represent data for another class of images whose detection efficiency curve has altogether a different slope as a function of

image complexity. Hence, although it seems clear that image complexity limits spatial integration of both irregular patterns and spatially ordered stimuli, the detection efficiency decreases faster for random stimuli because it is increasingly more difficult to deduce its spatial structures. As a consequence, it is increasingly difficult for the detection mechanism to form an accurate detection filter to match the stimulus. These inaccuracies then lead to poorer detection performance and a steeper decrease of detection efficiency as a function of stimulus complexity.

5.7 CONCLUSIONS

The effects of the complexity of the spatial frequency spectrum and its bandwidth, as well as the spatial spread of local contrasts in the image were studied in Sections 5.3-5.6 of this Chapter. The results obtained suggest that at the stage of image interpretation, the detection performance of the visual system is mainly restricted by the spatial structure of the stimulus rather than its spectral characteristics. Furthermore, one critical finding was that although the amount of details in the image is an important determinant, spatial integration is equally limited by the area across which contrast information has spread: Even if the nominal number of details in the image remained constant, detection efficiency decreased as the distance between the stimulus components increased: the decrease in detection efficiency is thus related to both the number of details in the image and the area over which the visual system needs to collect the information. The same determinant seemed to limit spatial integration of both complex stimuli and simple gratings supporting the view that the visual system is scale invariant irrespective of the spatial structure of the stimulus.

A new measure, image complexity, describing the amount and spread of details and contour in a stimulus was developed. The experimental data gathered suggest that this new measure of image complexity is the primary determinant of detection efficiency for a great variety of spatial stimuli. However, increase in image irregularity produced by phase randomisation also seems to contribute to the decrease of efficiency resulting in a steeper slope of decrease of detection efficiency as a function of image complexity. It seems that the human visual system is able to form a better detection filter for an image when the image is well structured that when it lacks of any ordered structure.

The present result agrees with the finding that in visual tasks the span of attention is limited, and only a small amount of information is processed in each glimpse (Verghese & Pelli, 1992). The finding of this study can be explained using various models of detection: We could assume an information collection window, called window of attention (van Essen & al., 1991) or sampling aperture (Burgess, 1990), which would collect

contrast information efficiently only at the centre of attention. The window would thus have gradually fading edges where the collection of information becomes increasingly inefficient. Another possibility is that the visual system could use a fixed number of samples from the image to form a detection filter. When the distances between these samples increases due to the spread of contrast information within the stimulus, the contrast energy collected at each location would decrease as a function of increasing extent of attention. Thus, efficiency of detection would be evenly reduced across the increasing stimulus area.

6. CONCLUDING SUMMARY

This thesis consisted of two major parts, one determining the masking characteristics of pixel noise and the other investigating the properties of the detection filter employed by the visual system. The purpose of this final chapter is to bring together all the major findings obtained.

Section 2.4 of the Chapter 2 pointed out that at in accordance with suprathreshold studies, the r.m.s contrast is a more valid measure describing human detection performance than Michelson contrast. Furthermore, it was demonstrated that contrast energy cannot be considered as a pure contrast metric due to its lack of scale invariance. It is, however, essential for the definition of detection efficiency.

The experiments of the *Chapter 3* showed that the masking effect of pixel noise can be increased by increasing the size of noise pixels as long as the side length in both horizontal and vertical direction is below the critical size. The minimum number of noise pixels depends only on the number of bars within the grating area. Therefore, when two-dimensional stimuli are used, the critical i.e. minimum number noise pixels per grating cycle is determined by the number of grating bars in each spatial dimension.

The maximum masking effect is obtained when the pixel size is at the critical size in each spatial direction. For one-dimensional grating there is no critical noise pixel side length along the grating bars and therefore the masking effect increases as the noise pixel height increases up to the height equal to the stimulus height producing one-dimensional noise. Therefore, the spectral density of one-dimensional noise should be calculated as the spectral density of two-dimensional noise, i.e. by taking into account the whole pixel area.

In *Chapter 4* Contrast sensitivity was measured with and without external spatial noise as a function of retinal illuminance, exposure duration, and grating area. The result showed that contrast sensitivity first increased similarly both with and without external noise as a function of the variable under study. However, in all the experiments contrast sensitivity with noise saturated earlier than contrast sensitivity without noise. After saturation contrast sensitivity with noise stayed constant and independent of the variable

under study. It thus seems that when contrast sensitivity is determined by external spatial noise, it is independent of the variable under study, if the physical signal-to-noise ratio remains constant. Contrast sensitivity thus depends only on the signal-to-noise ratio.

The results of *Chapter 3* were further supported by the results of *Chapter 4*: When contrast thresholds were determined by external noise (i.e. they were higher with than without noise), the one-dimensional spatial noise kept contrast threshold constant as a function of stimulus height. This suggests that signal-to-noise ratio remained constant. However, the physical signal-to-noise ratio stayed constant as a function of grating height only when both the spectral density of pixels noise and the contrast energy of the stimulus increased similarly as a function of stimulus height. Similarly, the third dimension, time, should be taken into account when calculating the spectral density of noise especially when the variable under study is exposure duration. It therefore seems that we should understand noise pixels as three dimensional "blocks" in order to describe the masking effect of spatial noise in the visual system.

Finally, *Chapter 5* studied the properties of the human detection mechanism by investigating the efficiency of spatial integration for stimuli with various spatial and spectral complexities. The results obtained suggest that at the stage of image interpretation, the detection performance of the visual system is mainly determined by the spatial structure of the stimulus rather than its spectral characteristics. Furthermore, one critical finding was that although the amount of contour and detail in the image is an important determinant, spatial integration is equally limited by the area across which contrast information has spread: Even if the number of details in the image remained constant, detection efficiency decreased as the distance between the stimulus parts increased: the decrease in detection efficiency is thus related to both the number of details in the image and the area over which the visual system needs to collect the information. The same determinant seemed to limit spatial integration of both complex stimuli and simple gratings supporting the view that the visual system is scale invariant irrespective of the spatial structure of the stimulus.

A new measure, image complexity, describing the amount of details and contour in stimuli was developed. The experimental data gathered suggest that this new measure of image complexity is the primary determinant of detection efficiency for a great variety of spatial stimuli. However, increase in image irregularity produced by phase randomisation also seems to contribute to the decrease of efficiency resulting in a steeper slope of decrease of visual detection efficiency as a function of image complexity. It seems that the human visual system is able to form a better detection filter for an image when the image is well structured than when it lacks any ordered structure.

The results of *Chapter 5* clearly suggest that the detection mechanism employed by the visual system is highly adaptive. The accuracy of the detection filter or model used for detection depends on the spatial structure of the stimulus and the area over which the stimulus is distributed.

PUBLICATIONS AND PRESENTATIONS

PUBLICATIONS

Papers

1) Näsänen R., Kukkonen H., and Rovamo J. (1993). Spatial integration of band-pass filtered patterns in noise. Vision Research, 33, 903-911.

2) Rovamo J., Kukkonen H., Tiippana K., and Näsänen R. (1993). Effects of luminance and exposure time on contrast sensitivity in spatial noise. Vision Research, 33, 1123-1129.

3) Kukkonen H., Rovamo J., Tiippana K., and Näsänen R. (1993). Michelson contrast, RMS contrast and energy of various spatial stimuli at threshold. Vision Research, 33, 1431-1436.

4) Näsänen R., Kukkonen H., and Rovamo J. (1994). Relationship between spatial integration and spatial spread of contrast energy in detection. Vision Research, 34, 949-954.

5) Kukkonen H., Näsänen R., and Rovamo J. (1994). Detection efficiency of circular gratings and band-pass filtered points with randomised phase spectra. Investigative Ophthalmology & Visual Science, 35, in press.

6) Kukkonen H., Rovamo J., and Näsänen R. (1994). Masking potency and whiteness of noise at various pixel sizes. Investigative Ophthalmology & Visual Science, under revision.

7) Kukkonen H. and Rovamo J. (1994). The effect of noise pixel size and shape on grating detectability. Vision Research, under revision.

Abstracts

8) Näsänen R., Kukkonen H., and Rovamo J. (1991). Effect of image structure on contrast detectability, poster abstract, Investigative Ophthalmology & Visual Science, 32/4, 1270

9) Näsänen R., Kukkonen H., and Rovamo J. (1991). Effect of image structure on contrast sensitivity in noise, paper abstract, Perception, Vol. 20 suplement

10) Rovamo J., Kukkonen H., and Näsänen R. (1991). Effect of image structure on contrast energy thresholds in noise, poster abstract, Eur. J. Neurosci, Supplement 4

11) Kukkonen H., Näsänen R., and Rovamo J. (1991). Efficiency for detecting band-pass filtered images, poster abstract, Ophthalmological and Physiological Optics, 11, 396

12) Näsänen R., Kukkonen H., and Rovamo J. (1991). Detection of band-pass filtered patterns in noise, poster abstract, Optics and Photonics News,2/9

13) Kukkonen H., Näsänen R., and Rovamo J. (1992). Effect of stimulus phase spectrum on contrast detection in noise, paper abstract, Investigative Ophthalmology & Visual Science 33/4, 1257

14) Kukkonen H., Rovamo J., Tiippana K., and Näsänen R. (1992). Contrast thresholds for gratings in spatial noise with various picture element areas and shapes, paper abstract, Optics and Photonics News,3/7

15) Kukkonen H., Rovamo J., and Näsänen R. (1993). Detection of gratings in pixel noise: The critical size of noise pixel, poster abstract, Perception vol. 22 suplement

16) Näsänen R., Kukkonen H., and Rovamo J. (1993). Image complexity and human detection efficiency, poster abstract, Perception vol. 22 suplement

PRESENTATIONS

Papers

1) Kukkonen H., Näsänen R., and Rovamo J. (1992). Effect of stimulus phase spectrum on contrast detection in noise. Annual Meeting of The Association for Research in Vision and Ophthalmology, 3-8 May 1992, Sarasota, Florida

2) Kukkonen H., Rovamo J., Tiippana K., and Näsänen R. (1992) Contrast thresholds for gratings in spatial noise with various picture element areas and shapes. The Optical Society of America 1992 Annual Meeting, 20.-25.9.1992, Albuquerque, New Mexico

3) Kukkonen H. (1992). The effect of noise structure on detection threshold for gratings. Internal Seminar Series, 13.10.1992, Department of Vision Sciences, University of Aston, Birmingham, UK

4) Kukkonen H., Rovamo J., Tiippana K., and Näsänen R. (1992). Contrast sensitivity in spatial noise as a function of luminance, grating area, and exposure time. AVA Postgraduate Open Contribution Meeting, 4.1.1992, London, UK

Posters

5) Kukkonen H., Näsänen R., and Rovamo J. (1991). Effect of image structure on the efficiency of contrast detection in noise, ScanVision Congress, 12-14 April 1991, Denmark

6) Näsänen R., Kukkonen H., and Rovamo J. (1991). Effect of image structure on contrast detectability, Annual Meeting of The Association for Research in Vision and Ophthalmology, 28 April -3 May 1991, Sarasota, Florida

7) Kukkonen H., Näsänen R., and Rovamo J. (1991). Efficiency for detecting band-pass filtered images, The 1991 Meeting of the Society of Experimental Optometry, 15-16 July 1991, Birmingham, UK

8) Kukkonen H., Rovamo J., Tiippana K., and Näsänen R. (1992). The effect of retinal illuminance, exposure time, and grating area on contrast sensitivity for gratings with and without spatial noise, The 15th European Conference on Visual Perception, 30.8.-3.9.1992, Pisa, Italy

9) Kukkonen H., Rovamo J., and Näsänen R. (1993). Detection of gratings in pixel noise: The critical size of noise pixel, The 16th European Conference on Visual Perception, 25.-29.8.1993, Edinburgh, Scotland, UK

REFERENCES

Ahumada Jr, A. J. (1987). Putting the visual system noise back in the picture. Journal of the Optical Society of America A4, 2372-2377.

Ahumada Jr, A. J. & Watson, A. B. (1985). Equivalent-noise model for contrast detection and discrimination. Journal of the Optical Society of America A2, 1133-1139.

Arend, L. E. Jr. (1976). Response of the human eye to spatially sinusoidal gratings at various exposure durations. Vision Research, 16, 1311-1315.

Baumgardt, E. (1972). Threshold quantal problems. In Jameson, D & Hurvich, L. M. (Eds.): Visual Psychophysics / Handbook of Sensory Physiology, Vol VII/4. Springer-Verlag Berlin.

Banks, M.S., Geisler, W.S. & Bennet, P.J. (1987). The physical limits of grating visibility. Vision Research, 27, 1915-1924.

Barlow, H. B. (1956). Retinal noise and absolute threshold. Journal of the Optical Society of America, 46, 634-639.

Barlow, H. B. (1957). Increment thresholds at low intensities considered as signal/noise discriminations. Journal of Physiology, 136, 469-488.

Barlow, H. B. (1977). Retinal and central factors in human vision limited by noise. In Barlow, H. B. & Fatt, P. (Eds.): Vertebrate Photoreception. Academic Press, London. 337-358

Breitmeyer, B. G. & Ganz, L. (1977). Temporal studies with flashed gratings: inferences about human transient and sustained channels. Vision Research, 17, 861-865.

Burgess, A.E. (1990). High level decision efficiencies. In Blakemore, C. (Ed.), Vision: Coding and efficiency (pp. 431-440). New York: Cambridge University Press.

Burgess, A. (1985). Visual signal detection. III. On Bayesian use of prior knowledge and cross correlation. Journal of the Optical Society of America, A2, 1498-1507.

Burgess, A.E. & Ghandeharian H. (1984). Visual signal detection. I. Ability to use phase information. Journal of the Optical Society of America, A1, 900-905.

Burgess, A.E. & Ghandeharian H. (1984). Visual signal detection. II. Signal-location identification. Journal of the Optical Society of America, A1, 906-910.

Bracewell, R. N. (1978). The fourier transform and its applications. McGraw-Hill Kogakusha.

Campbell, F. W. & Green D. G. (1965). Optical and retinal factors affecting visual resolution. Journal of Physiology, 181, 576-593.

Campbell, F. W. & Gubish, R. W. (1966). Optical quality of the human eye. Journal of Physiology, 186, 558-578.

Campbell, F.W., Kulikowski, J.J. & Levinson, J. (1966). The effect of orientation of the visual resolution of gratings. Journal of Physiology, London, 187, 427-436.

Campbell, F.W. & Robson, J.G. (1968). Application of Fourier analysis to the visibility of gratings. Journal of Physiology, 197, 551-566.

Carter, B. E. & Henning, G. B. (1971). The detection of gratings in narrow-band visual noise. Journal of Physiology, 219, 355-365.

Chesters, M. S. (1973). The influence of visual noise on visual detection thresholds, PhD thesis, University of Leeds.

Coltman, J. W. & Anderson, A. E. (1960). Noise limitations to resolving power in electronic imaging. Proceedings of the IRE, 48, 858-865.

Cornsweet, T. N. (1970). Visual Perception. New York: Harcourt (Brace & Jovanovich).

Curcio, C. A., Sloan, K. R., Packer, O., Hendrickson, A. E. & Kalina, R. E. (1987). Distribution of cones in human and monkey retina: Individual variability and radial asymmetry. Science, 236, 579-582.

Davila, K. D. & Geisler, W. S. (1991). The relative contributions of pre-neural and neural factors to areal summation in the fovea. Vision Research, 31, 1369-1380.

Davis, E.T. & Graham, N. (1981). Spatial frequency uncertainty effects in the detection of sinusoidal gratings. Vision Research, 21, 705-712.

Davis, E.T., Kramer, P. & Graham, N. (1983). Uncertainty about spatial frequency, spatial position, or contrast of visual patterns. Perception & Psychophysics, 33, 20-28.

Deeley, R.J., Drasdo, N. & Charman, W.N. (1991). A simple parametric model of the human ocular modulation transfer function. Ophthal. Physiol. Opt., 11, 91-93.

De Valois, R. L., Albrecht, D. G. & Thorell, L. G. (1982). Spatial frequency selectivity of cells in macaque visual cortex. Vision Research, 22, 545-559.

De Vries, H. L. (1943). The quantum character of light and its bearing upon threshold of vision, the differential sensitivity and visual acuity of the eye. Physica X, 553-564.

Elliot, P. (1964). Forced choice tables (Appendix 1). In Swets, J.A. (Ed.), Signal detection and recognition by human observers, (pp. 679-684). New York, Wiley.

van Essen, D. C., Olshausen, B., Anderson, C. H. & Gallant, J. L. (1991). Pattern recognition, attention, and information bottlenecks in the primate visual system. In Proceedings of the SPIE Conference on Visual Information Processing: From Neurons to Chips, 1473, 17-28.

Estévez, O & Cavonius, C. R. (1976). Low-frequency attenuation in the detection of gratings: sorting out the artefacts. Vision Research, 497-500.

Findlay, J. M. (1969). A spatial integration effect in visual acuity. Vision Research, 9, 157-166.

Georgeson, M. A. & Georgeson, J. M. (1987). Facilitation and masking of briefly presented gratings: time-course and contrast dependence. Vision Research, 27, 369-379.

Gontzalez, R. C. & Woods, R. E. (1992). Digital Image Processing. Addison-Wesley Publishing Company, Reading, Massachusetts.

Graham, N. (1989). Visual pattern analyzers. New York: Oxford University Press. ISBN 0-19-505154-8.

Graham, C. H., Brown, R. H. & Mote, F. A. (1939). The relation of size of stimulus and intensity in the human eye: I. Intensity thresholds for white light. Journal of Experimental Psychology, 24, 555-573.

Graham, N. & Hood, D. C. (1992). Quantal noise and decision rules in dynamic models of light adaptation. Vision Research, 32, 779-787.

Green, D. M. & Swets, J. A. (1966). Signal detection theory and psychophysics. Theory of Ideal observers, 151-179. John Wiley and Sons, Inc., New York.

Harmon, L. D. & Julesz, B. (1973). Masking in visual recognition: effects of two-dimensional filtered noise. Science, 1194-1197.

Harris, M. G. & Georgeson, M. A. (1986). Sustained and transient temporal integration functions depend on spatial frequency, not grating area. Vision Research, 26, 1779-1782.

Harvey, L. O. & Pöppel, E. (1972). Contrast sensitivity of the human retina. American Journal of Optometry, 49, 748-753.

Hauske, G., Wolf, W. & Lupp, U. (1976). Matched filters in human vision. Biological Cybernetics, 22, 181-188.

Henning, G.B., Hertz, B.G. & Hinton, J.L. (1981). Effects of different hypothetical detection mechanisms on the shape of spatial-frequency filters inferred from masking experiments: I. noise masks. Journal of the Optical society of America, 71, 574-581.

Hoekstra, J., Van der Goot, D.P.J., Van den Brink, G. & Bilsen, F.A. (1974). The influence of the number of cycles upon the visual contrast threshold for spatial sine wave patterns. Vision Research, 14, 365-368.

Howell, E.R. & Hess, R.F. (1978). The functional area for summation to threshold for sinusoidal gratings. Vision Research, 18, 369-374.

Hubel, D. H. & Wiesel, T. N. (1962). Receptive fields, binocular interaction and functional architecture in the cat's visual cortex. Journal of Physiology, London. 160,106-154.

Hubel, D. H. & Wiesel. T. N. (1968). Receptive fields and functional architecture of monkey striate cortex. Journal of Physiology, London. 195, 215-243.

Jamar, J. H. T. & Koenderink, J. J. (1983) Sine-wave gratings: scale invariance and spatial integration at suprathreshold contrast. Vision Research, 23,805-810.

Kersten, D. (1984). Spatial summation in visual noise. Vision Research, 24, 1977-1990.

Koenderink, J.J. & van Doorn, A.J. (1980). Spatial summation for complex bar patterns. Vision Research, 20, 169-176.

Lappin, J. S. & Uttal, W. R. (1976). Does prior knowledge facilitate the detection of visual targets in random noise. Perception and Psychophysics, 20, 367-374.

Legge, G. E. (1978). Sustained and transient mechanisms in human vision: temporal and spatial properties. Vision Research, 18, 69-81.

Legge, G. E. & Foley J.M. (1980). Contrast masking in human vision. Journal of the Optical Society of America, 1458-1471.

Legge, G. E., Kersten, D. & Burgess, A.E. (1987). Contrast discrimination in noise. Journal of the Optical Society of America, A4, 391-404.

Lillywhite, P. G. (1981). Multiplicative intrinsic noise and the limits to visual performance. Vision Research, 21, 291-296.

Lillywhite, P. G. & Laughlin, S. B. (1979). Tranducer noise in a photoreceptor. Nature, 277, 569-572.

Luntinen, O., Rovamo, J. & Näsänen, R. (1994). Contrast sensitivity as a function of grating area and spectral density of external spatial noise. Vision Research, under revision.

Mayhew, J.E.W. & Frisby, J.P. (1978). Suprathreshold contrast perception and complex random textures. Vision Research, 18, 895-897.

McCann, J. J. (1978). Visibility of gradients and low spatial frequency sinusoids: Evidence for a distance constancy mechanism. Photographic Science and Engineering, 22, 64-68.

McCann, J. J., Savoy, R. L., Hall, Jr. J. A. & Scarpetti, J. J. (1974). Visibility of continuous luminance gradients. Vision Research, 14, 917-927.

van Meeteren, A. & Barlow, H. B. (1981). The statistical efficiency for detecting sinusoidal modulation of average dot density in random figures. Vision Research, 21, 765-777.

van Meeteren, A. & Boogaard, J. (1972). Visual contrast sensitivity with ideal image intensifiers. Optik, 37, 179-191

van Meeteren, A. & Valeton, J.M. (1988). Effects of pictorial noise interfering with visual detection. Journal of the Optical Society of America, A5, 438-444.

Morrone, M. C., Burr, D. C. & Ross, J. (1983). Added noise restores recognizability of coarse quantized images. Nature, 305, 226-228.

Moulden, B., Kingdom, F. & Gatley, L.F. (1990). The standard deviation of luminance as a metric for contrast in random-dot images. Perception, 19, 79-101.

Mustonen, J., Rovamo, J. & Näsänen, R. (1993). The effects of grating area and spatial frequency on contrast sensitivity as a function of light level. Vision Research, 33. 2065-2072.

Nachmias, J. (1967). Effects of exposure duration on visual contrast sensitivity with square-wave gratings. Journal of the Optical Society of America, 57, 421-427.

Nachmias, J. (1968). Visual resolution of two-bar patterns and square-wave gratings. Journal of the Optical Society of America, 58, 10-13.

Nagaraja, N.S. (1964). Effect of luminance noise on contrast thresholds. Journal of the Optical Society of America, 54, 950-955.

Nakayama, K. (1990). The iconic bottleneck and the tenuous link between early visual processing and perception. In Blakemore C. (Ed.). Vision: Coding and Efficiency. Cambridge University Press, Cambridge, 411-422.

van Nes, F. L. & Bouman, M.A. (1967). Spatial modulation transfer in the human eye. J. Opt. Soc. Am., 57, 401-406.

van Nes, F. L., Koenderink, J. J., Nas, H. & Bouman, M. A. (1967). Spatiotemporal modulation transfer in the human eye. Journal of the Optical Society of America, 57, 1082-1088.

Näsänen, R. (1989). Effects of halftoning and noise on visual perception of spatial signals. PhD Thesis, Teknillinen Korkeakoulu, Helsinki, Finland.

Pelli, D. G. (1981). Effects of visual noise. PhD thesis. Cambridge: University of Cambridge.

Pelli, D. G. (1990). The quantum efficiency of vision. In Blakemore C. (Ed.). Vision: Coding and Efficiency. Cambridge University Press, Cambridge, 3-24.

Pelli, D.G. & Zhang, L. (1991). Accurate control of contrast on microcomputer displays. Vision Research, 31, 1337-1350.

Pointer, J. S. & Hess, R. F. (1989). The contrast sensitivity gradient across the human visual field: with emphasis on the low spatial frequency range. Vision Research, 29, 1133-1151.

Pointer, J. S. & Hess, R. F. (1990). The contrast sensitivity gradient across the major oblique meridians of the human visual field. Vision Research, 30, 497-501.

Pollehn, H. & Roehrig, H. (1970). Effect of noise on the modulation transfer function of the visual channel. Journal of the Optical Society of America, 60, 842-848.

Pöppel, E. & Harvey, L. O. (1973). Light-difference threshold and subjective brightness in the periphery of the visual field. Psychol. Forsch., 36, 145-161.

Quick, R.F. (1974). A vector model of contrast detection. Kybernetik. 16, 65-67.

Quick, R.F., Hamerly, J. R. & Reichert, T. A. (1976). The absence of a measurable "critical band" at low suprathreshold contrasts. Vision Research, 16, 351-355.

Ratliff, F. & Hartline, H. K. (1959). The responses of limulus optic nerve fibers to patterns of illumination on the receptor mosaic. J. Gen. Physiol., 42, 1241-1255.

Robson, J.G. & Graham, N. (1981). Probability summation and regional variation in contrast sensitivity across the visual field. Vision Research, 21, 409-418.

Rose, A. (1948). The sensitivity performance of the human eye on an absolute scale. Journal of the Optical Society of America, 38, 196-208.

Ross, J. & Speed, H. D. (1991). Contrast adaptation and contrast masking in human vision. Proceedings of the Royal Society of London B, 246, 61-69.

Rovamo, J. & Virsu, V. (1979). An estimation and application of the human cortical magnification factor. Experimental Brain Research, 37, 495-510.

Rovamo, J., Leinonen, L., Laurinen, P. & Virsu, V. (1984). Temporal integration and contrast sensitivity in foveal and peripheral vision. Perception, 13, 665-674.

Rovamo, J., Franssila, R. & Näsänen, R. (1992). Contrast sensitivity as a function of spatial frequency, viewing distance and eccentricity with and without noise. Vision Research, 32, 631-637.

Rovamo, J., Luntinen, O.& Näsänen, R. (1993). Modelling the dependence of contrast sensitivity on grating area and spatial frequency. Vision Research,33, 2773-2788.

Rovamo, J., Luntinen, O. & Näsänen, R. (1994e). Modelling the increase of contrast sensitivity with grating area and exposure duration. Vision Research, accepted for publication.

Rovamo, J., Mustonen, J. & Näsänen, R. (1994a). Two simple psychophysical methods for determining the optical modulation transfer function of the human eye, Vision Research, submitted.

Rovamo, J., Mustonen, J. & Näsänen, R. (1994b). Neural modulation transfer function of the human visual system at various eccentricities. Vision Research, submitted.

Rovamo, J., Mustonen, J. & Näsänen, R. (1994c). Modelling contrast sensitivity as a function of retinal illuminance and grating area. Vision Research, in press.

Rovamo, J., Ukkonen, O., Thompson, C. & Näsänen, R. (1994d). Spatial Integration of Compound Gratings with Various Numbers of Orientation Components. Investigative Ophthalmology and Visual Science,

Santamaria, J., Artal, P. & Bescos, J. (1987). Determining the point spread function of the human eyes using a hybrid optical-digital method. The Journal of the Optical Society of America A, 4, 1109-1114.

Savoy, R.L. & McCann, J.J. (1975). Visibility of low-spatial-frequency sine-wave targets: Dependence on number of cycles. Journal of the Optical Society of America, 65, 343-350.

Schade, O. H. (1956). Optical and photoelectric analog of the eye. Journal of the Optical Society of America, 46, 721-739.

Sheng, Y. & Arsenault, H.H. (1987). Noisy-image normalization using low-order radial moments of circular-harmonic functions. The Journal of the Optical Society of America A, 4, 1176-1184.

Sperling, G. (1989). Three stages and two systems of visual processing. Spatial Vision, 4, 183-207.

Stromeyer, C.F. & Julesz, B. (1972). Spatial frequency masking in vision: Critical bands and spread of masking. Journal of the Optical Society of America, 62, 1221-1232.

Tanner, W. P. and Birdsall, T. G. (1958). Definitions of d' and n as psychophysical measures. The Journal of the Acoustical Society of America, 30, 922-928.

Tiippana, K., Näsänen, R. & Rovamo, J. (1994) Contrast matching of two-dimensional compound gratings. Vision Research, in press.

Ukkonen, O., Rovamo, J. & Näsänen, R. (1993). The effect of orientation randomization on simple and compound gratings. Investigative Ophthalmology & Visual Science, 34/4 Suplement, 781.

Verghese, P. & Pelli, D. G. (1992). The information capacity of visual attention. Vision Research, 32, 983-995.

Virsu, V. & Rovamo, J. (1979). Visual resolution, contrast sensitivity, and the cortical magnification factor. Experimental Brain Research, 37, 475-494.

Watson, A. B. (1979). Probability summation over time. Vision Research, 19, 515-522.

Watson, A.B., Barlow, H.B. & Robson, J.G. (1983). What does the eye see best. Nature, 302, 419-422.

Westheimer, G. & McKee, S. P. (1977a). Integration regions for visual hyperacuity. Vision Research, 17, 89-93.

Westheimer, G. & McKee, S. P. (1977b). Spatial configurations for visual hyperacuity. Vision Research, 17, 941-947.

Wetherill, G.B. & Levitt, H. (1965). Sequential estimation of points on a psychometric function. The British Journal of Mathematical and Statistical Psychology, 18, 1-10.

Williams, D. R. (1985). Aliasing in human foveal vision. Vision Research, 25, 195-205.

Wright, M. J. (1982). Contrast sensitivity and adaptation as a function of grating length, Vision Research, 22, 139-149.

APPENDIX 1

THE LEAST SQUARES CURVES AND EXPLAINED VARIANCES

The least-squares curves were fitted to the data on a logarithmic scale. The goodness of the least-squares curves was estimated by calculating the variance of the experimental data from the least-squares values and expressing this as a proportion of the total variance of the experimental data. Logarithmic values were used instead of linear because the data were plotted on logarithmic axes.

The error variance of the experimental data (D) from the estimated values (D_{est}) is given by

$$\delta_e^2 = \frac{1}{n}\Sigma\,(logD - logD_{est})^2 \qquad (1)$$

The total variance of the experimental data is

$$\delta_{total}^2 = \frac{1}{n}\Sigma\,(logD - logD_{ave})^2, \qquad (2)$$

where D_{ave} is the average of logarithm of the experimental data:

$$D_{ave} = \frac{1}{n}\Sigma\, logD \qquad (3)$$

The explained percentage of the variance was then calculated as:

$$r^2 = 100[1 - \frac{\Sigma(\log D - \log D_{est})^2}{\Sigma(\log D - D_{ave})^2}]. \qquad (4)$$

APPENDIX 2

THE R.M.S CONTRAST ($c_{r.m.s}$) FOR A COSINE GRATING

According to definition r.m.s contrast in one spatial dimension is given by

$$c_{r.m.s}=[\frac{1}{n}\int_0^n c^2(x)\,dx]^{1/2}, \tag{1}$$

where c(x) is the contrast signal. The contrast signal is given by

$$c(x)=\frac{L(x)-L_0}{L_0}, \tag{2}$$

where L(x) is the luminance signal and L_0 is the mean luminance. For a cosine grating L(x) has a form

$$L(x)=L_0(c\cos(2\pi fx)+1)=L_0\,c\cos(2\pi fx)+L_0, \tag{3}$$

where c refers to the Michelson contrast of the cosine grating and f to its spatial frequency. From equations (2) and (3) we then get the contrast signal for a cosine grating:

$$c(x)=\frac{L_0\,c\cos(2\pi fx)+L_0-L_0}{L_0}=c\cos(2\pi fx)$$

The r.m.s contrast for a cosine grating is thus given by

$$c_{r.m.s}=[\frac{1}{n}\int_0^n[c\cos(2\pi fx)]^2\,dx]^{1/2}$$

$$\Rightarrow$$

$$c_{r.m.s}=[\frac{c^2}{n}\Big|_0^n\frac{x}{2}+\frac{\sin(4\pi fx)}{8\pi f}]^{1/2}$$

$$=[\frac{c^2}{n}(\frac{n}{2}+\frac{\sin(4\pi fn)}{8\pi f}]^{1/2}$$

$$=[\frac{c^2}{2}+\frac{c^2\sin(4\pi fn)}{8\pi fn}]^{1/2}.$$

The latter part of the right side of the above equation becomes smaller with increasing n i.e. with increasing number of cycles. Thus the r.m.s contrast of a cosine grating is approximately

$$c_{r.m.s}\cong\sqrt{\frac{c^2}{2}}=\frac{c}{\sqrt{2}},$$

where c was the Michelson contrast of the cosine grating. The equation above is accurate when $\sin(4\pi fn)=0$, that is when

$4\pi fn=k\pi \Rightarrow n=k/4f$, where k = 0, 1, 2, 3...

APPENDIX 3

THE SPECTRAL DENSITY OF PIXEL NOISE

The spectral density of pixel noise can be derived from the energy spectrum of a noise field. For simplicity, the definition of spectral density is here derived for one-dimension.

The waveform of static pixel noise can be considered as a sum of independent pulse functions. In one dimension a pulse function is given by:

$$rect(x) = \begin{cases} 1, when & |x| \le 1/2 \\ 0, when & |x| > 1/2 \end{cases} \quad (1)$$

When the width of each pixel is p, we can describe each pixel by rect(x/p).

The contrast of each pixel varies randomly in pixel noise. If contrast of the k^{th} pixel within a noise field is c_k, the waveform of a noise field [n(x)] can be described as a sum of pulse functions each displaced by kp and multiplied by the local contrast c_k:

$$n(x) = \sum_{k=0}^{n-1} c_k \, rect(\frac{x}{p} - kp) \quad (2)$$

The spectral density function is derived from the average energy spectrum of a noise field. The energy spectrum of one noise field is obtained as a product of the Fourier spectrum [F(u)] and its complex conjugate [F*(u)].

Fourier spectrum of the contrast waveform is

$$F(u) = \mathcal{F}\{n(x)\} = \sum_{k=0}^{n-1} c_k \int rect(\frac{x}{p} - kp) \, e^{-j2\pi ux} \, dx \quad (3)$$

When k = 0, the equation equals the Fourier transfrom of a single pulse function F(u) = p sinc(up) (Gonzalez & Woods, 1992). According to Shift Theorem (Bracewell, 1978)), for $k \neq 0$, the value of the function (i.e. its contrast c_k) is multiplied by $e^{-j2\pi kpu}$. Equation (3) can thus be rewritten

$$F(u) = p\,sinc(up) \sum_{k=0}^{n-1} c_k \, e^{-j2\pi kpu} \quad (4)$$

which is the Fourier spectrum of a noise field in one spatial dimension. The exact form of the Fourier spectrum of equation (4) depends on the value c_k, which varies from one pixel to another.

The energy spectrum of one noise field [n(x)] is given

$$|F(u)|^2 = p^2 sinc^2(up) [\sum_{k=0}^{n-1} c_k e^{-j2\pi kpu}] [\sum_{l=0}^{n-1} c_l e^{+j2\pi lpu}] \quad (5)$$

from which we get

$$|F(u)|^2 = p^2 sinc^2(up) \sum_{k=0}^{n-1} \sum_{l=0}^{n-1} c_l e^{+j2\pi lpu} \, c_k e^{-j2\pi kpu} \quad (6)$$

and

$$|F(u)|^2 = p^2 sinc^2(up) \sum_{k=0}^{n-1} \sum_{l=0}^{n-1} c_l \, c_k \, e^{+j2\pi (l-k)pu} \quad (7)$$

When k = l, the sum equals c_k^2. Therefore

$$|F(u)|^2 = p^2 sinc^2(up) [\sum_{k=0}^{n-1} c_k^2 + \sum_{k=0}^{n-1} \sum_{l=0; l \neq k}^{n-1} c_l c_k e^{+j2\pi (l-k)pu}] \quad (8)$$

In the average energy spectrum the latter part of the equation (8) approaches zero, because the values c_k and c_l are independent variables with zero mean. Therefore, the average energy spectrum is given by

$$\overline{|F(u)|^2} = p^2 sinc^2(up) \overline{\sum c_k^2} \tag{9}$$

The spectral density of pixel noise field [n(x)] (i.e. the power spectrum) is the average energy spectrum divided by the total width of the noise field (=np)

$$N(u) = p\, sinc^2(up) \overline{\sum c_k^2 / n} \tag{10}$$

The latter term equals to the r.m.s contrast of noise squared. The term $sinc^2(up)$ can be rewritten

$$sinc^2(up) = [\frac{\sin(\pi up)}{\pi up}]^2 \tag{11}$$

The spectral density function for pixel noise in one spatial dimension is thus given by

$$N(u) = p c_{r.m.s}^{\ 2} [\frac{\sin(\pi pu)}{\pi pu}]^2 \tag{12}$$

Because the spectral density of pixel noise is based on the Fourier transform, the spectral density function is considered to be two-sided, i.e. containing both positive and negative spatial frequencies symmetrically around origin.

APPENDIX 4

TABLES OF THE EXPERIMENTAL DATA OF THE THESIS.

CHAPTER 2

Figure 2.6a

Spatial frequency	grating 12.7 deg^2	grating 12 c	random 12.7 deg^2	random 12 c
0.25	117.0		86.62	
0.5	162.0	543.7	104.0	88.24
1.0	347.4	486.9	117.7	106.3
1.4		458.9		112.1
2.0	392.9	430.2	117.7	81.74
2.8		384.9		67.65
4.0	366.6	277.5	63.24	74.83
5.6		315.2		58.71
8.0	163.9	208.1	31.22	36.25
11		69.16		15.17
16	23.94	23.06	8.653	5.636
22		9.264		3.435

Figure 2.6b

Spatial frequency	grating 12.7 deg^2	grating 12 c	random 12.7 deg^2	random 12 c
0.25	127.0		81.25	
0.5	195.6	437.0	98.74	107.7
1.0	389.7	424.0	113.8	104.4
1.4		375.1		93.00
2.0	387.8	425.2	105.0	78.73
2.8		422.9		71.86
4.0	267.3	295.9	60.89	58.82
5.6		221.9		61.37
8.0	96.11	107.4	22.53	30.48
11		58.09		16.56
16	24.58	18.36	7.704	6.290
22		8.902		3.328

Figure 2.7a

Spatial frequency	grating 12.7 deg^2	grating 12 c	random 12.7 deg^2	random 12 c
0.25	165.5		208.9	
0.5	229.2	768.9	288.0	333.2
1.0	491.3	688.6	302.1	399.9
1.4		649.0		421.9
2.0	555.6	608.5	408.1	307.7
2.8		544.4		256.6
4.0	518.4	392.4	249.1	281.9
5.6		445.8		220.9
8.0	231.7	294.3	119.3	137.8
11		97.80		57.09
16	33.86	32.61	27.32	21.37
22		13.10		12.95

Figure 2.7b

Spatial frequency	grating 12.7 deg^2	grating 12 c	random 12.7 deg^2	random 12 c
0.25	179.7		196.0	
0.5	276.6	618.1	273.5	406.7
1.0	551.1	599.6	292.1	393.0
1.4		530.5		349.9
2.0	548.4	601.3	364.2	296.4
2.8		598.1		272.5
4.0	378.0	418.4	239.8	221.6
5.6		313.7		231.0
8.0	135.9	151.9	86.09	115.9
11		82.15		62.32
16	34.76	25.96	24.32	23.85
22		12.59		12.55

Figure 2.8a

Spatial frequency	grating 12.7 deg^2	grating 12 c	random 12.7 deg^2	random 12 c
0.25	2313		3474	
0.5	4240	927.0	6601	245.4
1.0	19170	4159	7263	1414
1.4		7241		3085
2.0	24390	12980	13250	3348
2.8		20310		4554
4.0	21190	21650	4936	11240
5.6		54680		13530
8.0	4231	46680	1132	10320
11		10520		3615
16	90.27	2285	59.40	991.1
22		756.8		744.0

Figure 2.8b

Spatial frequency	grating 12.7 deg^2	grating 12 c	random 12.7 deg^2	random 12 c
0.25	2726		3056	
0.5	6177	843.7	5952	365.6
1.0	24120	3154	6788	1365
1.4		4839		2123
2.0	23760	12680	10550	3107
2.8		24520		5138
4.0	11270	24610	4576	6944
5.6		27080		14790
8.0	1455	12440	589.8	7298
11		7420		4308
16	95.16	1449	47.08	1234
22		698.7		698.4

CHAPTER 3

Figure 3.3

r.m.s contrast of noise	1.5 c/deg HK	1.5 c/deg KT	6.0 c/deg HK	6.0 c/deg JM
0.0047	7.50 e-5	5.78 e-5	2.27 e-4	1.08 e-4
0.0094	9.31 e-5	6.72 e-5	1.73 e-4	1.06 e-4
0.019	7.25 e-5	6.01 e-5	3.01 e-4	1.26 e-4
0.038	8.01 e-5	4.92 e-5	2.33 e-4	1.28 e-4
0.075	1.00 e-4	7.99 e-5	2.62 e-4	2.24e-4
0.15	3.39 e-4	2.51 e-4	5.12 e-4	5.12 e-4
0.30	1.30 e-3	1.29 e-3	2.69 e-3	2.34 e-3

Figure 3.4a

noise pixel side length	1.5 c/deg	3 c/deg	6 c/deg
5.25 e-3			3.19 e-5
1.05 e-2		1.27 e-4	1.16 e-4
2.10 e-2	1.12 e-3	8.96 e-4	4.22 e-4
4.20 e-2	4.86 e-3	2.96 e-3	1.54 e-3
8.40 e-2	1.49 e-2	4.44 e-3	1.74 e-3
0.168	1.25 e-2	2.12 e-3	1.11 e-4
0.336	1.58 e-3	2.24 e-4	1.83 e-5
0.670	7.99 e-4	3.46 e-5	
1.34	8.17 e-5		

Figure 3.4b

noise pixel side length	1.5 c/deg	3 c/deg	6 c/deg
1.40 e-2			8.21 e-4
2.79 e-2		4.76 e-3	3.13 e-3
5.60 e-2	2.25 e-2	1.92 e-2	1.00 e-2
0.112	5.23 e-2	7.32 e-2	5.31 e-3
0.224	0.323	1.50 e-2	9.74 e-4
0.448	3.26 e-2	9.91 e-4	1.33 e-4
0.895	3.82 e-3	2.77 e-4	7.36 e-5
1.79	5.55 e-4	2.17 e-4	
3.58	4.98 e-4		

Figure 3.6a

noise pixel side length	1.5 c/deg	3 c/deg	6 c/deg
1.05 e-2			1.93 e-4
2.10 e-2		6.72 e-4	1.77 e-4
4.20 e-2	4.04 e-3	5.79 e-4	1.40 e-4
8.40 e-2	3.72 e-3	5.68 e-4	3.90 e-5
0.168	2.08 e-3	9.35 e-5	1.26 e-5
0.336	1.58 e-4	1.80 e-5	5.57 e-6
0.670	4.53 e-5	1.34 e-5	
1.34	4.49 e-5		

Figure 3.6b

noise pixel side length	1.5 c/deg	3 c/deg	6 c/deg
1.40 e-2			6.54 e-4
2.79 e-2		2.88 e-3	6.12 e-4
5.60 e-2	1.21 e-2	3.60 e-3	4.17 e-4
0.112	1.54 e-2	2.71 e-3	1.98 e-4
0.224	1.37 e-2	8.04 e-4	4.68 e-5
0.448	2.30 e-3	1.64 e-4	7.78 e-5
0.895	6.25 e-4	1.23 e-4	6.39 e-5
1.79	3.85 e-4	1.25 e-4	
3.58	5.88 e-4		

Figure 3.7

noise pixel side length	1 cycle 3 c/deg	1 cycle 3 c/deg	noise pixel side length	64 cycles 3 c/deg	64 cycles 3 c/deg
0.011	3.58 e-5	5.22 e-5	0.056	9.90 e-2	9.50 e-2
0.022	1.00 e-4	1.69 e-4	0.112	0.412	0.350
0.043	4.80 e-4	7.38 e-4	0.224	0.370	0.279
0.086	1.68 e-3	1.60 e-3	0.448	7.34 e-2	8.50 e-2
0.172	5.46 e-5	2.02 e-4	0.895	8.56 e-3	2.11 e-2

Figure 3.8

number of cycles	pixels/ cycle
1	4.10
4	4.36
4	4.78
16	2.90
16	3.24
64	2.12

Figure 3.10

noise pixel height	3.10a 3 c/deg	3.10a 0.75 c/deg	3.10b 3 c/deg	3.10b 0.75 c/deg
5.21 e-3	3.13 e-5			
1.04 e-2	4.38 e-5			
2.08 e-2	1.49 e-4	1.04 e-3	1.02 e-4	
4.17 e-2	2.21 e-4	2.15 e-3	1.10 e-4	
8.33 e-2	7.99 e-4	7.13 e-3	9.93 e-5	5.97 e-3
0.167	1.14 e-3	1.33 e-2	1.51 e-4	5.37 e-3
0.333	3.19 e-3	3.59 e-2	1.34 e-4	5.91 e-3
0.667	2.04 e-3	6.04 e-2	1.57 e-4	8.00 e-3
1.33	5.67 e-3	0.183	8.09 e-5	5.34 e-3
2.66		0.132		3.02 e-3
5.32		0.212		2.81 e-3

Figure 3.11/vertical grating

noise pixel width	3.11a 3 c/deg	3.11a 0.75 c/deg	3.11c 3 c/deg	3.11c 0.75 c/deg
5.21 e-3	3.13 e-5			
1.04 e-2	4.82 e-5			
2.08 e-2	9.44 e-5	1.04 e-3	1.07 e-4	
4.17 e-2	2.21 e-4	2.02 e-3	1.60 e-4	
8.33 e-2	3.26 e-4	4.88 e-3	1.54 e-4	6.90 e-3
0.167	3.30 e-4	6.93 e-3	5.02 e-5	8.71 e-3
0.333	1.19 e-4	2.08 e-2	2.15 e-5	9.25 e-3
0.667	3.82 e-5	6.57 e-3	2.09 e-5	2.10 e-3
1.33	2.32 e-5	2.66 e-3	2.21 e-5	8.18 e-4
2.66		1.08 e-3		2.94 e-4
5.32		5.94 e-4		2.76 e-4

Figure 3.11/circular grating

noise pixel height	3.11b 3 c/deg	3.11b 0.75 c/deg	3.11d 3 c/deg	3.11d 0.75 c/deg
5.21 e-3	6.50 e-5			
1.04 e-2	1.45 e-4		1.45 e-4	
2.08 e-2	2.20 e-4	2.09 e-3	1.61 e-4	
4.17 e-2	3.98 e-4	4.95 e-3	1.63 e-4	5.01 e-3
8.33 e-2	7.10 e-4	1.21 e-2	1.61 e-4	4.83 e-3
0.167	3.43 e-4	1.98 e-2	6.18 e-5	5.86 e-3
0.333	3.71 e-4	2.22 e-2	4.08 e-5	2.97 e-3
0.667	5.26 e-5	1.64 e-2	4.82 e-5	2.80 e-3
1.33	5.59 e-5	4.20 e-3	3.73 e-5	1.20 e-3
2.66		2.83 e-3		4.98 e-4
5.32		2.24 e-3		4.40 e-4

Figure 3.12

noise pixel width/height	vertical 3 c/deg	vertical 0.75 c/deg	circular 3 c/deg	circular 0.75 c/deg
3.92 e-3	5.72 e-3	0.116	6.49 e-5	1.69 e-3
0.0156	7.63 e-3	0.219	6.23 e-5	2.55 e-3
0.0625	1.18 e-2	0.343	9.37 e-4	1.06 e-2
0.250	5.91 e-3	0.365	3.91 e-3	1.85 e-2
1	7.73 e-3	0.107	7.58 e-3	5.26 e-2
4.00	7.79 e-4	2.19 e-2	2.91 e-3	3.00 e-2
16.0	1.74 e-4	6.66 e-3	9.96 e-4	1.09 e-2
64.0	4.31 e-5	1.36 e-3	6.72 e-5	2.93 e-3
255	2.77 e-5	8.04 e-4	5.65 e-5	2.52 e-3

CHAPTER 4

Figure 4.1

screen luminance cd/m^2	retinal illuminance phot. td	HK without noise	HK noise	KT without noise	KT noise
0.0139	0.698	11.7	8.50	7.27	6.75
0.0545	2.79	28.6	29.8	23.9	19.9
0.222	11.2	53.9	54.2	45.7	42.5
0.778	39.1	109	58.1	82.6	61.0
3.06	154	207	62.9	133	61.7
12.2	614	260	70.7	155	71.9
50.0	2510	375	63.0	235	56.1

Figure 4.2

screen luminance cd/m^2	retinal illuminance phot. td	HK without noise	HK noise	KT without noise	KT noise
50.0	2513	374	63.0	203	56.1
60.0	3016	431	102	233	83.8
70.0	3519	358	92.3	304	84.7
83.3	4189	400	105	236	111
122	6143	434	176	319	130
200	10053	450	261	369	212
333	16760	481	326	360	291
667	33510	449	524	384	299
778	39100	441	401	132	344

Figure 4.3

Added luminance cd/m^2	HK without noise	HK noise	KT without noise	KT noise
10	359	85.2	189	69.8
20	255	65.9	217	60.5
33.3	240	62.8	150	66.7
72	177	72.2	131	53.3
150	113	65.3	92.3	53.0
283	72.2	49.0	53.9	43.7
617	33.6	39.3	28.8	22.4
728	28.3	25.8	27.8	22.1

Figure 4.4 / 8 c/deg

exposure duration msec	HK without noise	HK noise	KT without noise	KT noise
16.7	33.6	27.3	23.4	16.3
33.3	61.0	44.0	40.2	35.3
66.7	94.0	56.4	65.3	42.7
133	136	60.5	97.0	40.9
267	159	62.4	114	50.3
533	187	71.0	158	60.0

Figure 4.4 / 0.75 c/deg

exposure duration msec	HK without noise	HK noise	KT without noise	KT noise
16.7	112	84.2	167	126
33.3	193	133	243	174
66.7	268	195	390	243
133	363	182	536	250
267	479	229	645	272
533	665	206	644	271

Figure 4.5

Area deg^2	HK without noise	HK noise	KT without noise	KT noise
1.97	202	178	142	156
3.95	328	285	237	240
7.89	359	271	302	272
15.8	408	321	339	295
31.5	484	350	409	302
62.7	580	318	464	303

CHAPTER 5

Figure 5.4, cosine

square cycles	1 deg^2 open	1 deg^2 closed	4 deg^2 open	4 deg^2 closed	16 deg^2 open	16 deg^2 closed
1	9237	35560	10960	5401	1363	952.2
4	28590	38900	7692	8816	1519	1218
16	18560	21120	5454	4050	840.7	775.9
64	14380	13240	2407	2170	569.4	614.9
256	2184	4160	1663	1720	304.9	217.0

Figure 5.4, random

square cycles	1 deg^2 open	1 deg^2 closed	4 deg^2 open	4 deg^2 closed	16 deg^2 open	16 deg^2 closed
1	13780	22050	6646	4095	1067	879.4
4	30110	38760	9704	12600	2140	1700
16	9164	7472	1670	1340	459.0	655.3
64	5461	4375	1447	1020	291.8	359.1
256	455.0	946.5	653.0	591.1	104.1	68.03

Figure 5.5, HK

square cycles	1 deg^2 cosine	4 deg^2 cosine	16 deg^2 cosine	1 deg^2 random	4 deg^2 random	16 deg^2 random
1	0.102	0.482	0.240	0.151	0.292	0.188
4	0.314	0.338	0.267	0.331	0.427	0.376
16	0.204	0.240	0.148	0.101	0.073	0.081
64	0.158	0.106	0.100	0.060	0.064	0.051
256	0.024	0.073	0.054	0.005	0.029	0.018

Figure 5.5, RN

square cycles	1 deg^2 cosine	4 deg^2 cosine	16 deg^2 cosine	1 deg^2 random	4 deg^2 random	16 deg^2 random
1	0.391	0.237	0.167	0.242	0.180	0.155
4	0.318	0.388	0.214	0.426	0.554	0.299
16	0.232	0.178	0.136	0.082	0.059	0.115
64	0.146	0.095	0.108	0.048	0.045	0.063
256	0.046	0.076	0.038	0.010	0.026	0.012

Figure 5.9a

centre frequency c/deg	H	K	O	+
1	0.342	0.230	0.491	0.264
2	0.289	0.150	0.258	0.213
4	0.103	0.077	0.063	0.105
8	0.049	0.059	0.036	0.082
16	0.023	0.021	0.011	0.032

Figure 5.9b

centre frequency c/deg	H	K	O	+
1	0.365	0.277	0.430	0.300
2	0.136	0.104	0.174	0.240
4	0.114	0.064	0.098	0.106
8	0.052	0.042	0.051	0.066
16	0.030	0.034	0.016	0.071

Figure 5.10a

bandwidth octaves	H	K	O	+
0.25	0.085	0.043	0.092	0.082
0.5	0.046	0.091	0.087	0.168
1	0.084	0.071	0.113	0.066
2	0.098	0.126	0.128	0.131
4	0.250	0.319	0.312	0.254

Figure 5.10b

bandwidth octaves	H	K	O	+
0.25	0.072	0.052	0.068	0.083
0.5	0.059	0.058	0.083	0.099
1	0.103	0.071	0.064	0.098
2	0.212	0.100	0.125	0.113
4	0.324	0.367	0.329	0.294

Figure 5.11

Symbols with various centre frequencies

Relative image area	H hk	H rn	Relative image area	K hk	K rn
1.26	0.342	0.365	1.39	0.230	0.277
5.85	0.289	0.136	6.03	0.150	0.104
32.3	0.103	0.114	32.1	0.077	0.064
86.6	0.049	0.052	84.4	0.059	0.042
210	0.023	0.030	201	0.021	0.034
Relative image area	O hk	O rn	Relative image area	+ hk	+ rn
1.43	0.491	0.430	1.74	0.265	0.300
4.98	0.258	0.174	4.05	0.213	0.240
35.2	0.063	0.098	20.1	0.105	0.106
82.5	0.036	0.051	59.5	0.082	0.066
189	0.011	0.016	131	0.032	0.071

Symbols with various bandwidths

Relative image area	H hk	H rn	Relative image area	K hk	K rn
34.2	0.085	0.072	34.6	0.043	0.052
39.5	0.046	0.059	34.6	0.091	0.058
32.3	0.086	0.103	32.1	0.071	0.071
14.4	0.098	0.212	17.3	0.126	0.100
6.27	0.250	0.324	6.35	0.319	0.367
Relative image area	O hk	O rn	Relative image area	+ hk	+ rn
36.0	0.092	0.068	31.8	0.082	0.083
36.9	0.087	0.083	26.5	0.168	0.099
35.2	0.113	0.064	20.9	0.066	0.098
23.1	0.128	0.125	9.63	0.131	0.113
5.14	0.312	0.329	4.31	0.254	0.294

Relative image area	cosine hk	cosine rn	Relative image area	random hk	random rn
3.22	0.309	0.301	1.09	0.376	0.413
12.6	0.197	0.181	5.86	0.084	0.082
53.3	0.121	0.117	29.3	0.058	0.051
217	0.047	0.052	119	0.014	0.015

Figure 5.14

area	hk patched	hk uniform	rn patched	rn uniform
0.64	0.155	0.155	0.273	0.273
3.24	0.085	0.100	0.147	0.105
7.84	0.052	0.072	0.097	0.096
23.0	0.039	0.030	0.057	0.035

Figure 5.16

Complexity uniform	hk	rn	Complexity patched	hk	rn
4.54	0.155	0.273	4.54	0.155	0.273
25.3	0.100	0.105	36.2	0.085	0.147
58.8	0.072	0.096	83.4	0.052	0.097
142	0.030	0.035	121	0.039	0.057

Figure 5.16, Previous data
Symbols with various centre frequencies

Complexity	H hk	H rn	Complexity	K hk	K rn
1.79	0.342	0.365	1.58	0.230	0.277
3.92	0.289	0.136	4.64	0.150	0.104
22.4	0.103	0.114	24.1	0.077	0.064
80.6	0.049	0.052	86.9	0.059	0.042
331	0.023	0.030	355	0.021	0.034
Complexity	O hk	O rn	Complexity	+ hk	+ rn
1.40	0.491	0.430	1.59	0.265	0.300
4.34	0.258	0.174	2.64	0.213	0.240
27.7	0.063	0.098	13.8	0.105	0.106
90.0	0.036	0.051	50.4	0.082	0.066
363	0.011	0.016	198	0.032	0.071

Symbols with various bandwidths

Complexity	H hk	H rn	Complexity	K hk	K rn
29.0	0.085	0.072	26.7	0.043	0.052
29.1	0.046	0.059	25.5	0.091	0.058
22.4	0.086	0.103	24.1	0.071	0.071
8.43	0.098	0.212	9.19	0.126	0.100
2.75	0.250	0.324	2.75	0.319	0.367
Complexity	O hk	O rn	Complexity	+ hk	+ rn
28.1	0.092	0.068	20.7	0.082	0.083
28.0	0.087	0.083	17.0	0.168	0.099
27.8	0.113	0.064	13.8	0.066	0.098
8.45	0.128	0.125	5.19	0.131	0.113
2.91	0.312	0.329	1.81	0.254	0.294

complexity	cosine hk	cosine rn	complexity	random hk	random rn
1.97	0.309	0.301	2.03	0.376	0.413
8.20	0.197	0.181	7.69	0.084	0.082
32.2	0.121	0.117	32.0	0.058	0.051
109	0.047	0.052	136	0.014	0.015

Figure 5.18

phase range	2 oct hk	1 oct hk	0.5 oct hk	0.25 oct hk	circular hk
0	0.578	0.408	0.466	0.224	0.081
90	0.317	0.277	0.204	0.148	0.082
180	0.270	0.210	0.135	0.120	0.062
270	0.042	0.053	0.035	0.038	0.044
360	0.018	0.042	0.039	0.052	0.054

phase range	2 oct rn	1 oct rn	0.5 oct rn	0.25 oct rn	circular rn
0	0.466	0.328	0.286	0.220	0.085
90	0.459	0.403	0.219	0.155	0.080
180	0.107	0.193	0.104	0.097	0.047
270	0.039	0.045	0.041	0.037	0.053
360	0.018	0.041	0.030	0.054	0.038

Figure 5.19

Spatial spread deg^2	2 oct hk	2 oct rn	Spatial spread deg^2	1 oct hk	1 oct rn
0.005	0.578	0.446	0.026	0.408	0.328
0.429	0.317	0.459	0.443	0.277	0.403
1.20	0.270	0.107	1.21	0.210	0.193
1.85	0.042	0.039	2.10	0.053	0.045
2.10	0.018	0.018	2.33	0.042	0.041
Spatial spread deg^2	0.5 oct hk	0.5 oct rn	Spatial spread deg^2	0.25 oct hk	0.25 oct rn
0.113	0.466	0.286	0.467	0.224	0.220
0.456	0.204	0.219	0.733	0.148	0.155
1.19	0.135	0.104	1.49	0.120	0.097
2.05	0.035	0.041	2.26	0.038	0.037
2.04	0.039	0.030	2.22	0.052	0.054
Spatial spread deg^2	circular hk	circular rn			
2.10	0.081	0.085			
2.05	0.082	0.080			
2.19	0.062	0.047			
1.91	0.044	0.053			
2.25	0.054	0.038			

Figure 5.20

complexity	2 oct hk	2 oct rn	complexity	1 oct hk	1 oct rn
0.118	0.578	0.446	0.465	0.408	0.328
9.98	0.317	0.459	7.77	0.277	0.403
28.0	0.270	0.107	21.3	0.210	0.193
43.0	0.042	0.039	36.8	0.053	0.045
49.0	0.018	0.018	40.9	0.042	0.041
complexity	0.5 oct hk	0.5 oct rn	complexity	0.25 oct hk	0.25 oct rn
1.85	0.466	0.286	7.54	0.224	0.220
7.47	0.204	0.219	11.8	0.148	0.155
19.5	0.135	0.104	24.0	0.120	0.097
33.5	0.035	0.041	36.5	0.038	0.037
33.3	0.039	0.030	35.9	0.052	0.054
complexity	circular hk	circular rn			
28.9	0.081	0.085			
28.2	0.082	0.080			
30.1	0.062	0.047			
26.3	0.044	0.053			
31.0	0.054	0.038			